To the Graduate Council:

I am submitting herewith a thesis written by Scott Gayton Liter entitled "High Heat Rate Testing of Thermal Response of Carbon-Phenolic FM-5055." I have examined the final copy of this thesis for form and content and recommend that it be accepted in partial fulfillment of the requirements for the degree of Master of Science, with a major in Mechanical Engineering.

Majid Keyhani 12/18/95

Majid Keyhani, Major Professor

We have read this thesis and recommend its acceptance:

Accepted for the Council:

Associate Vice Chancellor and
Dean of The Graduate School

HIGH HEAT RATE TESTING OF THERMAL RESPONSE OF CARBON-PHENOLIC FM-5055

A Thesis

Presented for the

Master of Science

Degree

The University of Tennessee, Knoxville

Scott Gayton Liter

May 1996

Dedication

This thesis is dedicated to my parents

Mr. Melvin Earl Liter

and

Mrs. Cherry Lynn Liter

for their unwavering support and unequaled friendship and love.

Acknowledgments

Above all things, I acknowledge and am thankful for the mercy and grace afforded me by God. It is by His power and providence that I can do anything at all. I am also thankful for the unwavering support and unparalleled friendship of my family, especially of my parents, Melvin and Cherry Liter, and of my brother, Michael Liter. Without them, I would not have been here. Thank you to Amanda Gutwein whose unconditional love helped me to maintain my focus on the important things in life.

Joyfully, I take this opportunity to thank my major professor, Dr. Majid Keyhani. His wise counsel on everything from my thesis to life in general has enriched my graduate school experience at UTK beyond measure. I consider myself honored to have worked with him. I would like to also express sincerest appreciation to Dr. R. V. Arimilli and Dr. M. Milligan for their service and help as my committee members.

I very much appreciate the support through funding and materials by the National Aeronautics and Space Administration at Marshall Space Flight Center, by Analysis and Measurement Services Corporation of Knoxville, TN, and by the Mechanical and Aerospace Engineering Department of UTK. The assistance and expertise of Dennis Higdon with the experimental set-up and technical equipment is much appreciated. Also the friendship of Cathy Graves and her assistance with making the x-rays is much appreciated

And last, but not least, I am grateful to all my fellow graduate students and all of my professors at UTK for establishing an environment conducive to learning, discovering, and engineering.

Abstract

A test facility was constructed for measurement of thermal response of decomposing polymers exposed to initial heating rates up to 250 °C/sec and maximum temperatures exceeding 2000 °C. Eight experimental runs were performed with the facility on blocks of carbon-phenolic FM-5055. During these experiments, temperature and heating rates at various locations in the block, the aggregate mass loss, and "char" depth were found. A boundary condition for the heated surface was also measured to allow for numerical predictions of the experiments. The results of these experiments are discussed and are presented as a database with which numerical codes may be verified.

Numerical predictions were made for these experiments using PEACH, a two-dimensional finite-difference code, and comparisons were drawn. The mass loss and "char" depth are shown to be under-predicted in all of the experiments. The temperature is shown to have poor agreement at locations in the block exposed to high heating rates (close to the heated surface) and good agreement at locations exposed to low heating rates (far from the heated surface). It is suggested that the part of the code modeling the kinetics of the pyrolysis process be re-evaluated.

Table of Contents

Chapter 1 1

1.0 Introduction 1

Chapter 2 8

2.0 Experimental Setup 8

2.1 Procedure 17

2.2 Brief Description of Numerical Predictions 19

Chapter 3 22

3.0 Experimental Results and Analysis 22

3.1 RUN #1 22

3.2 RUN #2 32

3.3 RUN #3 46

3.4 RUN #4 55

3.5 RUN #5 68

3.6 RUN #6 83

3.7 RUN #7 94

3.8 RUN #8 101

Chapter 4 111

4.0 Conclusions and Future Considerations 111

References 114

Appendices 118

Appendix A High heating rate database 119

Appendix B Material properties 131

Vita 137

List of Figures

1 Regions of a composite undergoing heating 3

2 Schematic of experimental set-up 9

3 Experimental test stand: (a) top view; and (b) front view 11

4 Test sample and graphite heater assembly 13

5 Schematic of electrical leakage detection circuit 15

6 Calculated resistive power dissipation for run #1 23

7 Measured temperatures for run #1 25

8 Comparison of run #1 in-depth temperatures with prediction 29

9 Predicted degree of char after 13.3 sec of heating and 15 minutes cooling for run #1 31

10 Measured thermocouple temperatures for run #2 35

11 Comparison of run #2 in-depth temperatures with prediction 41

12 Predicted degree of char after 9.8 sec of heating and near 15 minutes cooling for run #2 41

13 Time history of heating rates of run #2 thermocouples 45

14 Comparison of measured temperatures for runs #1 and 2 45

15 Comparison of measured thermocouple temperatures for selected thermocouples for run #3 48

16 Measured thermocouple temperatures for run #3 49

17 Comparison of run #3 in-depth temperatures with prediction 54

18 Predicted degree of char after 32.3 sec of heating and 15 minutes of cooling for run #3 54

19 Time history of heating rates of run #3 thermocouples 56

20 Comparison of measured thermocouple temperatures for thermocouples #1 and 2 for run #4 60

21 Comparison of measured thermocouple temperatures for thermocouples #3 and 4 for run #4 60

List of Figures (cont.)

22 Comparison of measured thermocouple temperatures for thermocouples #5 and 6 for run #4 61

23 Measured thermocouple temperatures for run #4 63

24 Comparison of run #4 in-depth temperatures with prediction 67

25 Predicted degree of char after 46.7 sec of heating and 15 minutes cooling for run #4 67

26 Time history of heating rates of run #4 thermocouples 69

27 Comparison of measured thermocouples temperatures for run #5 71

28 Comparison of run #5 cement-potted in-depth thermocouple measurements with prediction using original CMA kinetics coefficients ...74

29 Comparison of run #5 air-potted in-depth thermocouple measurements with prediction using 50 times larger kinetics coefficients 76

30 Thermal resistance vs. temperature for different potting materials 80

31 Effective time constant vs. temperature for diferent potting materials 80

32 Predicted degree of char after 30.9 sec of heating and near 15 minutes cooling for run #5 82

33 Time history of heating rates of run #5 air-potted thermocouples 84

34 Comparison of measured thermocouples temperatures for run #6 86

35 Measured thermocouple temperatures for run #6 88

36 Comparison of run #6 in-depth temperatures with prediction 90

37 Predicted degree of char after 33.9 sec of heating and near 15 minutes cooling for run #6 92

38 Time history of heating rates of run #6 thermocouples 93

39 Comparison of measured thermocouple temperatures for run #7 95

40 Measured thermocouple temperatures for run #7 97

41 Comparison of run #7 in-depth temperatures with prediction 99

List of Figures (cont.)

42 Predicted degree of char after 27.9 sec of heating and near 15 minutes cooling for run #7 100

43 Comparison of measured thermocouple temperatures for thermocouples #1 and 2 for run #8 104

44 Comparison of measured thermocouple temperatures for thermocouples #3 and 4 for run #8 104

45 Comparison of measured thermocouple temperatures for thermocouples #5 and 6 for run #8 105

46 Measured thermocouple temperatures for run #8 107

47 Comparison of run #8 in-depth temperatures with prediction 109

48 Time history of heating rates of run #8 thermocouples 109

List of Tables

1 List of equipment and material 10

2 Thermocouple locations for run #1 25

3 Predicted and measured mass loss for run #1 29

4 Comparison of the predicted "char" depth with the "Scratch" Test for run #1 ...33

5 Thermocouple locations for run #2 33

6 Predicted and measured mass loss for run #2 39

7 Comparison of the predicted "char" depth with the "Scratch" Test for run #2 ...42

8 Thermocouple locations for run #3 48

9 Predicted and measured mass loss for run #3 52

10 Comparison of the predicted "char" depth with the "Scratch" Test for run #3 ...56

11 Thermocouple locations for run #4 57

12 Predicted and measured mass loss for run #4 65

13 Comparison of the predicted and "observed" "char" depth of run #4 69

14 Thermocouple locations for run #5 71

15 Predicted and measured mass loss for run #5 74

16 Comparison of the predicted and "observed" "char" depth for run #5 82

17 Thermocouple locations for run #6 86

18 Predicted and measured mass loss for run #6 90

19 Comparison of the predicted and "observed" "char" depth for run #6 92

20 Thermocouple locations for run #7 95

21 Predicted and measured mass loss for run #7 99

22 Comparison of the predicted and "observed" "char" depth for run #7 100

23 Thermocouple locations for run #8 102

A-1 Instrumented test sample dimensions for each experiment 119

List of Tables (cont.)

A-2 Uninstrumented test sample dimensions for each experiment 119

A-3 Uncoated graphite heater dimensions for each experiment 120

A-4 Current, voltage, resistance, and calculated surface heat flux at the end of heating for each experiment 120

A-5 Total mass loss and "char" depth of uninstrumented test sample for each experiment 121

A-6 Experimental temperature data for run #1 122

A-7 Experimental temperature data for run #2 123

A-8 Experimental temperature data for run #3 124

A-9 Experimental temperature data for run #4 125

A-10 Experimental temperature data for run #5 126

A-11 Experimental air-potted temperature data for run #5 127

A-12 Experimental temperature data for run #6 128

A-13 Experimental temperature data for run #7 129

A-14 Experimental temperature data for run #8 130

B-1 Temperature-dependent material properties for carbon-phenolic 131

B-2 Porosity and permeability for carbon-phenolic 133

B-3 Decomposition kinetics for carbon-phenolic 134

B-4 Material properties used for POCO graphite, grade EDM3 135

B-5 Material properties used for Boron Nitride paint 135

B-6 Thermophysical properties of thermocouple potting materials and carbon-phenolic 136

B-7 Material properties used for Hot Pressed Boron Nitride (HPBN) plates 136

Nomenclature

A_i	Surface area of thermocouple bead, m^2
c_p	Specific heat, J/Kg-K
C_t	Thermal capacitance, J/K
E	Activation energy, J/mole
I	Current, Amperes
k	Themal conductivity, W/m-K
K	Pre-exponential factor for kinetic rate equation, sec^{-1}
m	Mass, Kg
q	Power dissipated, W
r	radius, m
R	Universal gas constant, J/mol-K; Radius, m
R_t	Thermal resistance, K/W
t	Time, sec
T	Temperature, ^oC or K
V	Voltage, Volt

Greek Variables

β	Degree of Char, Argument of Bessel's function
ε	Emissivity
φ	Exponent for kinetic rate equation
Γ	Resin fraction
θ	Phase angle

Greek Variables (cont.)

ρ	Density, Kg/m^3
σ	Stefan-Boltzmann Constant, $W/m^2\text{-}K^4$
τ	Time constant, sec

Subscripts

A	Component material index for composite solid density model
bead	Of thermocouple bead
B	Component material index for composite solid density model
c	Char solid
cp	Carbon-phenolic
C	Component material index for composite solid density model
eff	Effective
i	Index for component material of composite for kinetic rate equation
inner	Of thermocouple bead or inner sphereical shell
initial	At beginning of heating time
n	denotes zero of Bessel's function
o	of cylinder
s	solid
tc, TC	Thermocouple
v	Virgin solid

Abbreviations

BN	Boron Nitride paint
CMA	Charring Material Ablators code by Aerotherm
DOC	Degree of char
HPBN	Hot pressed boron nitride
MSFC	Marshal Space Flight System
SRM	Solid Rocket Motor
TC	Thermocouple
TGA	Thermogravimetric Analysis

Chapter 1

1.0 Introduction

An exhaust nozzle of a solid rocket motor (SRM) on an orbital lifter experiences extreme and potentially destructive heating conditions where exhaust gas temperatures exceed 3000 °C. The temperature of the structural shell of the nozzle must be maintained below its maximum-use temperature or else it would be weakened and cause catastrophic failure. One method of maintaining the temperature of the structural shell below its maximum allowable temperature is by placing an ablative, sacrificial insulating liner between it and the exhaust gases. Carbon-phenolics have been shown to be effective insulators for this purpose. Weight is a major consideration on any orbital lifter, therefore the liner should only be as thick as necessary to safely insulate the shell. Thus, to create the optimum design, in terms of performance and cost, it is imperative to be able to accurately predict the thermal response of these ablative insulating materials when subjected to very high heating conditions. A number of computer codes have been developed in attempts to predict the thermal response, but as with any codes, their predictions depend on the accuracy of the material properties used for input.

The highly temperature dependent thermophysical properties of carbon-phenolic are very difficult to determine. "Virgin," or non-pyrolysized, carbon-phenolic consists of woven carbon cloth glued together with a phenolic resin. It has orthotropic properties in the "with-ply" direction, in plane with the cloth, and the "across-ply" direction, perpendicular to the cloth. As it is heated, the resin pyrolysizes into a complex mixture of gases, rendering the material "charred," and then escapes from the carbon substrate.

Figure 1 shows the different regions of a composite undergoing heating. One should be aware that the thickness of the pyrolysis region is sensitive to the rate of heating of the material. During the firing of an actual SRM, the nozzle liner, in addition to having the heating rate-dependent pyrolysis region propagating through it, experiences surface recession from ablation into the exhaust stream of the heated surface of the char region.

The degree of charring depends on the amount of resin pyrolysized and thus also depends on the time and spatial location in the material domain. The local degree of char (DOC) can be related to the local density of the material. The thermophysical properties, such as thermal conductivity, specific heat, permeability, and porosity, depend on the DOC as well as the local temperature. The DOC itself depends on time due to the rate at which the resin is pyrolysized. The rate of gas generation due to pyrolysis has also been shown to be dependent on the heating rate [2]. As the resin is pyrolysized, the local porosity (and permeability) increases until the local DOC becomes unity. To escape the material substrate, the generated pyrolysis gases flow in the direction of least resistance, towards the heated surface through the char region. While resident in this region, the gases can absorb additional heat, cooling the carbon substrate. As heating continues, the pyrolysis region propagates into the virgin region. Obviously, the transient, temperature dependent nature of the material properties is very complex.

Much research has been done to develop a numerical model for the prediction of the thermal response of carbon-phenolic. A currently accepted model is the one-dimensional Charring Material Ablation code (CMA90S) developed by Ross and Strobel [15] at Aerotherm. Keyhani and Krishnan presented another one-dimensional code (UT1D) for predicting the temperature and pore pressure of a decomposing polymer [5].

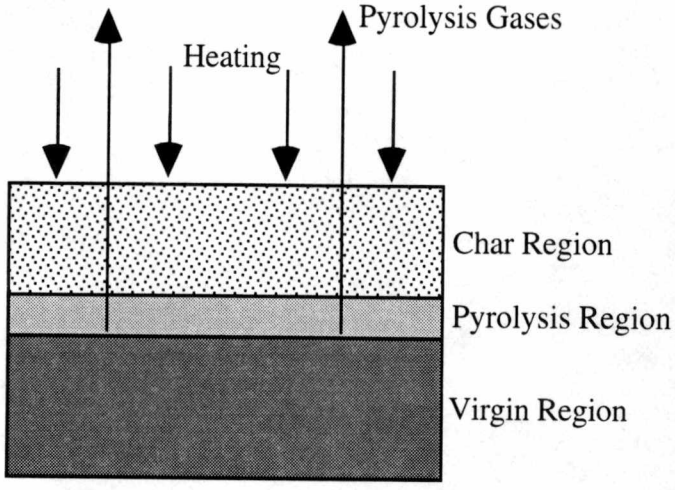


Figure 1 Regions of a composite undergoing heating

Then they extended their code to include surface recession [6] and used it to predict the thermal response in a radiatively heated and glass-filled thermoset composite designated as H41N [2]. UT1D was found to run up to two times faster than CMA90S.

The latest version of UT1D as presented by Krishnan [9] was further extended by Keyhani and Polehn [8,13] to model two-dimensional anisotropic flows. Polehn, Keyhani, and Parang [14] discussed the transient nature of compressible flow in variable permeability media, and Polehn and Keyhani [12] explored different schemes for predicting pore pressures for flow through variable permeability media. Polehn [11] presented the latest version of the two-dimensional model (PEACH) and numerically analyzed the general transient thermal response of an ablating, decomposing composite for the two-dimensional case.

Studies were performed to find an empirical expression for each of the properties that are needed to predict the thermal response of the material, but accurate numbers for some of the properties, for example those dealing with the rate of generation of pyrolysis gases, at heating rates experienced in an SRM nozzle, exceeding 500 ^{o}C/sec [3], are not available. The quantitative values for the model of the pyrolysis process used in the CMA90S and PEACH models were found through thermogravimetric analysis of carbon-phenolic. Keyhani and Liter [7] noted that these quantitative input values were found at much lower than actual heating rates and temperatures, and therefore predictions of actual flight responses made by these models cannot be used with confidence. Stokes [17] also recognized this problem and performed a thermogravimetric analysis over a range of heating rates, but only to a maximum of 50 ^{o}C/sec, still unacceptably low. Some of the responses that must be predicted to optimize the liner design include: the temperature

profile, the surface recession rate due to ablation, the pore pressure profile, the depth of the char region, the solid density profile (DOC), and the aggregate mass loss. The input properties necessary to predict these responses are very difficult to measure at actual flight conditions. The properties of FM 5055 used for predictions in this project were found by Acurex [1,15] and Southern Research Institute (SoRI) [16,18], and are given in Appendix B. Some of the required input properties are:

-for the solid material

- virgin and char density (currently accepted as accurate)
- thermal conductivity (accuracy suspect)

  with-ply - virgin, char, and as a function of DOC and temperature

  across-ply - virgin, char, and as a function of DOC and temperature
- heat capacity (accuracy suspect)

  virgin, char, and as a function of DOC and temperature
- heat of formation (accuracy suspect)

  virgin, char, and as a function of DOC and temperature
- porosity (accuracy suspect)

  as a function of degree of char
- permeability (currently accepted as accurate)

  with-ply and across-ply, and as a function of DOC and temperature
- decomposition kinetics (rate of pyrolysis process) (inaccurate)

  as a function of heating rate and temperature

-for the pyrolysis gas

- molecular weight (accuracy suspect)
- viscosity (accuracy suspect)
- enthalpy (accuracy suspect)

Obviously, with only two properties considered accurate, predictions made with these properties cannot be made with great confidence. Slight "tweaking" of such properties as the rate of pyrolysis gas generation tend to improve some predictions, but these predictions cannot be quoted with confidence without verifying the "tweaking" by somehow justifying the amount of "tweaking" and by accurately predicting comparable experimental test cases.

Small scale experiments can be performed to remove some of the complexities of the actual phenomenon to facilitate verification of numerical models. Specifically, high heating can be applied in a controlled manner in which surface recession, a difficult numerical problem, is not experienced, thus allowing efforts to be concentrated on other unsolved aspects of modeling the phenomenon. The avoidance of surface recession would also allow for accurate temporal measurements of the heated surface providing a quality numerical boundary condition.

Pitman [10] presented a facility for gathering of high heat rate thermal response of decomposing polymers for the purpose of code verification. His facility used contact heating of the samples in such a way as to minimize multi-dimensional effects and to allow for accurate boundary condition measurements. He used metallic foil as a resistive heating element in his apparatus and was limited by the melting point of the foil. Polehn [11] improved on Pitman's design by using POCO (polycrystalline) graphite as the heating element theoretically allowing heating to temperatures in excess of 3300 ^{o}C.

The purpose of this thesis is twofold: (1) to develop a facility for collection of accurate data on the thermal response of a decomposing polymer subjected to initial

heating rates near 200 °C/sec and temperatures exceeding 2000 °C; and (2) to use this facility to generate a limited database of such responses for carbon-phenolic samples. The results from these experiments could be used to validate numerical models and to more easily allow for the isolation of those thermophysical properties that are highly dependent on heating rate.

Chapter 2

2.0 Experimental Setup

The desired database of the thermal response of carbon-phenolic for various heating rates will consist of the temperature histories at various depths from the heated surface, the aggregate mass loss, the depth of the char region, and a measured boundary condition. The following facility is presented as a means of generating this database. It is a revision of the facility presented by Polehn [11], which in turn was a revision of the facility presented by Pitman [10]. The proposed facility will improve on that of Polehn by allowing for higher heat rate tests while decreasing experimental errors.

A schematic of the equipment setup is shown in Fig. 2 and a list of the equipment used is given in Table 1. An electrical circuit with a resistive heating element (POCO graphite) was the chosen device for heating of the test samples. A regulated AC power supply was used as the energy source for the circuit. This power was directed through two AC power transformers in series to reduce the voltage by approximately a factor of ten to better match the low electrical resistance of the heater. The tests were controlled by a Hewlett-Packard emulator board in an IBM compatible personal computer. This board sent a signal to a Hewlett-Packard DC power supply that actuated a relay which toggled the power flow to the transformers. The output from the transformers was applied across two parallel sets of copper bus bars as shown in Fig. 3 (a). The graphite plate (the heater) was suspended between these bus bars completing the circuit.

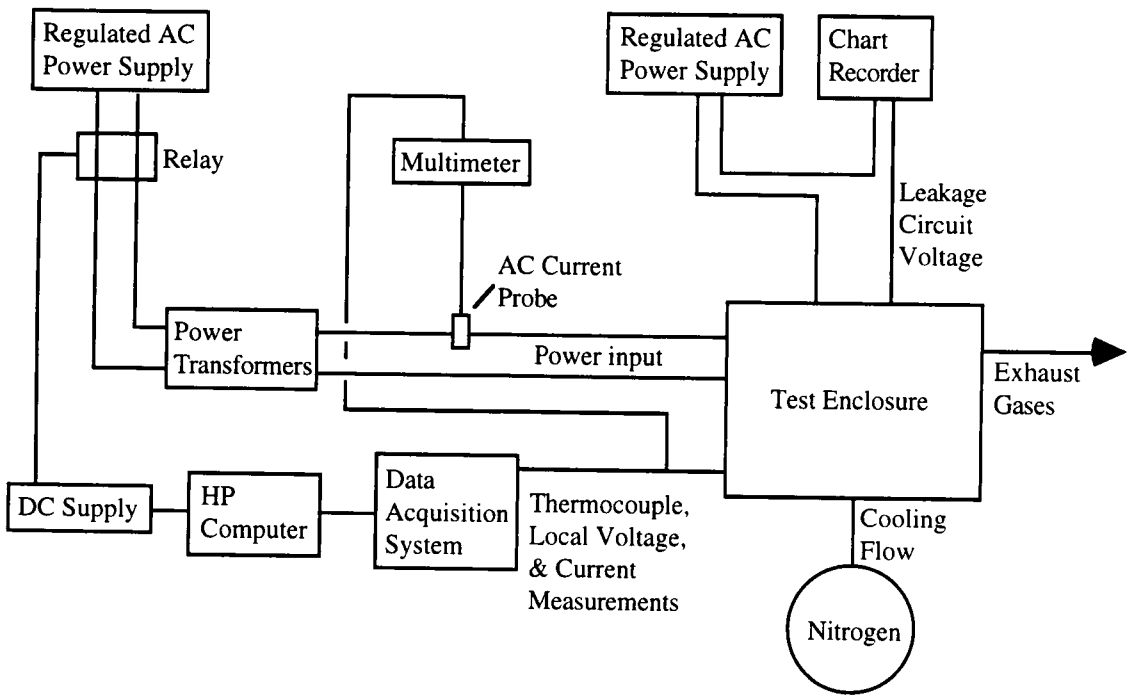
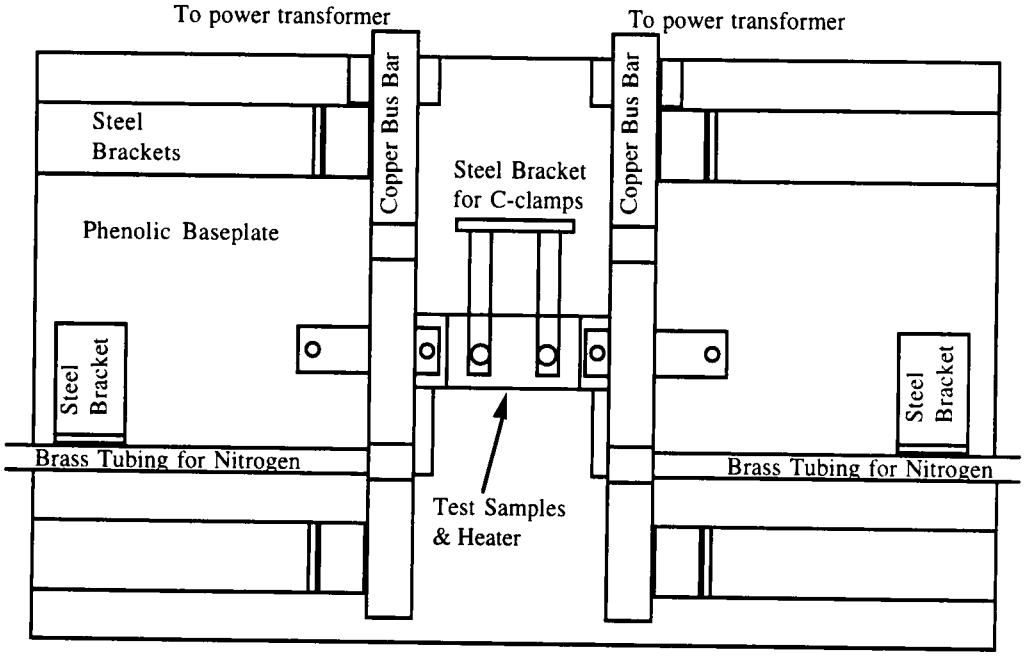


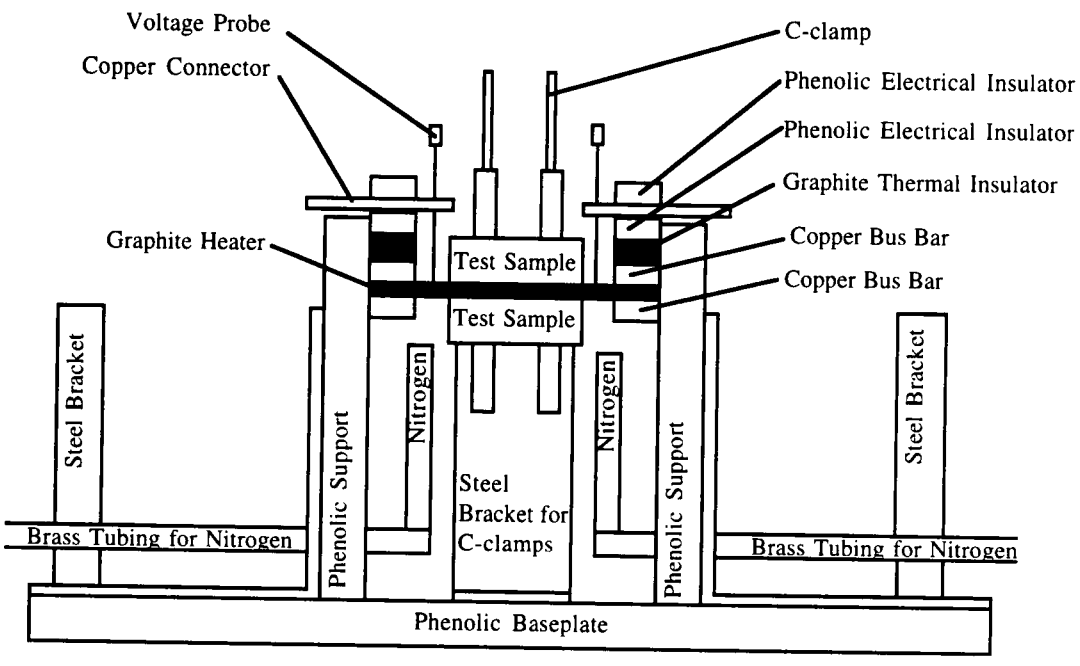
Figure 2 Schematic of experimental set-up

Table 1 List of equipment and material

Description	Equipment and Materials Used
AC current probe	Fluke Model 80i-600
AC power supply	Sorenson AC regulator, ACR 7500
Chart recorder	Gould Brush 2400
DC supply	Hewlett-Packard Model 6634A
Regulated DC supply	Lambda Regulated Power Supply
Data acquisition unit	Hewlett-Packard Model 3497A
Dial caliper	Mitutoyo #505-637-50, ±0.001"
Digital voltmeter	Hewlett-Packard Model 3456A
Electrically insulating plate	Carborundum hot pressed Boron Nitride plates (20 mm x 40 mm x 2.5 mm)
Electrically insulating paint	ZYP Coatings Boron Nitride, liquid
Electrically conductive paint	GC Electronics Silver Paint 22-201
Heater element	UNOCAL POCO Graphite, Grade EDM-3
Multimeter A	Keithley Model 177
Multimeter B	Fluke Model 87
Oscilloscope	Tektronix Model 465
Power transformers	2 Square D 2 KVA, 2S43F
Pyrometer	Fast-response, two color
Relay	Potter & Brumfield SSR-240D80, 80 amp
Thermocouple wire	Teflon coated, 0.127 mm, Type K chromel-alumel Bare, 0.127 mm, Type C tungsten-rhenium Glass braided, 0.254 mm, Type J iron-constantan
Thermocouple reference	Kaye Instruments Ice Point / reference
Thermocouple potting compounds	Sauereisen INSULTEMP NO.10 Insulating cement ZYP Coatings RS-1000 cement ORPAC Alumina Paste Cotronics C-7030, C-989, and C-903-HP cements
Test samples, composites	FM 5055 carbon-phenolic provided by NASA
Weighing device	Ohaus triple beam balance, ±0.05 grams



(a)



(b)

Figure 3 Experimental test stand: (a) top view; and (b) front view

To measure a heat flux boundary condition, the power dissipated in the heater must be found. Local AC voltage across and AC current flow through the heater was measured by the Hewlett-Packard data acquisition system. The local voltage was measured across two tactile probes on the heater between the test samples and copper bus bars, and was stored by the computer. The AC current flow through the heater was measured over time with a Fluke clamp-on AC current probe. The output from this probe was converted from AC current to a proportional DC voltage using a Keithley multimeter and was then measured by the Hewlett-Packard data acquisition system. The measured current data was then timed, processed, and stored by the Hewlett-Packard emulator. The power dissipated was calculate by

$$q = V\ I\ \cos(\theta) \tag{1}$$

where $\cos(\theta)$ is the power factor and θ is the phase angle between the voltage and current sinusoids. There was little inductance in the power circuit and as expected, the power factor was found to be $\cos(\theta) = 1.0$. A Tektronix oscilloscope was used to superimpose the sinusoids of the AC current readings and the AC voltage readings, and the phase angle θ was seen to be negligible.

A typical test sample and heater assembly is shown in Fig. 4. The heater was made of fine-grained polycrystalline (POCO) graphite with well documented isotropic properties. It was machined as thin as practical to minimize multi-dimensional effects. The ends of the graphite heater were painted with an electrically conductive silver paint to enhance the electrical conduction across the graphite and copper bus bar interfaces. To

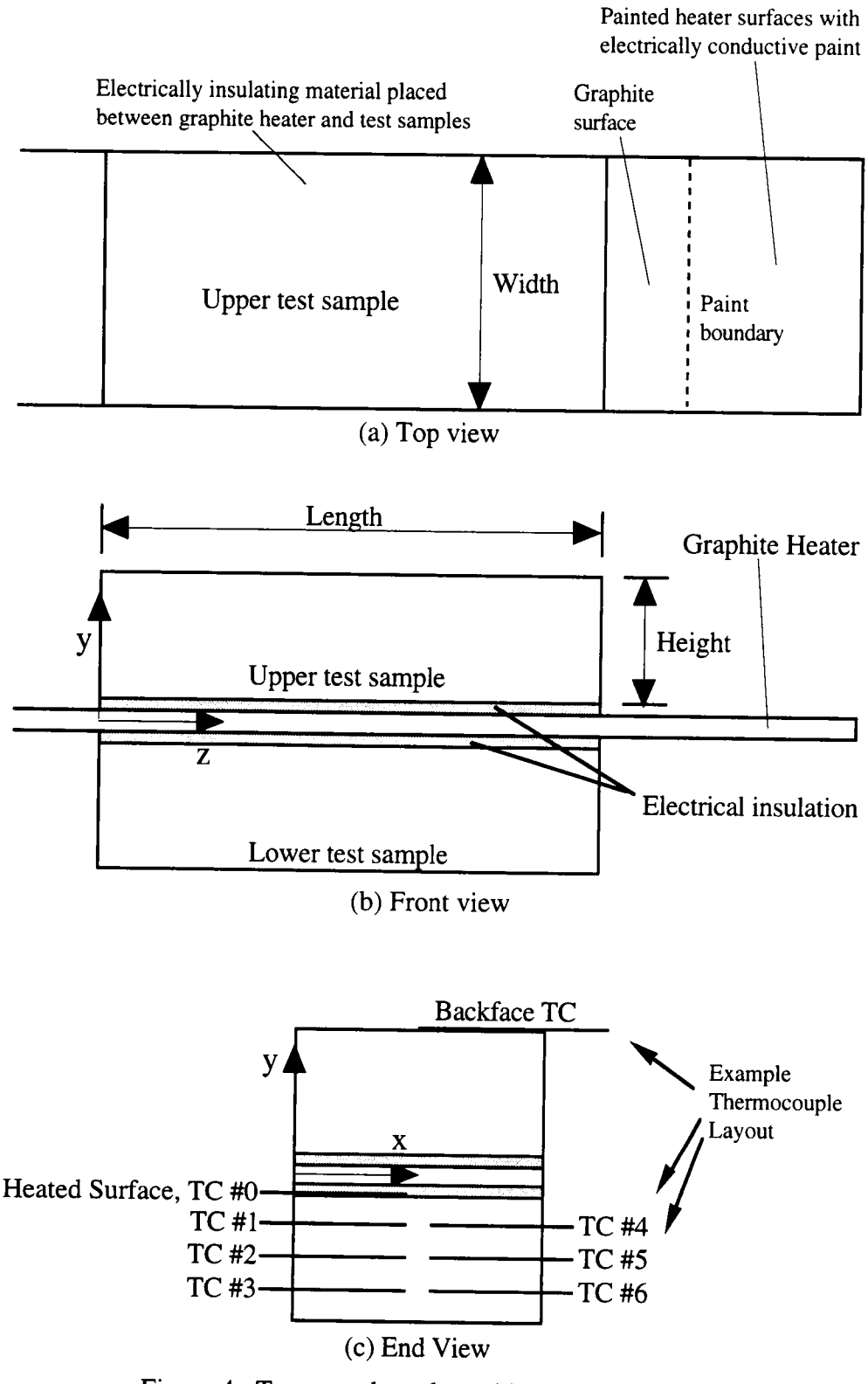


Figure 4 Test sample and graphite heater assembly

achieve a symmetrical heat flow from the upper and lower surfaces of the heater, two test samples of nearly equal dimensions were placed against the heater as shown in Fig. 4 (b). FM 5055 carbon-phenolic samples of nominal dimension 1 x 2 x 4 cm (H x W x L) were used as test samples. Electrical insulation was placed between the graphite heater and test samples to minimize any electrical current that may "leak" into the test samples from the graphite. Such current would create additional resistive, or Joulean, heating inside the test sample which would corrupt the heat flux boundary condition by an unquantifiable amount. The exposed surface areas of the heater between the test samples and copper bus bars were left bare for the local voltage probes.

Since the effectiveness of the electrical insulation is a function of temperature, it is desirous to determine when it breaks down and "leakage" occurs. Figure 5 shows a schematic of the "leakage" circuits used for such determination for both the bottom and top test samples. A Lambda regulated DC power supply was used to supply a low voltage across the electrical insulation. The electrical insulation, when in tact, easily stands off this voltage due to its high dielectric strength and renders the circuit effectively open. When the electrical insulation breaks down, a circuit is closed across the insulation over which the voltage can be measured. It is at this time that electrical "leakage" can occur to result in Joulean heating of the test samples. The voltage across the insulation was measured with respect to time by the Gould chart recorder showing approximately when the insulation became ineffective.

In-depth temperature measurements were made using Type K and Type J thermocouples. Holes of 0.75 mm diameter were drilled into one of the pair of test samples parallel to the plane of heat application from the front or back surfaces at half

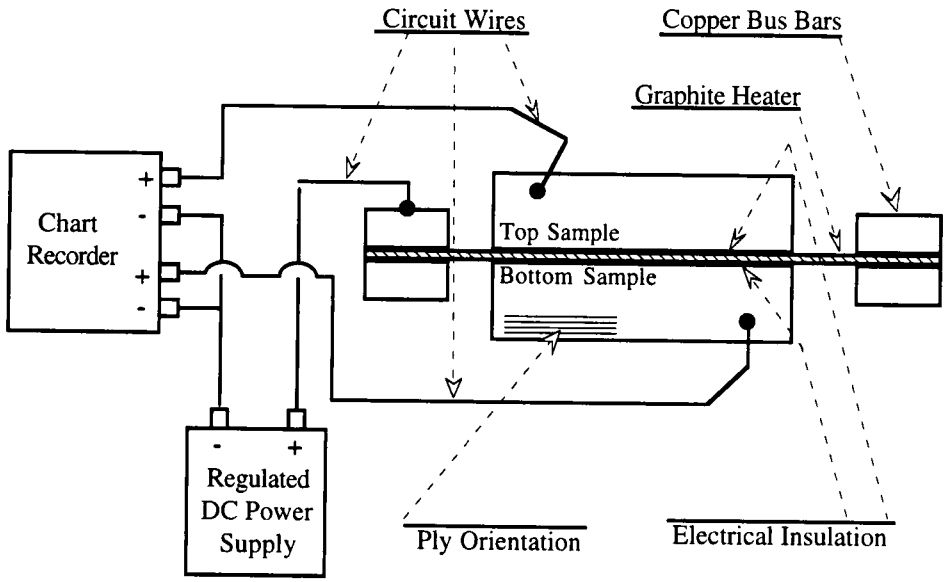


Figure 5 Schematic of electrical leakage detection circuit

span in the lengthwise direction to a depth of half span in the width direction. The orientation of these holes allowed the thermocouples to be placed in such a way as to inhibit axial conduction into or out of the instrumented thermocouple bead along the thermocouple's lead wires. The other test sample was left uninstrumented to facilitate an accurate mass loss measurement. One thermocouple was inserted and potted in each hole of the drilled sample. The locations of these holes were selected to minimize both multi-dimensional effects and heat transfer interference from other holes. A Type C thermocouple, arc-welded from 0.127 mm diameter wire was placed at the interface for some tests to measure a known temperature boundary condition for the heated surface. An example was shown in Fig. 4 (c). Type K and C thermocouples were arc-welded from 0.127 mm diameter wire. Type J thermocouples were arc-welded from 0.254 mm diameter wire. The Type K and Type J thermocouple beads and exposed wires were thinly coated with an electrically insulating thermocouple potting compound to prevent secondary junctions. After the coating had dried, the thermocouples were potted into the drilled holes with the compound.

The instrumented test samples were x-rayed and the in-depth thermocouple bead locations were measured on the x-rays with a dial caliper. The output of these thermocouples were measured by the Hewlett-Packard data acquisition system and stored by the computer. A Kaye ice point reference was run continuously before any experiments to attain an equilibrium reference for the thermocouples.

The dimensions of the test samples, and graphite heater were also measured with the dial caliper. The reported dimension measurement uncertainty of the test samples and graphite heater include the uncertainty of the dial caliper ($\pm$ 0.001 in) plus variations in

size due to manufacturing. The mass of test samples was measured with a triple beam balance. The reported mass uncertainty was that of the triple-beam balance (± 0.05 grams). The maximum reading uncertainties of the Type J, K, and C thermocouples were ± 6 °C (@750 °C), ±10 °C (@1250 °C), and ±28 °C (@2760 °C), respectively.

The 35 x 25 x 23 cm test enclosure was made from sheet metal with a Plexiglas front side and base. During the heating of the carbon-phenolic, the generated pyrolysis gases were removed and vented to the building exterior. Nitrogen was used to create an oxygen poor atmosphere inside the test enclosure and thus suppress ignition of the ambient gases around the test samples. The test stand, shown in Fig. 3, fit within the test enclosure and held the test sample/heater assembly, local voltage probes, copper bus bars, "leakage" probes, and nitrogen tubing. Clamps were used to hold the test samples against the heater. The Fluke AC clamp-on current probe was placed outside the test enclosure around the output power line of the transformers. All AC lines were routed through a different access port on the test enclosure than DC lines to minimize the parasitic noise effect from the high power AC lines on the measured DC wires.

2.1 Procedure

Prior to running each test, the test sample/heater assembly was carefully prepared and instrumented. The dimensions of the test samples and heater were measured with a dial caliper. The test samples were weighed with a triple-beam balance. Once the sample

was instrumented with the thermocouples it was weighed again. Then the test sample was x-rayed and the thermocouple bead locations were measured with the dial caliper.

The end portions of the graphite heater that contact the copper bus bars were painted with silver paint to enhance electrical conduction between the porous graphite and copper. The heater was then securely suspended between the bus bars, and two test samples, one on top and one on bottom, were pressed firmly to the heater by clamps as shown in Fig. 3. An electrically insulating ceramic was placed between the heater and each sample as shown in Fig. 5. The thickness of this insulation and the form or method of application depended on which insulation was used.

All the electrical units of the experimental setup were turned on thirty minutes or more before each experimental run to allow equipment warm-up. The regulated AC power supply was adjusted from experience, at about a 10:1 ratio, to provide the desired voltage across the heater. Just before each experimental run, the chart recorder was started recording. At operator command, a mark event button on the Gould chart recorder was manually pushed and the computer program which activates the power relay, initiating heating of the test samples, and collects the data was executed. At the end of the run, the timed thermocouple data was converted to temperature and saved with the current and voltage data to an output file. All runs were video taped for further review.

From 1000 to 3000 ^{o}C, the electrical resistivity of POCO graphite, the heater material, is 9400 $\mu\Omega$-mm $\pm$ 11%. The power supply and transformers provided a near constant power input over time. Preliminary testing of the local voltage and current across the heater at various power levels showed the voltage exhibited less variation in

magnitude over time. Statistically, voltage measurements exhibited standard deviations near 0.03 and variances near 0.001 while current measurements exhibited standard deviations near 0.12 and variances near 0.015. Therefore, the local voltage was assumed constant and was measured once by the Hewlett-Packard data acquisition system just before power was turned off, while the current was measured over the entire heating period. The changes in current would account for the changes in resistance of the POCO allowing a time-dependent expression for the heat flux into the samples to be measured. Once the power was turned off, the test samples were cooled in place and then weighed.

2.2 Brief Description of Numerical Predictions

Numerical predictions of the experiments performed for this project were done using PEACH, a transient two-dimensional code written by Polehn (Polehn, 1994). These predictions were done to provide a platform from which observations could be made concerning which material input properties require further refinement. Presented here are some details of Polehn's numerical modeling to clarify some of the discussion in this thesis.

The char density, ρ_c, and the virgin density, ρ_v, are considered to be accurately known. The local dry solid density at any instant of time, ρ_s, is defined as a combination of ρ_c and ρ_v as

$$\rho_s = \beta\rho_c + (1 - \beta)\rho_v \qquad (2)$$

where β is the DOC.

The carbon-phenolic is modeled as a combination of three different component materials (A, B, and C), each decomposing. Defining Γ as the resin fraction, or fraction of the material consisting of components A and B, the time rate of change (decomposition) of ρ_s is

$$\frac{\partial \rho_s}{\partial t} = \Gamma\left(\left(\frac{\partial \rho}{\partial t}\right)_A + \left(\frac{\partial \rho}{\partial t}\right)_B\right) + (1 - \Gamma)\left(\frac{\partial \rho}{\partial t}\right)_C . \tag{3}$$

The decomposition of the components are calculated from a modified form of the Arrhenius rate equation. The modified form of this equation is

$$\left(\frac{\partial \rho}{\partial t}\right)_i = -(K\rho_v)_i \left(\left(\frac{\rho - \rho_c}{\rho_v}\right)^{\varphi}\right)_i \exp\left(-\frac{E_i}{RT}\right) . \tag{4}$$

In Eq. 4, K_i represents the pre-exponential kinetic factor of the i-th component. This is the aspect of the kinetics model that is "tweaked" in this project to show how the predictions behave.

Two different types of boundary conditions were modeled for this project. Half of the resistive power dissipated in the graphite heater, the power going to one of the samples, was plotted from the current and voltage measurements as a function of time. This function was then approximated as a second order polynomial in time which was in turn divided by the area of the heated surface of the sample to provide a known time dependent heat flux boundary condition. The highest order polynomial that can be used

for input by PEACH is second order. The second type of boundary condition was a known time dependent surface temperature. The measured output trace from a thermocouple located at the heated surface of a test sample was divided into up to six consecutive curves in time, each of which was approximated by a second order polynomial. The interval lengths of these divisions were defined to provide good agreement between the measured and approximated surface temperatures. These divisions were done to provide, within the input limitations of the program, a more accurate approximation of the boundary condition for predictions .

Chapter 3

3.0 Experimental Results and Analysis

Eight experimental test runs were performed for this project. Each experimental run is presented individually. Tabulated results for these runs can be found in Tables A-1 through A-14 in Appendix A.

3.1 Run #1

The electrical insulation used for run #1 consisted of a 0.16 mm coating of Boron Nitride paint and a 0.02 mm layer of mica. Boron Nitride paint was used to coat the surface areas of the heater and test samples that would come in contact with each other. The use of this paint in previous experiments had been unsuccessful as a high temperature electrical insulator. Post-run observations of these insulations led to the supposition that carbon residue, or soot, was being outgased from the carbon-phenolic and deposited in the pores of the Boron Nitride, thus electrically bridging across the insulation the distance from the graphite heater to the sample [11]. The paint would be white before heating and dark gray afterwards. The thin sheet of mica, although it loses its electrical resistance at about 700 ^{o}C [10], much lower than temperatures experienced, was placed between the Boron Nitride coatings as an impermeable barrier to reduce this soot deposition.

This experimental run (run #1) attained a mean heat flux of 80.5 W/cm^2. The power as a function of time is shown in Fig. 6. Note that the measured heat flux is nearly

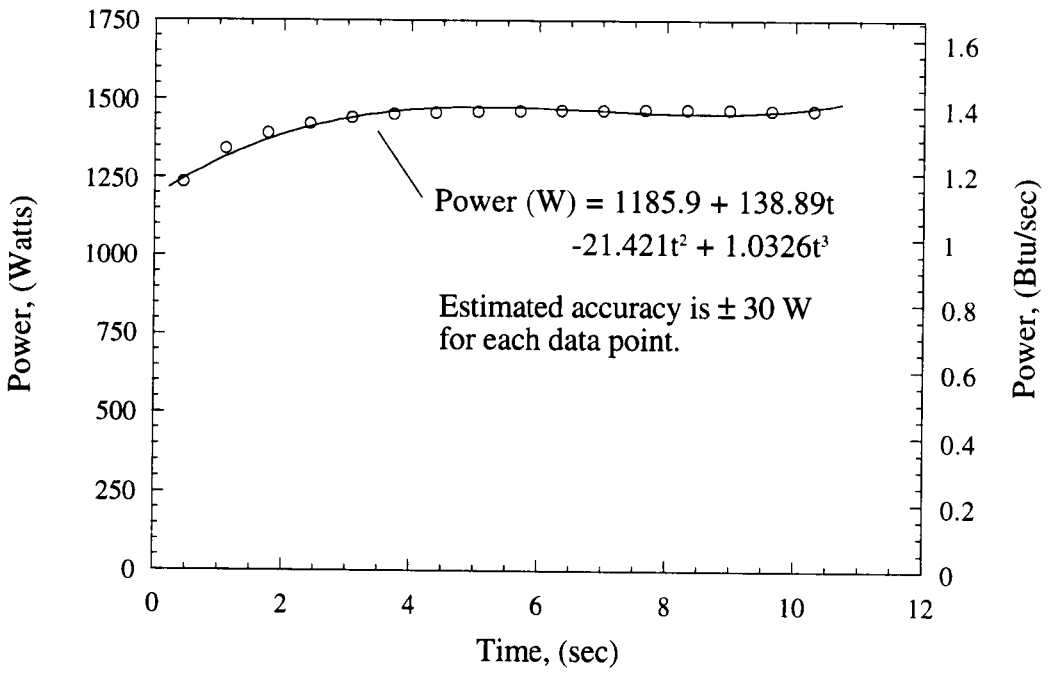


Figure 6 Calculated resistive power dissipation for run #1

constant after t = 3 sec. The estimates in uncertainty for the calculated power were obtained using the method of Kline and McClintock. The measured dimensions of the test samples and of the graphite heater between the local voltage probes for this and all following runs are given in Appendix A (Tables A-1,-2, and -3). The distances of the thermocouples from the heated surface of the test sample, as measured from the x-ray, are listed in Table 2. The thermocouples for this run (run #1) were potted using Sauereisen #10 electrically insulating cement, an Alumina-based cement.

Figure 7 shows the measured temperatures for run #1. At the start of the run the heater first glowed red at the center, then the glow quickly spread outward in both directions. Pyrolysis gas flow from the test assembly was very strong. During the last part of the run (best guess is about 6 seconds, based on review of the video tape), these gases ignited in a small fireball behind the test samples. This is believed to be due to the ventilation system of the test enclosure. The path of suction for the venting of gases from the enclosure was behind the test samples. Therefore, this area had the potential of being nitrogen poor and pyrolysis gas rich, allowing gaseous ignition. It was suggested that the venting rate be reduced in further runs to allow the nitrogen to remain in the test enclosure in higher concentrations. The back ground fireball likely did not corrupt the temperatures measured by the embedded thermocouples because of the high internal thermal resistance of the carbon-phenolic. At the conclusion of the experiment, it was noted that at the entry points for thermocouples, some of the Teflon insulation (melting temperature 310 ^{o}C) for the wires had burned off, but because the thermocouple traces shown in Fig. 7 do not appear to have been corrupted, the bare thermocouple wires likely did not touch.

Table 2 Thermocouple locations for run #1

Thermocouple	Distance from Heated Face (mm)
TC #1	1.7±0.08
TC #2	5.4±0.08
TC #3 (backface)	10.1±0.15

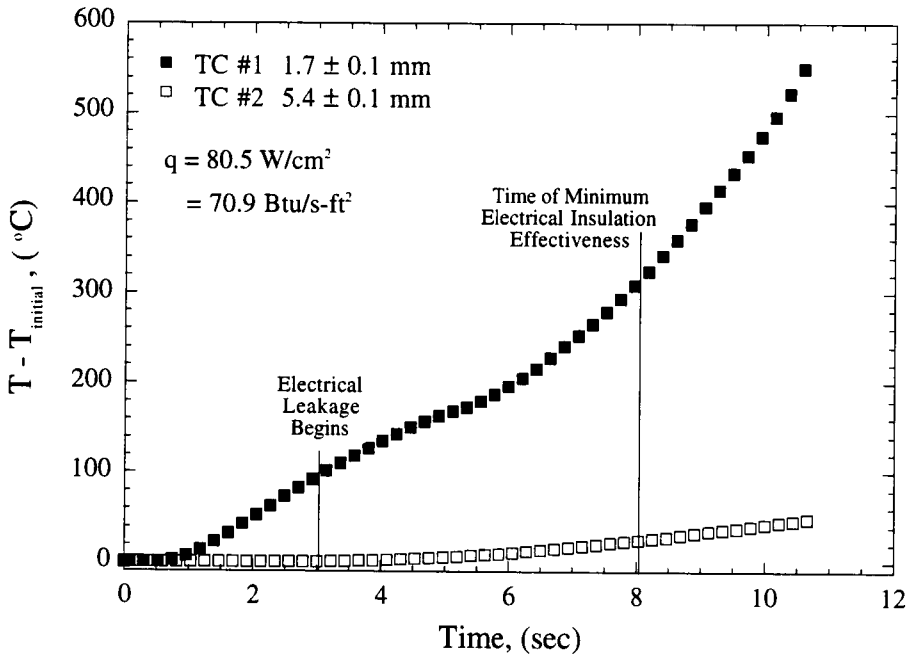


Figure 7 Measured temperatures for run #1

From the traces of the recorded DC voltage due to electrical "leakage," it was seen that the Boron Nitride coatings for the top and bottom test samples lost their electrically insulating effectiveness at nearly the same time. These voltages became non-zero at about three seconds after power-on indicating when the electrical insulation began to break down and the leakage circuits began to close. The maximum voltages, as set by the Lambda DC power supply, were achieved at about 8 seconds after power-on. It is at this time that the insulation lost all effectiveness, i.e. was no longer electrically resistive. A low electrical resistance for the Boron Nitride implies that some of the electrical energy traveling through the graphite heater might cross the insulation and travel through the sample as well, resulting in some volumetric (Joulean) heating within each test sample. Halfway between when the breakdown of the insulation begins and when it is rendered ineffective, near 5.5 seconds, Fig. 7 shows a noticeable upward trend in the measured temperature of TC #1, the thermocouple nearest the heated surface. This is similar to upward trends noted in similar heat flux tests performed by Polehn [11]. The timing of this trend lends credence to the supposition that Joulean heating is occurring.

The backface thermocouple trace and the two electrical "leakage" voltage traces from the Gould chart recorder showed small vibrations during the time the power was applied, as if there were small variations in the readings with time. Inspection of the traces showed that pen vibration started exactly as the power started, before the carbon-phenolic could decompose, and that the pen vibration stayed the same magnitude throughout the duration of the run. Subsequent tests showed these vibrations to be repeatable and revealed these variations to exhibit a 60 Hz frequency. Electrical interference from the high AC current in the power cable due to its close proximity to the wires is a possible explanation.

The Boron Nitride coatings were white before the run, but were a dark gray after. Only trace amounts of the mica remained. It was noted that the insulation did not regain its effectiveness upon cooling, so the temperature dependence of the dielectric strength of the Boron Nitride can not fully explain the experienced reduction in electrical resistance. Two explanations for this reduction seem possible. The pyrolysis gases may have penetrated the mica and deposited carbon in the pores of the Boron Nitride coating. As previously mentioned, once sufficient soot was deposited, carbon may have bridged the distance electrically from the graphite heater to the carbon-phenolic sample. Also, this soot could have originated from the heater itself, bridging the distance from the other direction. Another possibility is that the Boron Nitride underwent a chemical change (oxidation of Boron Nitride begins near 1000 ^{o}C). At the high temperatures experienced, a chemical reaction between the complex mixture of pyrolysis gases and the Boron Nitride paint is likely. Significant changes in the chemical composition of the material coating would result in changes in its electrically resistive properties. An x-ray diffraction was performed on a Boron Nitride coating after the run of a previous experiment at similar power levels and on an unheated Boron Nitride coating. Using the unheated coating as a control, no different chemical compositions were discernible in the heated Boron Nitride [11]. This suggests that a chemical reaction significantly changing the composition of the coating was unlikely.

Another explanation for the upward trend of the temperature history of TC #1 at t = 5.5 sec, as seen in Fig. 7, could be the difference in coefficients of thermal expansion between the test sample and the Sauereisen #10 cement used to install the thermocouples. At the high heating rate experienced at the surface, the different expansion rates of the two materials could cause reduced contact between them. This would result in the

appearance of a layer of air between the cement and the carbon-phenolic. The high thermal diffusivity of air at the resulting elevated temperatures, as compared to the cement and carbon-phenolic, would affect the thermocouple response by increasing the effective "thermal contact" with the host material. The presence of the air would improve the time response of the temperature probe. This is described in more detail in run #5. The increasing slope of the temperature measurement profile of TC #1 at 5.5 seconds, as seen in Fig. 7, is probably due to both the failure of the Boron Nitride coating allowing Joulean heating of the test sample, and the different thermal expansions of the potting compound and test sample temporally affecting the effective thermal contact resistance. A trend similar to that in the change of the slope of TC #1 was noted for the response of the thermocouples located close to the heated surface in all subsequent runs. A more in-depth explanation of the two possible solutions stated above is given in run #5.

Table 3 lists the mass loss of the uninstrumented test sample. Predictions were made using PEACH for two cases, the first using the original gas pyrolysis kinetics coefficients used in CMA90S [15] and the second using an arbitrary 50 times larger pre-exponential kinetic factor, (faster kinetics). In the latter predictions, the kinetics coefficients (pre-exponential factors K_i), were multiplied by 50 to try to better match the high heating rate. As can be seen from the table, the experimental measurement (0.3 grams) was matched very well by the prediction of the first case (0.291), but not by the second (0.846). The temperatures listed in this table are the predicted maximum temperatures found at the heated surface.

Figure 8 shows the temperature predictions for the two cases at the locations of TC's #1 and #2 with the measured data. The difference between the two cases in the

Table 3 Predicted and measured mass loss for run #1

Case	Heating (13.3 sec.)		Approximated Cool Down (15 min.)		Total Mass Loss
	Mass Loss (grams)	End Temp.[a] (^oC)	Mass Loss (grams)	End Temp.[a] (^oC)	(grams)
Orig. CMA Kinetics Coefficients	0.064	1396	0.227	91	0.291
50 times Larger Kinetics	0.379	1241	0.467	65	0.846
Measurement					0.3 ± 0.05

[a]Maximum predicted temperature in the sample (located at the heater surface) at end of time period.

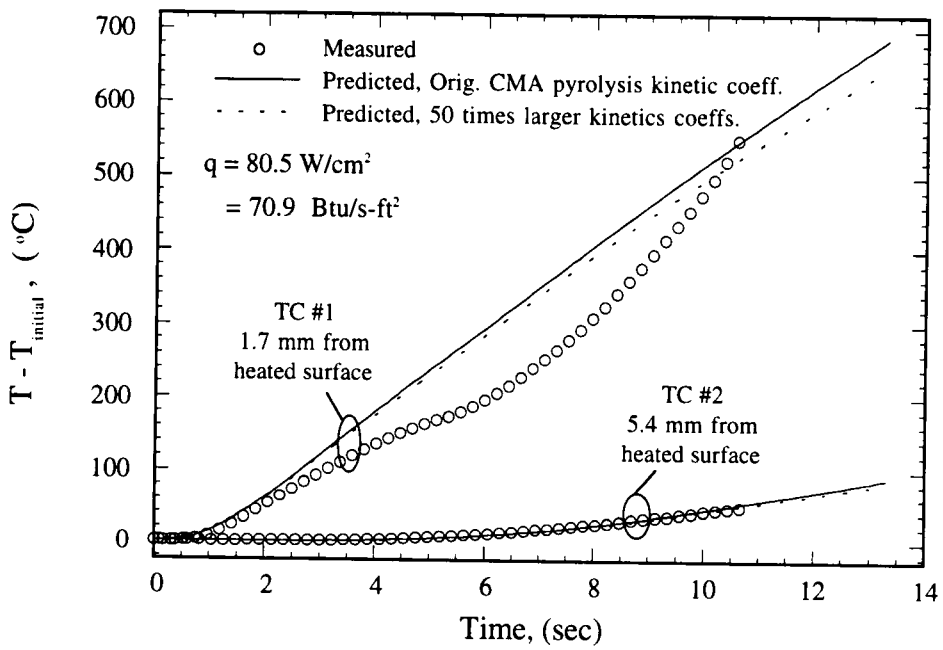


Figure 8 Comparison of run #1 in-depth temperatures with predictions

predicted temperature is slight compared to the large difference in predicted mass loss (degree of char). It would appear that the original CMA kinetics coefficients are more applicable to this type of experiment, but more tests at different heating rates should be performed to verify this. The pyrolysis process (changes in the DOC), modeled by Eq. 4, may affect the temperature prediction in two ways. One, since the process is endothermic, a finite amount of energy would be used to char the material; and two, since the thermophysical properties of the charred and virgin material are different, energy transfer through the sample would be governed by effective properties of a mixture of the two materials. The properties for the char and virgin materials are listed in Appendix B. Note that the listed data for the specific heat and thermal conductivity of the virgin material are not substantially different than those for the charred material. This would suggest that these properties have a low dependence on the degree of char and thus, the slight differences in the predicted temperatures of the two cases, along with the significant differences in the predicted mass loss, are not surprising.

Figure 8 shows that the TC #1 data is over predicted. Moreover, the prediction does not capture the curved trend of the measured data. The prediction of TC #2 is in good agreement with the measured data. Over the time of heating, the location of this measurement was subjected to a low heating rate. Possible explanations for the differences between the prediction and the measured thermocouple data will be discussed in run #5.

Figure 9 shows the predicted DOC as a function of depth from the heated surface at the end of heating (t = 13.3 sec) and after cooling (t = 913.3 sec). Predictions were made for both the case using the original CMA coefficients and that using 50 times larger

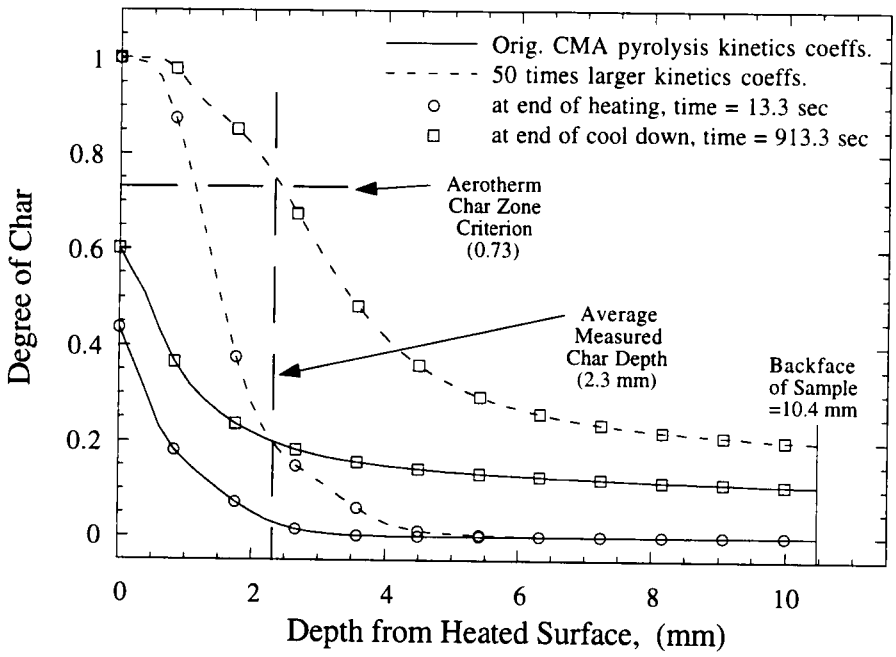


Figure 9 Predicted degree of char after 13.3 sec of heating and 15 minutes cooling for run #1

pre-exponential coefficients. The samples were sent to NASA Marshall Space Flight Center (MSFC) to have their degree of char measured. The "scratch" test at MSFC returned an average "char" depth for these samples of 2.3 mm. The Aerotherm criterion for predicted "char" depth is DOC = 0.73, which means the region where DOC $\geq$ 0.73 is considered to be charred. Table 4 lists the predicted "char" depth for both predicted cases based on the Aerotherm criterion. The prediction based on the 50 times larger kinetics coefficients (2.42 mm) is close to the measured value, while the prediction based on the original CMA coefficients of zero "char" depth is clearly unacceptable.

3.2 Run #2

In run #2 run, 2.5 mm thick Hot Pressed Boron Nitride plates, hereafter referred to as HPBN, were used for electrical insulation. The HPBN was chosen as the electrical insulator for its high thermal conductivity, high electrical resistivity, and refractory characteristics. The thermophysical of HPBN are listed in Table B-7 in Appendix B. A Type C thermocouple was placed at the HPBN-carbon-phenolic interface, the heated surface of the test sample, and was used to provide a known temperature boundary condition for numerical modeling. The mean heat flux was not found due to a failure in recording of the current measurements.

Six thermocouples were used in run #1; one Type C, three Type K, and two Type J. The distances of thermocouple beads from the heated surface of the test sample, as measured from the x-ray, are listed in Table 5. The thermocouples were potted using various compounds in an attempt to optimize thermal contact in the holes.

Table 4 Comparison of the predicted "char" depth with the "Scratch" Test for run #1

Time	Char Depth (mm)		
	Original CMA Kinetics Coefficients[1]	50 times Larger Kinetics Coefficients[1]	"Scratch" Test[2] (MSFC)
End of the Heating (t = 13.3 sec)	0	1.11	--
End of the Cool-down (t = 913.3 sec)	0	2.42	2.3

[1]Aerotherm char criterion of 0.73 is used to determine the predicted values.

[2]The listed value is the average of 4 experimental measurements made by MSFC.

Table 5 Thermocouple locations for run #2

Thermocouple (Type)	Distance from Heated Face (mm)
TC #0 (C)	Surface Boundary
TC #1 (K)	1.9±0.05
TC #2 (K)	2.9±0.05
TC #3 (K)	6.6±0.08
TC #4 (J)	8.0±0.05
TC #5 (J)	10.2±0.05

Thermocouples #1, 3, and 5 were potted with Aluminum Oxide (Alumina) paste while thermocouples #2 and 4 were potted with a mixture of Alumina paste and Boron Nitride paint. The HPBN plates were cut flush with the width and length dimensions of the samples and placed between the samples and the heater. Boron Nitride paint was used between the HPBN and heater, and the HPBN and samples to decrease thermal contact resistance. The Type C thermocouple used to record the heated surface temperature was placed in a shallow groove cut in the side of the HPBN plate adjacent to the instrumented sample. Boron Nitride paint was then used to seal the lead wires in the HPBN such that the bead was just exposed to contact the test sample.

Figure 10 shows the temperature measurements of thermocouples #0, 1, 2, and 3 for this run. As in the previous test, the heater began glowing red in the center at the start of this run, then the glow quickly spread outward in both directions. Pyrolysis gas flow from the samples was again very strong. Power input was stopped at about 9.8 seconds. During the last part of the run, the pyrolysis gases ignited in a small fireball around the test samples. At the conclusion of the experiment, it was noted, as in Run #1, that at the entry points for thermocouples #1, 2, and 3, some of the Teflon insulation for the wires had burned off. Again, the bare thermocouple wires likely did not touch. As previously stated, it is believed that because of the high internal thermal resistance of the carbon-phenolic, the fireball had little effect on the temperatures measured by the embedded thermocouples.

A two-color pyrometer was used to measure the maximum temperature experienced by the exposed side of the graphite heater in between the two samples. It recorded a maximum temperature of 1570 ^{o}C. This appears to be a reasonable

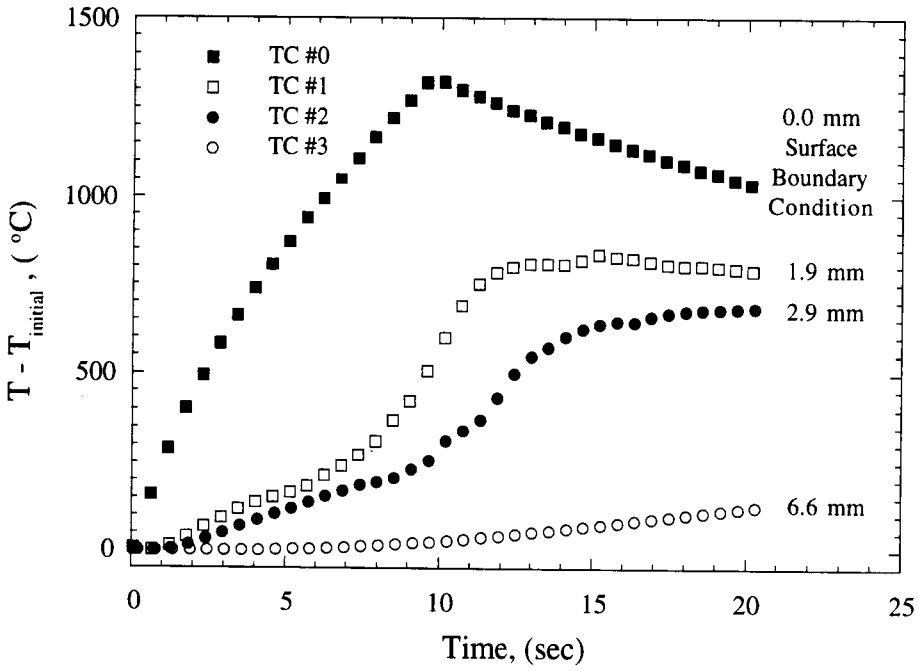


Figure 10 Measured thermocouple temperatures for run #2

temperature compared to the 1347 °C maximum temperature measured by the Type C thermocouple at a distance of 2.5 mm from the heater surface (the location of the heated sample surface). But, since the diameter of the target area of the pyrometer was larger than the thickness of the heater, and since the effects of the participating media in the path of the pyrometer's measurement (the Plexiglas front face of the enclosure and the unquantifiable amount of the unsteady escaping pyrolysis gases) could not be accurately evaluated, the measurements of the pyrometer were considered unreliable. Due to the failure in measuring the current data, the dissipated power was not known and the temperature on the heater surface could not be predicted for comparison.

The recorded traces of the electrical "leakage" showed that for the HPBN which was insulating the instrumented (bottom) sample, the voltage became non-zero at about t = 4 sec . The plate maintained its insulating effectiveness until about t = 8.5 sec, when the maximum voltage, as set by the Lambda DC power supply, was achieved. The measured voltage across the plate insulating the uninstrumented (top) sample became non-zero after about three seconds and the insulation lost its effectiveness after about 5.5 seconds. The HPBN plates were white before the experimental run. After firing, what appeared to be carbon was noted to have unevenly diffused a short distance into the plates, but the electrical resistance was in tact upon cooling. Therefore, the electrical insulation was not compromised by soot deposition electrically bridging the thickness of the HPBN. This fact seems to indicate that the temporary loss in insulating effectiveness was more likely due to the adverse temperature dependence of its dielectric strength. HPBN has a manufacturer's listed maximum use temperature in oxidizing and inert atmospheres of 850 °C and 3000 °C, respectively. Since current flow seeks the path of least resistance, it would seem likely that any errant current flow that may leave the graphite heater would

penetrated only a short distance into the HPBN plate, therefore not subjecting the test sample to Joulean heating.

Due to the high thermal conductivity of the HPBN in the plane parallel to the heater, any possible volumetric energy generation in the HPBN is assumed to have been distributed equally over the heated surface of the test sample, and thus is accounted for by the measured temperature boundary condition. However, if any volumetric heat generation occurs in the test sample, it would not be accurately accounted for by the measured boundary condition. Figure 10 shows that the surface temperature of the instrumented test sample is near 1150 ^{o}C when the HPBN loses its insulating effectiveness. This indicates that the HPBN had exceeded its maximum use temperature in an oxidizing atmosphere. Similar to Run #1, the upward change in the slope of the interior thermocouple closest to the heated surface (TC #1, 1.9 mm) began near the same time ($t > 7$ sec) the HPBN lost its insulating effectiveness. Thus the question of this change in slope of the thermocouple measurement being caused by Joulean heating due to the encroachment of electrical "leakage" into the sample can not yet be resolved.

As in run #1, the traces of the two Type J thermocouples and the two electrical "leakage" circuits from the Gould chart recorder exhibited 60 Hz noise during the time the power was applied. For this run, all DC voltage lines were routed through a different port in the test enclosure than the AC lines. These fluctuations were attributed to the same reasons given for Run #1.

Thermocouples #4 and 5 were continuously recorded using the Gould chart recorder. Post firing observations showed that at the entry points for these

thermocouples, the wires had become loose in their holes. It is unclear whether they were loosened during the firing, or during inadvertent twisting or bending of the wires when the sample assembly was either placed in the test stand before, or removed after firing. The loosening of the thermocouple wire, coupled with their large diameters relative to the diameter of the holes, suggest the presence of secondary junctions. The chart recorder trace of thermocouple #4 shows unexpected fluctuations during t = 7 to 9.5 sec of the heating period. Two explanations are possible, the first being secondary junctions as discussed, and the second being poor and inconsistent thermal contact around the bead due to insufficient potting material securing the thermocouple in-depth in the hole. Because of the uncertainty in the installation of the Type J thermocouples, TC's #4 and 5 are not included here as part of the thermal response database for this run.

Table 6 lists the mass loss of the uninstrumented test sample. Predictions were made for two cases. The first prediction was made using the original CMA pyrolysis kinetics coefficients as supplied by Aerotherm, and the second prediction using a set of arbitrary 50 times larger kinetics coefficients. As can be seen from the table, the experimental measurement of the mass loss (0.7 grams) was matched fairly well by the prediction based on the larger kinetics coefficients (0.857 grams), while it was substantially under-predicted based on the original kinetics. The temperatures listed in Table 6 for the first two time periods (Heating and Measured Cool-down) are the measured heated surface temperatures at the end of these times. The temperature listed for the last time period is the predicted temperature for the heated surface at the end of this time. After the measured cool-down period, an adiabatic surface boundary condition was imposed in the numerical model.

Table 6 Predicted and measured mass loss for run #2

Case	Heating (9.8 sec.)		Measured Cool-down (10.6 sec.)		Approximated Cool Down (15 min.)		Total Mass Loss
	Mass Loss (grams)	End Temp.[a] (°C)	Mass Loss (grams)	End Temp.[a] (°C)	Mass Loss (grams)	End Temp.[b] (°C)	(grams)
Orig. CMA Kinetics Coefficients	0.039	1347	0.078	1048	0.173	85	0.290
50 times Larger Kinetics	0.220	1347	0.248	1048	0.389	60	0.857
Measurement							0.7 ± 0.05

[a]Measured temperature at end of time period by thermocouple #0 at heated surface.

[b]Maximum predicted temperature in the sample (located at the heater surface) at end of time period.

Figure 11 compares the temperature predictions for the two cases at the locations of thermocouples #1, 2, and 3 with the measured data. Similar to run #1, the difference between the two cases in the predicted temperature is slight compared to the large difference in predicted mass loss (DOC). As in run #1, the prediction for the location subjected to a low heating rate, in this case TC #3, is in very good agreement with the data, while the relatively higher heating rate locations, in this case TC #1 and 2, are under-predicted for $t > 9.5$ sec.

The predicted DOC as a function of depth from the heated surface is shown in Fig. 12. Predictions for both cases, that using the CMA kinetics coefficients and that using ones 50 times larger were made. From visual observations of the samples for both runs #1 and 2, the sample of run #2 appeared to be more "charred" than that of run #1, and therefore would appear to be better predicted by the case with 50 times larger kinetics coefficients. "Scratch" test measurements performed by MSFC and presented in Fig. 12 show that indeed the sample of run #2 had a larger average "char" depth (2.9 mm) than that of run #1 (2.3 mm). Table 7 shows that the case using 50 times larger kinetics coefficients predicts a "char" depth of 3.22 mm, while, as in run #1, the original CMA kinetics predicts a clearly unacceptable zero "char" depth. It appears that the prediction made with the 50 times larger kinetics coefficients results in a rather accurate mass loss for run #2 while the prediction made with the original CMA kinetics appears to be more accurate in the predicting of the mass loss of run #1. But the 50 times larger kinetics coefficients provides a good prediction of the "char" depth of both runs #1 and 2, while the predictions using original CMA kinetics are clearly inaccurate (zero "char" depth). As can be seen from Figs. 8 and 11, the temperature has little dependence on the gas pyrolysis kinetic coefficients for either run.

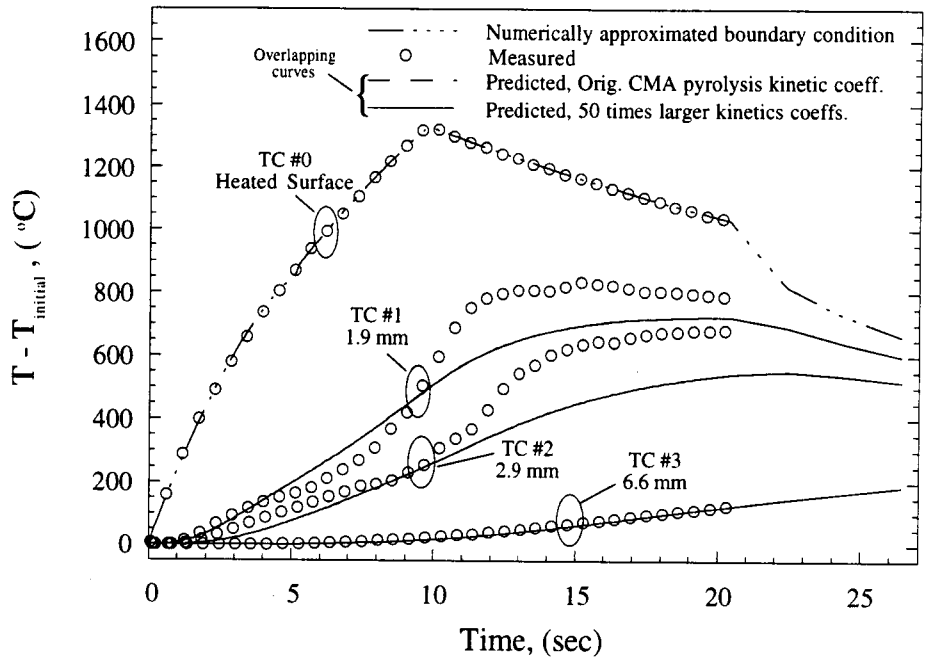


Figure 11 Comparison of run #2 in-depth temperatures with prediction

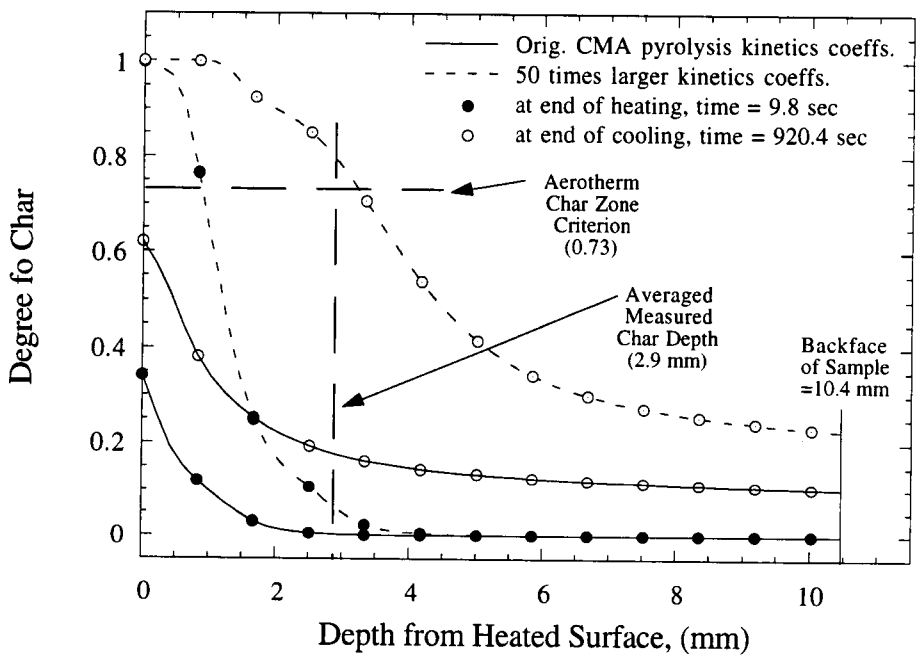


Figure 12 Predicted degree of char after 9.8 sec of heating and near 15 minutes cooling for run #2

Table 7 Comparison of the predicted "char" depth with the "Scratch" Test for run #2

Time	Char Depth (mm)		
	Original CMA Kinetics Coefficients[1]	50 times Larger Kinetics Coefficients[1]	"Scratch" Test[2] (MSFC)
End of the Heating (t = 9.8 sec)	0	0.88	--
End of the Cool-down (t = 900 sec)	0	3.22	2.9

[1] Aerotherm char criterion of 0.73 is used to determine the predicted values.
[2] The listed value is the average of 4 experimental measurements made by MSFC.

It is interesting to note that although the numerical boundary condition for the predictions of run #1 and 2 are different, the predicted mass losses for these runs are nearly the same with respect to the set of kinetics coefficients used. However, the measured mass loss for run #2 (0.70 grams) is substantially higher than that of run #1 (0.30 grams). While for Run #1 the original kinetics coefficients seemed to better predict the measured mass loss, the case using 50 times larger kinetics coefficients appears to better predict the mass loss for Run #2. The mass loss can be directly related to the DOC profile across the sample. In the design of a SRM, it is important that the "char" depth in the carbon-phenolic liner material of the nozzle at the end of firing is accurately predicted. Recall that the predicted "char" depth is defined as the region in the material with DOC ≥ 0.73 (Aerotherm criterion). To predict this "char" depth accurately, a good model for the kinetics of the pyrolysis process is needed. Thermogravimetric analysis (TGA) of the material is used to develop the kinetics models, but this type of analysis on phenolic resin based composites is highly sensitive to heating rate [17]. Stokes [17], at the high heat rate TGA facility at Southern Research Institute (SoRI) has obtain TGA data at heating rates ranging from 0.05 to 50 ^{o}C/sec. This data was used in the CMA three-reaction kinetics model with constant coefficients (Eq. 4) which Polehn utilized in PEACH [11]. This model used a single set of constant coefficients to represent all heating rates over this range. Clayton [2] has shown that such a model is unsuited for modeling the pyrolysis process over a range of heating rates and suggests that a five reaction model would be better in handling heating rates over a range of values But again, the range used by Clayton is very low (0.05 to 50 ^{o}C/sec) to be extrapolated into actual flight condition heating rates. In this present study, the three-reaction kinetics model over-predicts the mass loss at low heating rates (too fast kinetics) and under-

predicts the mass loss at high heating rates (too slow kinetics). Thus, the accuracy of the predicted mass loss and DOC of the experimental data is highly suspect.

The heating rate of the thermocouples in run #2 are presented in Fig. 13. These were found by numerical differentiation of the discrete measured data and are considered to only show the general magnitude and trend of the heating rates at different locations. Note that our test facility was able to heat the surface of the test sample at an initial heating rate of near 250 ^{o}C/sec. Thermocouples #1, located at 1.9 mm from the heated surface, experienced heating rates as high as 170 ^{o}C/sec near t = 10 sec; and TC #2, located at 2.9 mm from the heated surface, experienced heating rates as high as 110 ^{o}C/sec near t = 12 sec. Recall that 50 ^{o}C/sec is the highest heating rate at which TGA data has been obtained for the pyrolysis kinetics model.

Figure 14 compares selected thermocouple data of runs #1 and 2 that are at similar distances from the heated surface. Since the measured temperatures of the run #2 thermocouples which were located further from the heated surface than the run #1 thermocouples (1.9 mm vs. 1.7 mm and 6.6 mm vs. 5.4 mm) are nearly the same as the run #1 values, it may be concluded that the heating rate for run #2 was slightly higher than that for run #1. If Joulean heating did occur in the samples due to electrical leakage across the electrical insulations placed between the samples and respective heater, the differences in the insulations (0.159 mm of BN paint for run #1 as opposed to a 2.5 mm HPBN plate for run #2) would have created different effects of the Joulean heating on the measured temperatures. Note the similarity in the trend of the change in the slope of the measured temperature data for the two thermocouples located at 1.7 mm (run #1) and 1.9

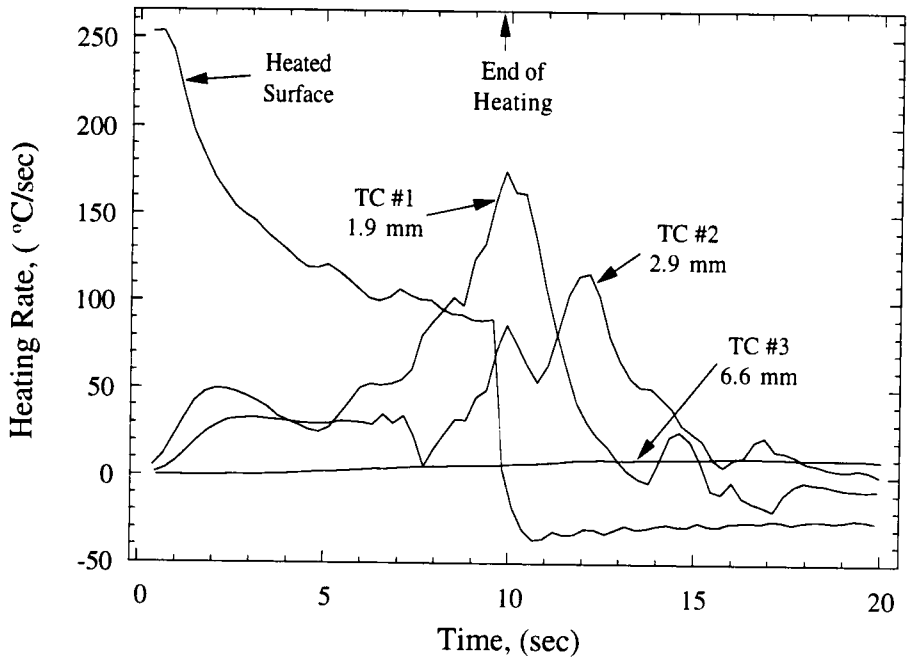


Figure 13 Time history of heating rates of run #2 thermocouples

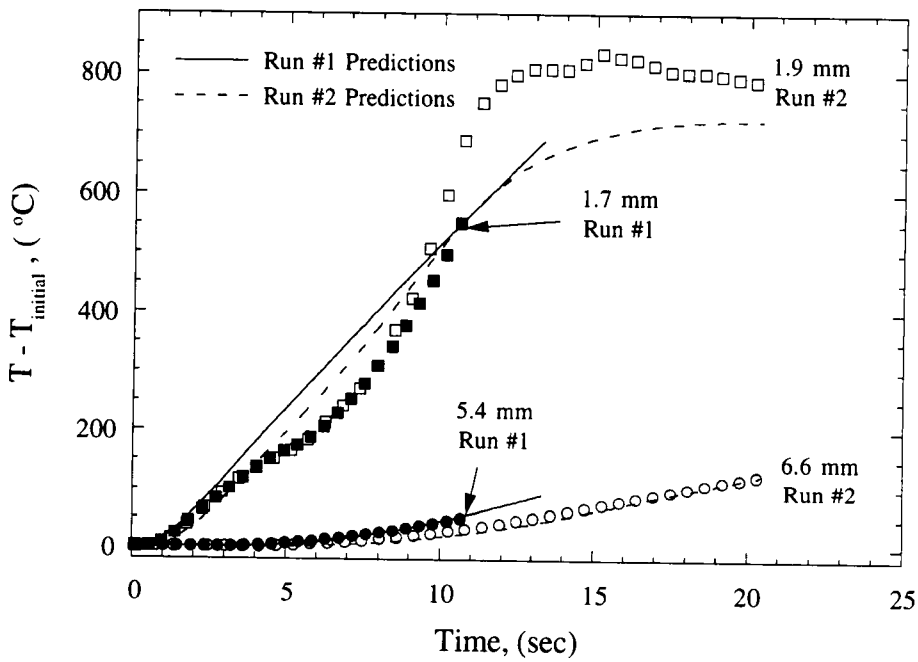


Figure 14 Comparison of measured temperatures for runs #1 and 2

mm (run #2) from the heated surface. This similarity supports the theory that the trend in the change in slope is not due to Joulean heating.

For t < 10 sec, the prediction of TC #1 of run #2 (1.9 mm) and its measured output are in better agreement than the prediction of TC #1 of run #1 (1.7 mm) and its measured output. This suggests that: (1) the measured heat flux boundary condition used for predictions of run #1 is higher than the experimental condition it represents, and that boundary conditions obtained by the same method are unreliable; and (2) the measured surface temperature boundary condition is more realistic.

3.3 Run #3

In this and all subsequent runs, 2.5 mm thick HPBN plates were used for electrical insulation between the samples and heater and a Type C thermocouple was placed at the HPBN-sample interface, the heated surface of the test sample, to provide a known temperature boundary condition for numerical modeling. The mean heat flux also was not found since, from the discussion of Fig. 14, its use as a boundary condition modeling the actual experiment conditions was considered less realistic than that of the measured heated surface temperature. To provide a comparison between different runs, the heat flux at the end of the heating periods of each run except run #2 was calculated and listed in Appendix A, Table A-4. For run #3, this heat flux was found to be 83 ± 6 W/cm^2.

Seven thermocouples were used in this run; one Type C, and six Type K. The distances of thermocouple beads from the heated surface of the test sample, as measured from the x-ray, are listed in Table 8. The thermocouples were potted using two compounds. Thermocouples #1, 3, and 5 were potted with RS-1000, an Alumina-based cement while thermocouples #2 ,4 and 6 were potted with Boron Nitride paint.

Figure 15 shows the temperature measurements of two pairs of thermocouples (#3 and 4 , and #5 and 6) for this run, each pair at a representative depth from the heated surface. Output from thermocouples #3 and 6 (5.0 mm and 8.3 mm from the heated surface) can be seen to be corrupted for time $t > 23.5$ sec. Post run observations revealed that these two thermocouples had become loose in their holes during execution of the test allowing for possible secondary junctions along their lead wires. Thermocouples #4 and 5 (5.1 mm and 7.2 mm from the heated surface) remained secure in their respective holes throughout the firing and exhibited plausible output traces over the entire heating range. Since the two sets of measured output from thermocouples #3 and 6 are suspect and not representative of the temperatures in the sample over the entire heating range at their respective depths from the heated surface, they are not included here as part of the thermal response database for this run.

The temperature measurements of thermocouples #0, 1, 2, 4, and 5 (the heated surface, 2.1 mm, 2.6 mm, 5.1 mm, and 7.2 mm, respectively), the thermocouples considered to have made reliable measurements, are shown in Fig. 16. As in previous tests, the heater began glowing red in the center at the start of this run, then the glowing quickly spread outward in both directions, and pyrolysis gas flow from the samples was very strong. The rate of Nitrogen addition to the test enclosure was increased for this run

Table 8 Thermocouple locations for run #3

Thermocouple	Distance from Heated Face (mm)	Potting Compound
TC #0 (C)	Surface Boundary	BN paint
TC #1 (K)	2.1±0.05	RS-1000[a]
TC #2 (K)	2.6±0.05	BN paint
TC #3 (K)	5.0±0.05	RS-1000[a]
TC #4 (K)	5.1±0.05	BN paint
TC #5 (K)	7.2±0.05	RS-1000[a]
TC #6 (K)	8.3±0.05	BN paint

[a]RS-1000 is an Alumina-based cement.

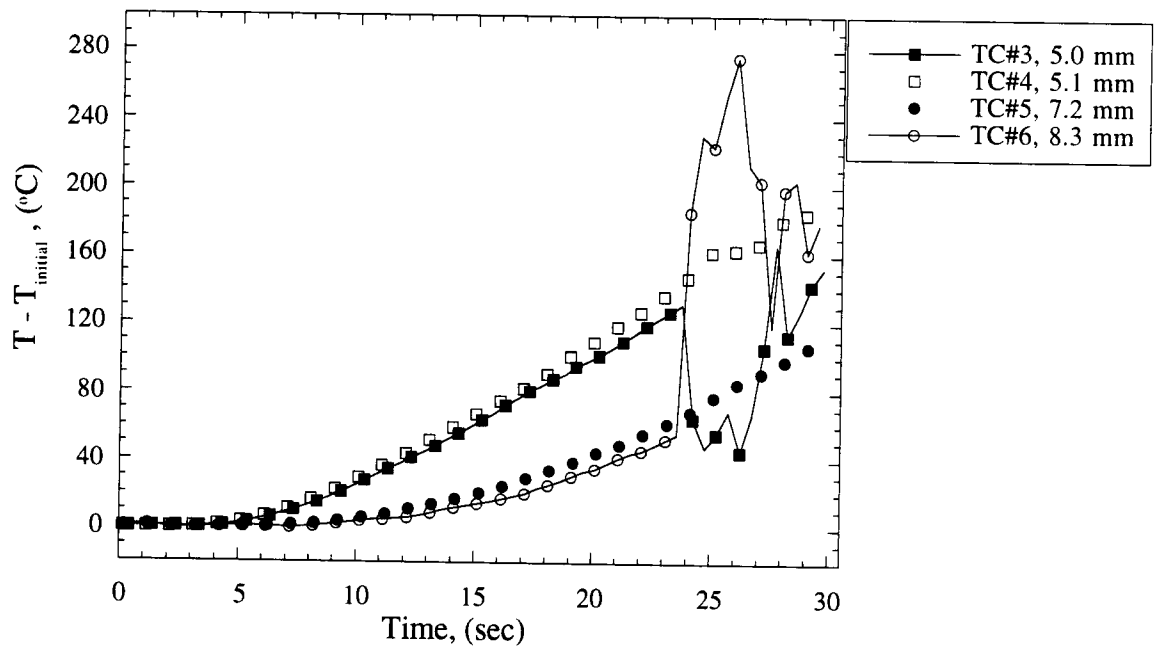


Figure 15 Comparison of measured thermocouple temperatures for selected thermocouples for run #3

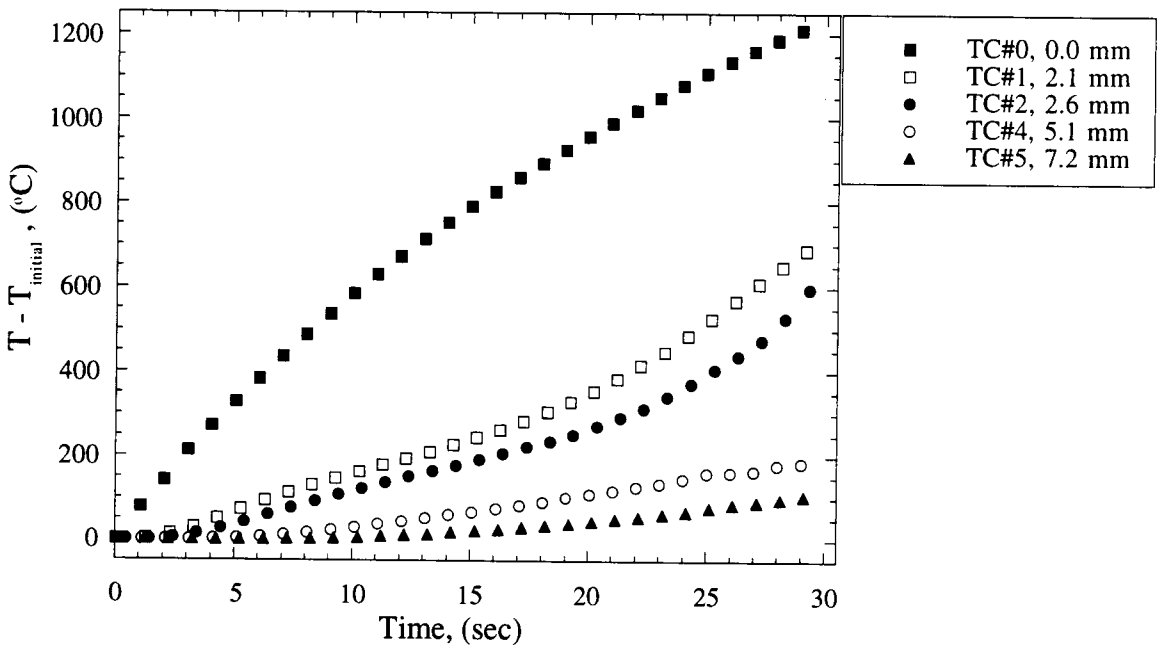


Figure 16 Measured thermocouple temperatures for run #3

and no ignition of the pyrolysis gases was observed. Thermocouple measurements were recorded until t = 29.9 sec and power input was stopped near t = 32.3 sec. At the conclusion of the experiment, as in previous and all subsequent runs, it was noted that at the entry points for Type K thermocouples some of the Teflon insulation for the wires had burned off. For the bared lead wires of the thermocouples that remained secure in their respective holes, it is believed that secondary junctions likely did not occur.

The recorded traces of the electrical "leakage" showed that for the HPBN which was insulating the instrumented (bottom) sample, the voltage became non-zero near t = 12.5 sec. The plate maintained its insulating effectiveness until about t = 18 sec, when the maximum voltage, as set by the Lambda DC power supply, was achieved. The measured voltage across the plate insulating the uninstrumented (top) sample became non-zero near t = 13.5 sec and it lost its effectiveness after about t = 19.5 seconds. The HPBN plates were white before the experimental run. After firing, similar to run #2, what appeared to be carbon was noted to have unevenly diffused a short distance into the plates, but the electrical resistance of the insulation was in tact upon cooling. It is interesting to note that, as in previous runs, the measured surface temperature of the instrumented test sample at the time insulating effectiveness was lost was near the maximum use temperature of HPBN in oxidizing conditions (850 ^{o}C), and that the upward trend in the slope of the response of the in-depth thermocouples near the heated surface (TC's #1&2, 2.1 & 2.6 mm) occurred after this insulation breakdown.

As in runs #1 and 2, the traces of the two electrical "leakage" circuits from the Gould chart recorder exhibited the 60 Hz noise during the time the power was applied. These fluctuations were again attributed to the same reasons given in Run #1. Since the

amplitude of the trace of this noise was small compared to the amplitude of the voltage output trace, and since only the temporal trend of the "leakage" rather than an exact value of the "leakage" voltage is needed to determine insulation effectiveness, the noise was disregarded in subsequent tests. The noise was present for all eight tests performed in this project.

Table 9 lists the mass loss of the uninstrumented test sample. A prediction was made using original CMA pyrolysis kinetics coefficients as supplied by Aerotherm. As can be seen from the table, the experimental measurement of the mass loss (1.1 grams) was substantially under-predicted based on these original kinetics (0.326 grams). The prediction using a set of arbitrary 50 times larger kinetics coefficients was not performed for this run. Using this set of arbitrary coefficients in performing additional predictions of runs #1 and 2 was useful in that it illuminated shortcomings in the kinetics model of the pyrolysis process used by PEACH and suggested an area for inspection for possible correction. While the original CMA kinetics coefficients were found through thermogravimetric analysis of carbon-phenolics, there is no rigorous experimental evidence to justify the use of a set of 50 times larger kinetics coefficients. What is suggested here is that the three reaction (three component) model of the pyrolysis kinetics process be either reformulated for high heating rate conditions or even replaced by a new model better suited for a range of these conditions such as an extension of the model proposed by Clayton [2].

The temperature listed in Table 9 for the first time period (heating) is the measured heated surface temperature of the test sample at the end of power input. After the measured heating period, an adiabatic surface boundary condition was imposed in the

Table 9 Predicted and measured mass loss for run #3

Case	Heating (32.3 sec.)		Approximated Cool Down (15 min.)		Total Mass Loss
	Mass Loss (grams)	End Temp.[a] (°C)	Mass Loss (grams)	End Temp.[b] (°C)	(grams)
Orig. CMA Kinetics Coefficients	0.119	1274	0.207	95	0.326
Measurement					1.1 ± 0.05

[a]Measured temperature at end of time period by thermocouple #0 at heated surface.
[b]Maximum predicted temperature in the sample (located at the heater surface) at end of time period.

numerical model. The temperature listed for the last time period (cool down) is the predicted temperature for the heated surface at the end of this time using the adiabatic surface boundary condition.

Figure 17 compares the temperature predictions based on the original CMA kinetics coefficients at the locations of thermocouples #1, 2, 4, and 5 with the measured data. As seen in previous runs, the predictions for the locations subjected to a low heating rate, in this case TC's #4 and 5, are in very good agreement with the data, while the predictions of the relatively higher heating rate locations follow a now familiar trend. As was similarly shown in Fig. 14 for the thermocouples located at 1.7 mm (run #1) and 1.9 mm (run #2) from the heated surface, the predictions of the temperatures at the relatively high heating rate locations (2.1 and 2.6 mm), shown in Fig. 17, seem to follow three consecutive patterns: (1) they are initially in good agreement with the measured data, in this case for $t <$ near 7 sec; (2) then they tend to over predict the measured data for a finite time, in this case near 7 sec to near 27 sec; and (3) they under-predict the measured data, in this case for $t >$ near 27 sec. For the prediction at the location subjected to the relatively low heating rate (7.2 mm) it appears, as mentioned earlier, that the numerical model has a canceling of errors that allows for accurate predictions. Eventhough predictions and measurements of temperatures close to the heated surface are in disagreement, the numerical model accounts for the delivery of the correct amount of energy through this region of the test sample to accurately predict the measured temperature at the further in-depth location subjected to a relatively low heating rate.

The predicted DOC as a function of depth from the heated surface is shown in Fig. 18. The Prediction shown is based on the original CMA kinetics coefficients. From

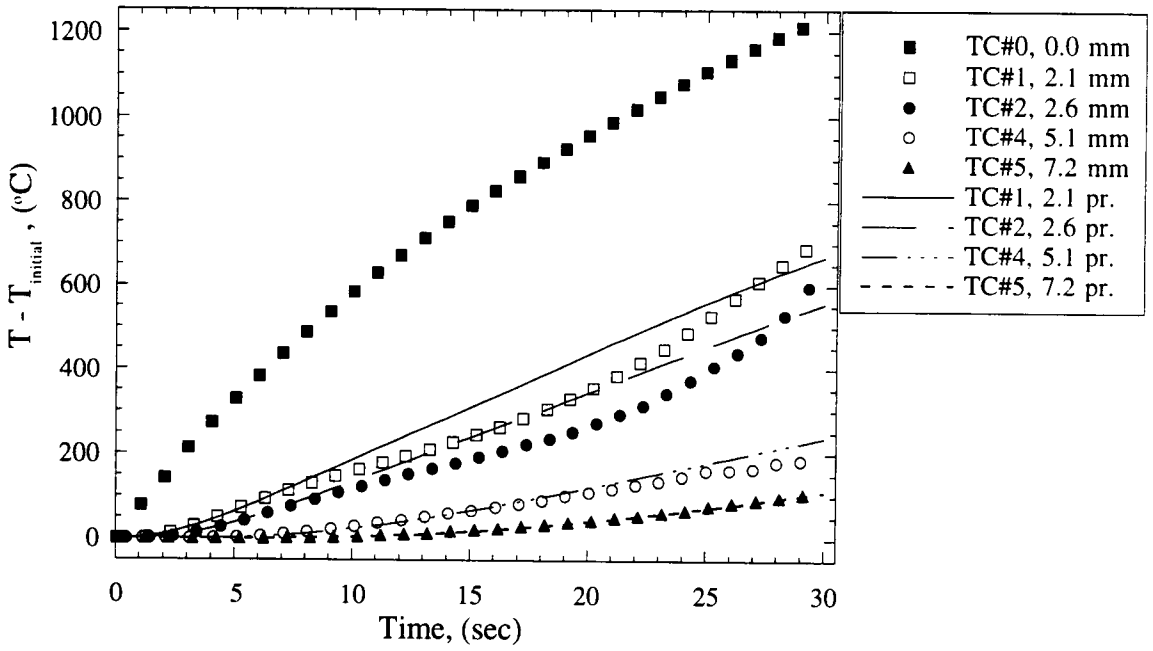


Figure 17 Comparison of run #3 in-depth temperatures with prediction

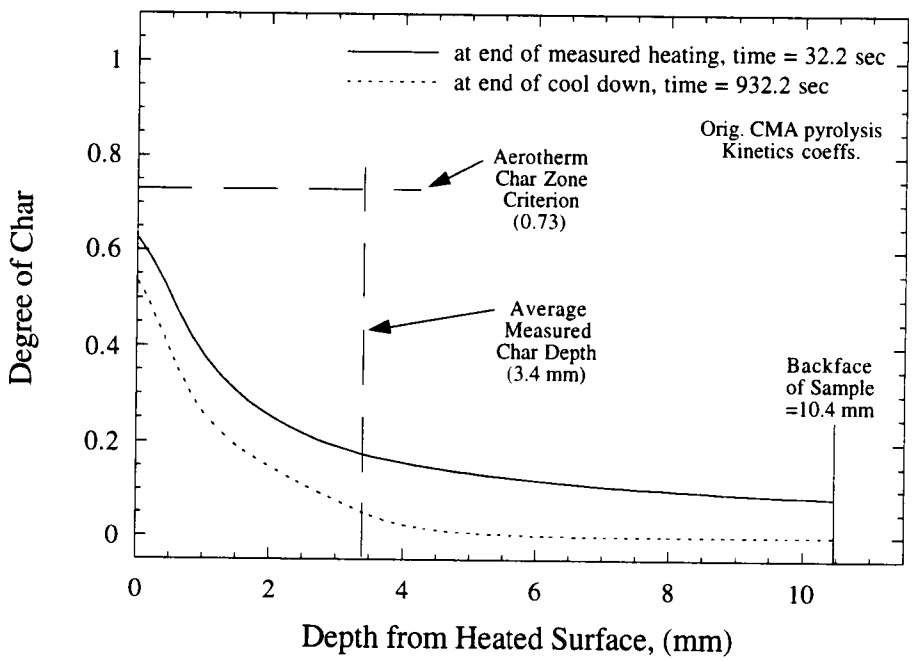


Figure 18 Predicted degree of char after 32.3 sec of heating and 15 minutes cooling for run #3

visual observations of the samples for runs #1, 2, and 3, the sample of run #3 appeared to be the most "charred." The time of heating for run #3 was nearly three times as long as those for runs #1 and 2. "Scratch" test measurements performed by MSFC and presented in Table 10 show that indeed the sample of run #3 had a larger average "char" depth of 3.4 mm versus 2.3 mm for run #1 and 2.9 mm for run #2. The predicted "char" depth of run #3 based on the original CMA kinetics coefficients is, as was the case for both runs #1 and 2, a clearly unacceptable zero "char" depth.

The heating rate of the thermocouples in run #3 are presented in Fig. 19. Recall, these were found by numerical differentiation of the discrete measured data and are considered to only show the general magnitude and trend of the heating rates at different locations. For this run, our test facility heated the surface of the test sample at an initial heating rate of near 80 ^{o}C/sec, only 30 ^{o}C/sec over the maximum of 50 ^{o}C/sec for the range of heating rates over which TGA data has been obtained for the pyrolysis kinetics model, yet the numerical model substantially under-predicted the mass loss and DOC for this run.

3.4 Run #4

Seven thermocouples were used in this run; one Type C, and six Type K. The distances of thermocouple beads from the heated surface of the test sample, as measured from the x-ray, are listed in Table 11. The thermocouples were potted using various compounds in an attempt to find which gave optimum thermal contact in the holes. Thermocouples #1, 4, and 5 were potted with Alumina paste while thermocouples #2 ,3

Table 10 Comparison of the predicted "char" depth with the "Scratch" Test for run #3

Time	"Char" Depth (mm)	
	Original CMA Kinetics Coefficients[1]	"Scratch" Test[2] (MSFC)
End of the Heating (t = 32.3 sec)	0.0	--
End of the Cool-down (t = 900 sec)	0.0	3.4

[1] Aerotherm char criterion of 0.73 is used to determine the predicted values.
[2] The listed value is the average of 4 experimental measurements made by MSFC.

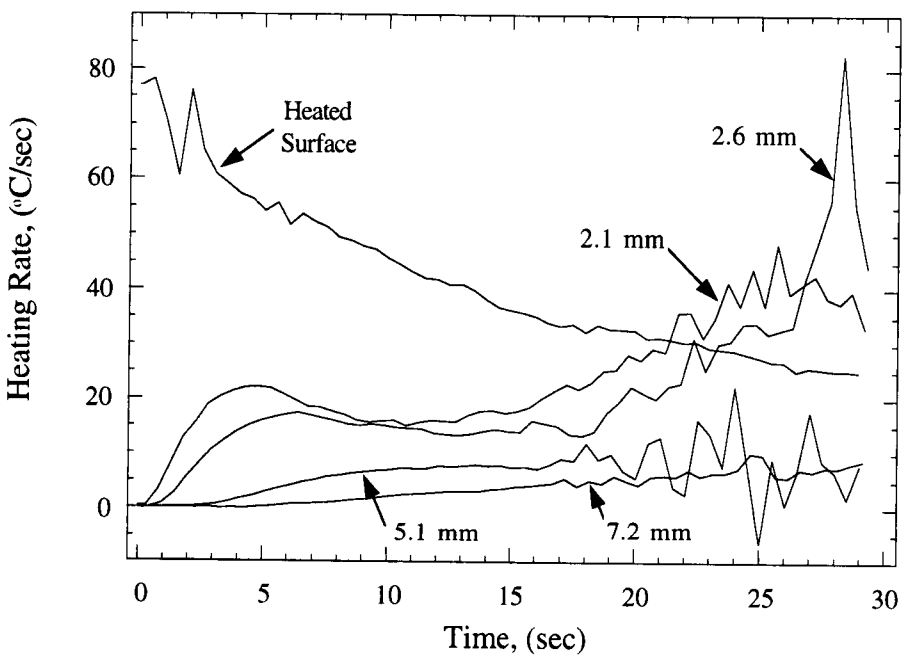


Figure 19 Time history of heating rates of run #3 thermocouples

Table 11 Thermocouple locations for run #4

Thermocouple	Distance from Heated Face (mm)	Potting Compound
TC #0	Surface Boundary	BN paint
TC #1	2.8±0.05	Alumina paste
TC #2	2.8±0.05	RS-1000[a]
TC #3	5.2±0.05	RS-1000[a]
TC #4	5.5±0.05	Alumina paste
TC #5	7.9±0.05	Alumina paste
TC #6	8.0±0.05	RS-1000[a]

[a]RS-1000 is am Alumina-based cement.

and 6 were potted with RS-1000, an Alumina-based cement. Heating was applied to the samples for 46.7 seconds. The heat flux at the end of the heating period was calculated to be 113 ± 3 W/cm^2. The output of all seven thermocouples was recorded over this heating period and over a 15 minute cooling period.

As in previous tests, the heater began glowing red in the center at the start of this run before the glowing quickly spread outward in both directions, and pyrolysis gas flow from the samples was very strong. After about 14 seconds of the 46.7 second heating period of this run, a vigorous flame was observed on the side of the test sample facing the back of the test enclosure. In this run a slightly stronger pump was used to provide suction to the pyrolysis gas venting system while the nitrogen flow rate was not adjusted properly to compensate. It is believed, as in run #1, that since the path of suction for the venting of pyrolysis gases is along the back of the test enclosure, the area behind the test sample became nitrogen poor and pyrolysis gas rich. This allowed for gaseous ignition of the pyrolysis gases.

The thermocouples of run #4 can be divided into three sets, each set consisting of two thermocouples at similar depths from the heated surface: (1) TC's #1 and 2 both at 2.8 mm from the heated surface, (2) TC's #3 and 4 at 5.2 and 5.5 mm from the heated surface, and (3) TC's #5 and 6 at 7.8 and 8.0 mm from the heated surface. Figures 20, 21, and 22 show the temperature measurements of each of these pairs, respectively. The thermocouples located on the flame side of the test sample, TC's 2, 4, and 5, are represented by dashed lines in these figures. For short periods of time the measured output of these thermocouples appear to have been corrupted by the adverse conditions created by the flame. After these periods, the thermocouples appear to have regained

their measurement integrity. Post-firing observations of the thermocouples at the points of insertion into the sample revealed that the Teflon insulation around the wires had burned off as in previous runs, as was expected, and that the thermocouples had become loose in their holes during the experiment. The temporary corruptions noted in Figs. 20, 21, and 22 are possibly due to secondary junctions along the lead wires of the thermocouples. Another possibility is that the temporary corruptions are due to axial conduction heat transfer along the lead wires to the thermocouple beads because of the external fire. Because the corruptions occur over different time intervals, and because these regions don't appear to all be coincident with the time the flame appeared, this possibility is considered less likely.

It is interesting to note the remarkable agreement between TC's #1 and 2 (both measured at 2.8 mm from the heated surface) from t = 0 sec to near t = 30 sec shown in Fig. 20. This agreement is a testament to the installation procedure used in this project. Recall TC #1 was potted with Alumina paste and TC #2 was potted with RS-1000 cement. Though both compounds are Alumina-based and exhibit similar thermal properties, they do have very different physical working characteristics. The paste was a smooth pre-mixed compound while the cement was supplied as a powder and was mixed into a mildly gritty compound.

Thermocouples #1, 3, and 6 (2.8 mm, 5.2 mm, and 8.0 mm from the heated surface) remained secure in their respective holes throughout the firing and exhibited plausible output traces over the entire heating range. These thermocouples span the set of three pairs defined above and thus represent the full range of locations from the heated

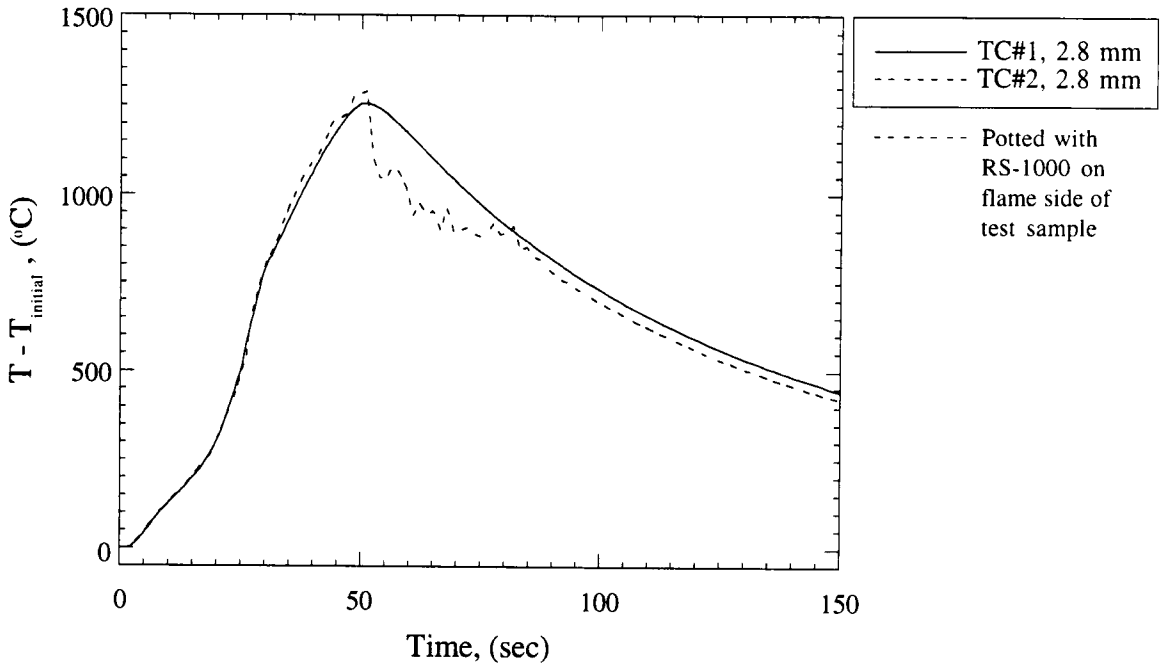


Figure 20 Comparison of measured thermocouple temperatures for thermocouples #1 and 2 for run #4.

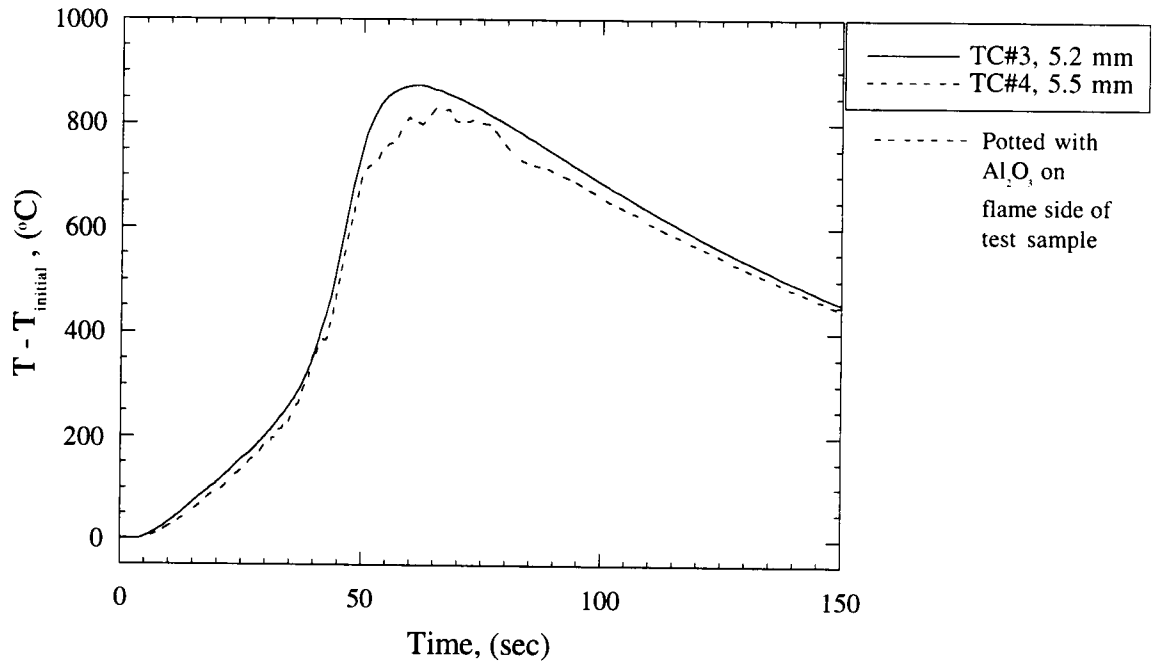


Figure 21 Comparison of measured thermocouple temperatures for thermocouples #3 and 4 for run #4.

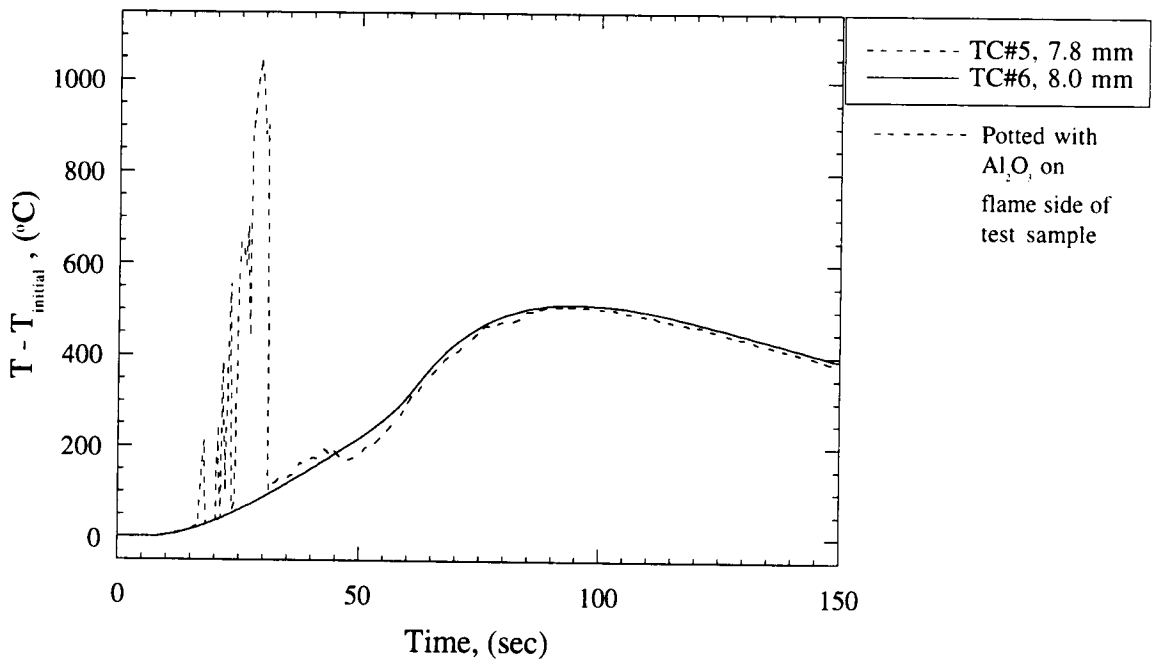


Figure 22 Comparison of measured thermocouple temperatures for thermocouples #5 and 6 for run #4.

surface for which measurements were taken. Since the measured output from thermocouples #1, 4, and 5 are not representative of the temperatures in the sample over the entire range of measurements at their respective depths from the heated surface, and since they provide no additional quality thermal response data beyond that provided by TC's 1, 3, and 6, they are not included here as part of the thermal response database for this run.

The temperature measurements of thermocouples #0, 1, 3, and 6 (the heated surface, 2.8 mm, 5.2 mm, and 8.0 mm, respectively), the thermocouples considered to have been reliable over the complete measurement period and to be representative of each location in the sample for which measurements were taken, are shown in Fig. 23. Note a maximum temperature near 2047 ^{o}C was achieved at the surface at the end of the heating period (t = 46.7 sec).

The recorded traces of the electrical "leakage" showed that for the HPBN which was insulating the instrumented (bottom) sample, the voltage became non-zero near t = 8.0 sec. The plate maintained its insulating effectiveness until about t = 11.8 sec, when the maximum voltage, as set by the Lambda DC power supply, was achieved. The measured voltage across the plate insulating the uninstrumented (top) sample also became non-zero near t = 8.0 sec and the insulation lost its effectiveness after about t = 11.1 seconds. The HPBN plates were white before the experimental run. After firing, similar to run #2, what appeared to be carbon was noted to have unevenly diffused a short distance into the plates, but the electrical resistance of the insulation was in tact upon cooling. Therefore, Joulean heating of the sample likely did not occur.

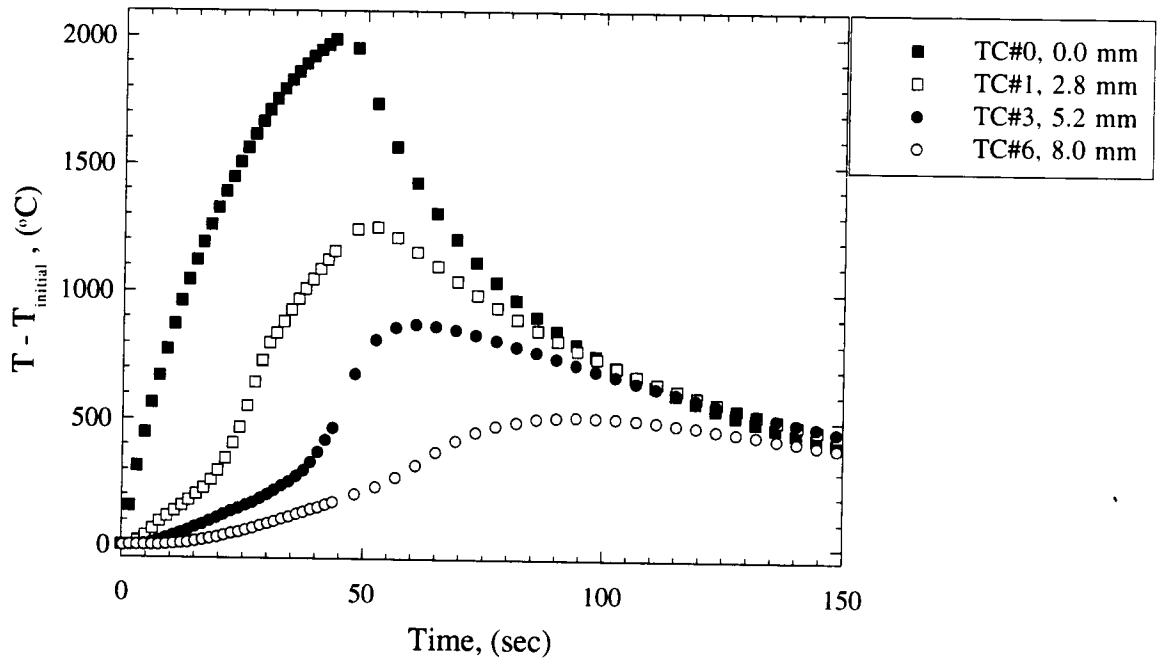


Figure 23 Measured thermocouple temperatures for run #4

Table 12 lists the mass loss of the uninstrumented test sample. A prediction was made using original CMA pyrolysis kinetics coefficients. As can be seen from the table, the experimental measurement of the mass loss (1.3 grams) was under-predicted based on these original kinetics (0.909 grams). This predicted mass loss of 0.909 grams would seem to not under-predict enough compared to the under-predicted results based on the original CMA kinetics coefficients of runs #1, 2 and 3, but the prediction for run #4 utilizes a different heated surface boundary condition during the cool-down period than did the predictions of the previous runs. The temperature (2046 °C) listed in Table 12 for the first time period (heating) is the measured heated surface temperature of the test sample at the conclusion of power input. The temperature (76 °C) listed in Table 12 for the second time period (cooling) is the measured heated surface temperature of the test sample after 15 minutes of unassisted cooling in place in the test stand. In runs #1, 2 and 3, an adiabatic boundary condition was used as an approximation of the heated surface during the cool-down period. The "true" adiabatic condition is the plane of symmetry located at the center of the graphite heater, near 5.7 mm from the heated surface of the sample (one-half of the heater thickness, 0.6 mm, plus the insulation thickness, 2.5 mm). Using this adiabatic approximation for the heated surface would provide lower than actual values for temperatures of this surface during the cool-down period. This lower temperature boundary condition would numerical result in a lower predicted aggregate mass loss for the heated sample during the cool-down period and thus an under-predicted total mass loss. The measured heated surface temperature of the sample during the heating and cool-down periods provide a more realistic boundary condition over the whole period in which predictions are made. This higher temperature boundary condition results in higher local temperatures in the sample that are maintained longer above the activation temperature for which pyrolysis can occur. Thus, while the predicted total

Table 12 Predicted and measured mass loss for run #4

Case	Heating (46.7 sec.)		Cool-Down (15 min.)		Total Mass Loss
	Mass Loss (grams)	End Temp.[a] (°C)	Mass Loss (grams)	End Temp.[a] (°C)	(grams)
Orig. CMA Kinetics Coefficients	0.431	2046	0.478	76	0.909
Measurement					1.3 ± 0.05

[a]Measured temperature at end of time period by thermocouple #0 at heated surface.

mass loss of the uninstrumented sample for run #4 (0.909 grams) under-predicts the measured aggregate mass loss (1.3 grams) due to stated shortcomings in the three-reaction constant coefficients model of the pyrolysis process, it does not under-predict the mass loss as substantially as previous runs because of the utilization of the more realistic (measured) known heated surface temperature boundary condition over both the heating and cooling periods.

Figure 24 compares the temperature predictions based on the original CMA kinetics coefficients at the locations of thermocouples #1, 3 and 6 with the measured data. As seen in previous runs, the predictions do not capture the trend in the change of the slope of the temperature measurement profile during heating of the thermocouple locations. For example, the prediction does not exhibit (over-predicts) the noticeable concave dip in the temperature measurement profile of TC #1 (2.8 mm) between about t = 8 and t = 28 sec, and of TC #2 (5.2 mm) between about t = 16 and 46 sec.

The predicted DOC as a function of depth from the heated surface is shown in Fig. 25. The prediction shown is based on the original CMA kinetics coefficients. The "scratch" test was not performed on the uninstrumented sample of run #4, so a "measured" char depth with which to compare the numerically predicted "char" depth was found in the following manner. Observations made on the side surfaces perpendicular to the plane of heat application of the burned samples from runs #1, 2, and 3 revealed a semi-uniform strip of area adjacent to the heated surface that had a darker, more porous appearance. The thickness of this strip roughly corresponded to the measured "char" depth found from the "scratch" test. Thus, since visual observations of the discoloration and surface roughness of the samples for runs #1, 2, and 3, compared to

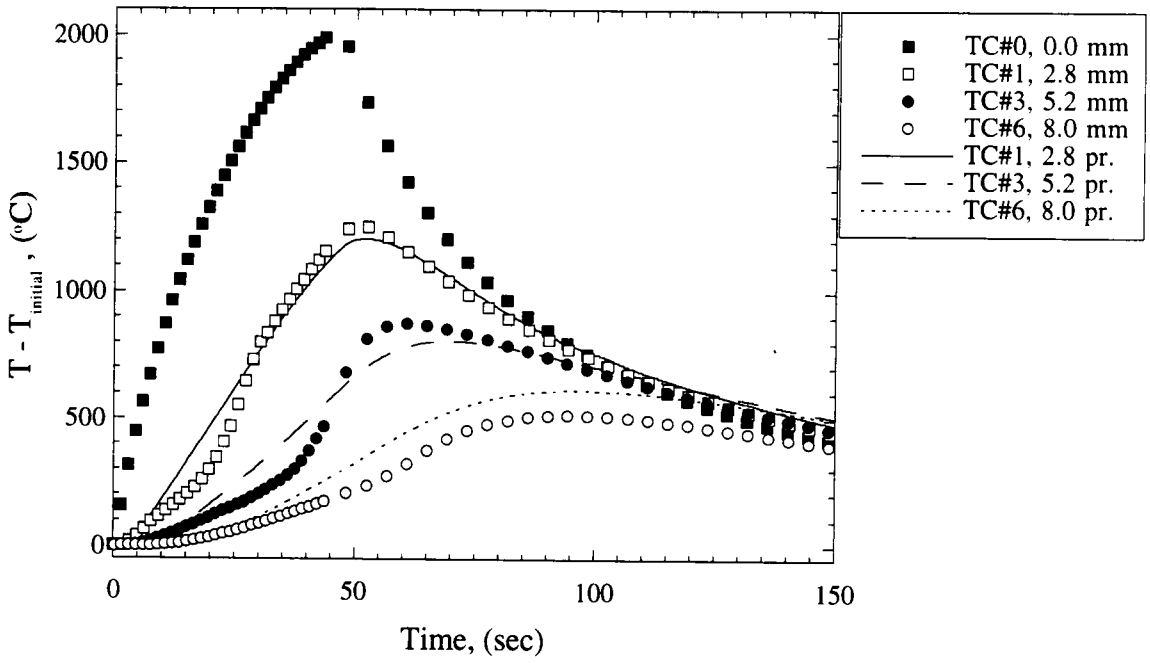


Figure 24 Comparison of run #4 in-depth temperatures with prediction

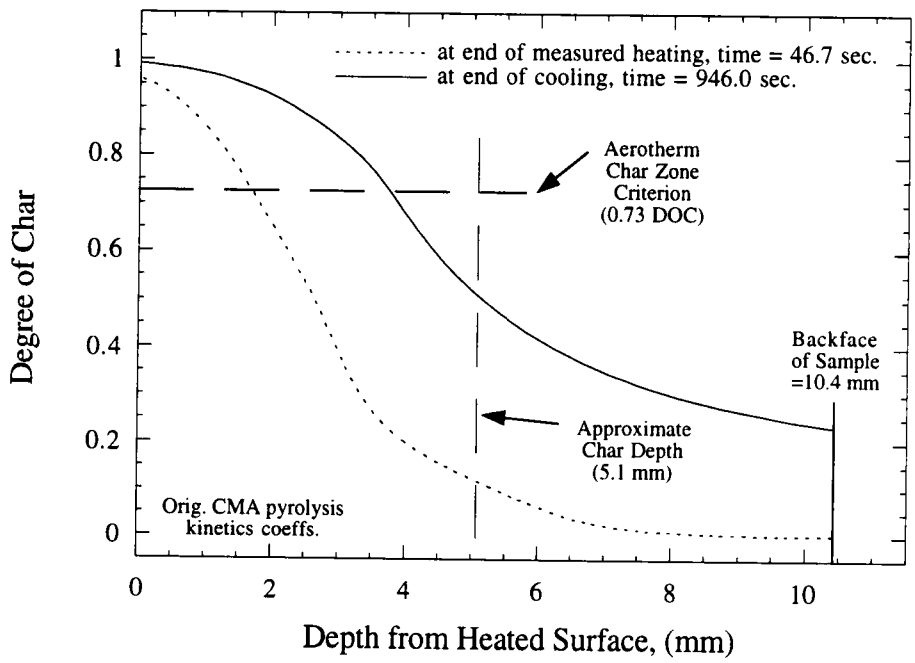


Figure 25 Predicted degree of char after 46.7 sec of heating and 15 minutes cooling for run #4

the "char" depths measured by the "scratch" test at MSFC, an approximation based on likewise visual observations was made for the "char" depth of run #4. As shown in Fig. 25, the approximate "char" depth for run #4 was found to be 5.1 mm. The predicted "char" depth based on the Aerotherm char criterion was found to be 3.56 mm.

The approximated and predicted "char" depths are listed in Table 13. In runs #1, 2, and 3, an unacceptably under-predicted "char" depth of zero was found using the original CMA kinetics coefficient. The "char" depth of run #4 is also under-predicted, but not as grossly as in the previous experiments. This is as expected in view of the above discussion on the use of the more realistic measured heated surface temperature boundary condition since the DOC can be directly related to mass loss.

The heating rate of the thermocouples in run #4 are presented in Fig. 26. For this run, our test facility heated the surface of the test sample at an initial heating rate of near 100 ^{o}C/sec, two times the maximum of 50 ^{o}C/sec for the range of heating rates over which TGA data has been obtained for the pyrolysis kinetics model. Even with the more realistic measured temperature boundary condition used in the predictions during the cool-down period, the pyrolysis kinetics model still under-predicts the mass loss and "char" depth and thus is too slow to adequately represent higher heating rates.

3.5 Run #5

Seven thermocouples were used in this run; one Type C, and six Type K. The distances of thermocouple beads from the heated surface of the test sample, as measured

Table 13 Comparison of the predicted and "observed" "char" depth of run #4

Time	"Char" Depth (mm)	
	Original CMA Kinetics Coefficients[1]	Approximated Char Depth[2]
End of the Heating (t = 46.7 sec)	1.56	--
End of the Cool-down (t = 946.0 sec)	3.58	5.1

[1] Aerotherm char criterion of 0.73 is used to determine the predicted values.
[2] The listed value is an estimation based on observation.

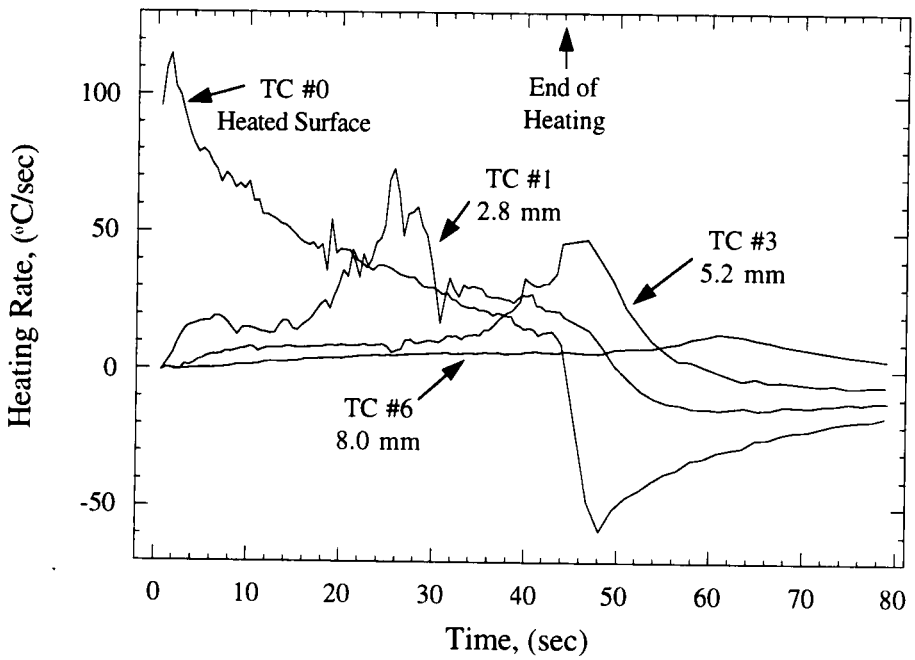


Figure 26 Time history of heating rates for run #4 thermocouples

from the x-ray, are listed in Table 14. The thermocouples were potted in various ways in an attempt to find which gave optimum thermal contact in the holes. Thermocouples #1, 4, and 6 were instrumented in the holes without any potting compound except for a small amount at the entry point to secure the probe in place. These thermocouples are designated in Table 14 as being potted in air. They were potted this way to establish a reference that could possibly be used to compare three Alumina-based cements supplied by Cotronics: C-903-HP, C-989, and C-7030. Thermocouples #2 ,3 and 5 were potted with C-903-HP, C-989, and C-7030, respectively. Heating was applied to the samples for 30.9 seconds. The heat flux at the end of the heating period was calculated to be 138 ± 3 W/cm^2. The output of all seven thermocouples was recorded over this heating period and over a near 15 minute cooling period.

As in previous tests, the heater began glowing red in the center at the start of this run before the glowing quickly spread outward in both directions, and pyrolysis gas flow from the samples was very strong. For this run, the mass flow of nitrogen into the test enclosure was increased and the air flow through the pump was partially baffled to decrease the amount of suction used for venting of the pyrolysis gases. No flame was observed during this test.

As in run #4, the thermocouples of run #5 can be divided into three sets, each set consisting of two thermocouples each at similar depths from the heated surface: (1) TC's #1 and 2 at 2.6 and 2.8 mm, (2) TC's #3 and 4 at 5.3 and 5.5 mm, and (3) TC's #5 and 6 at 8.1 and 8.6 mm. Figure 27 shows the measured temperatures for the seven thermocouples. As can be seen, there are no apparent anomalies in the thermocouple output traces. The thermocouples potted in air in the test sample, TC's 1, 4, and 6, are

Table 14 Thermocouple locations for run #5

Thermocouple	Distance from Heated Face (mm)	Potting Compound
TC #0	Surface Boundary	BN paint
TC #1	2.6±0.05	Air
TC #2	2.8±0.05	C-903-HP[a]
TC #3	5.3±0.05	C-989[a]
TC #4	5.5±0.05	Air
TC #5	8.1±0.05	C-7030[a]
TC #6	8.6±0.05	Air

[a]Various Alumina-based cements supplied by Cotronics.

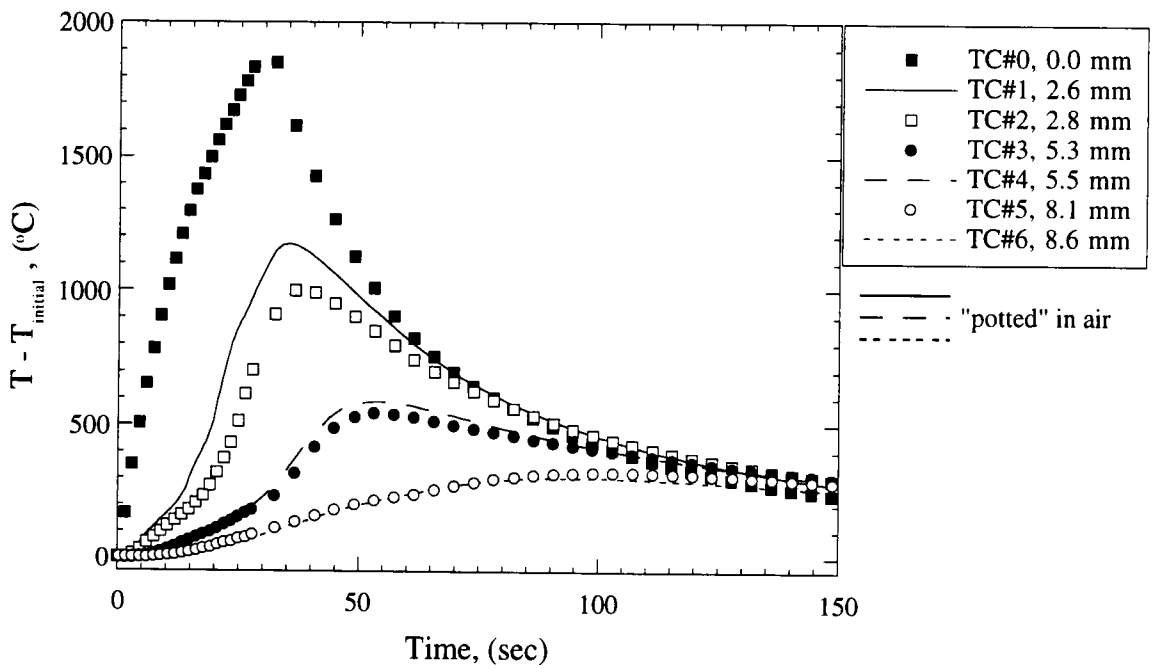


Figure 27 Comparison of measured thermocouple temperatures for run #5.

represented by different line styles. Note a maximum temperature near 1934 °C was achieved at the surface at the end of the heating period (t = 30.9 sec).

The air-potted thermocouples #1, 4, and 6 (2.6, 5.5, and 8.6 mm from the heated surface) remained secure in their respective holes throughout the firing and exhibited plausible output traces over the entire heating range. Thermocouples #2, 3, and 5 (2.8, 5.3, and 8.1 mm from the heated surface) also remained secure in their respective holes throughout the firing. These three thermocouples also span the set of three pairs defined above and thus represent the full range of locations from the heated surface for which measurements were taken. These thermocouples exhibit similar trends and orders of magnitude with their respective air-potted partners. However, it may be noted that the air-potted thermocouples at y = 5.5 mm (TC #4) and 8.6 mm (TC #6) measured equal or higher temperatures than the Alumina-based cement-potted thermocouples located at y = 5.3 mm (TC #3) and 8.1 mm (TC #5), even though the cement-potted thermocouples are closer to the heated surface. Considering the fact that the thermocouples, regardless of the potting compound used, will always measure a lower temperature than the actual temperature of the host material, one can conclude that the measured temperatures by the cement-potted thermocouples are in substantial error.

The recorded traces of the electrical "leakage" showed that for the HPBN which was insulating the instrumented (bottom) sample, the voltage became non-zero near t = 6.4 sec. The plate maintained its insulating effectiveness until about t = 8.4 sec, when the maximum voltage, as set by the Lambda DC power supply, was achieved. The measured voltage across the plate insulating the uninstrumented (top) sample became non-zero near t = 6.2 sec and the insulation lost its effectiveness after about t = 8.2 seconds. The HPBN

plates were white before the experimental run. After firing, similar to run #2, what appeared to be carbon was noted to have unevenly diffused a short distance into the plates, but the electrical resistance of the insulation was in tact upon cooling. The measured surface temperature of the instrumented (bottom) test sample after the insulation lost its effectiveness (t = 8.4 sec) was near 970 °C. The upward change in slope of the measured in-depth thermocouple responses is noted to begin after the loss of insulating effectiveness. This same occurrence is observed for all experimental test runs and thus prohibits the assertion that Joulean heating is not, at least in part, responsible for the change in slope of the in-depth thermocouple responses.

Table 15 lists the mass loss of the uninstrumented test sample. A prediction was made using original CMA pyrolysis kinetics coefficients as supplied by Aerotherm, and using 50 times larger kinetics coefficients. As can be seen from the table, the experimental measurement of the mass loss (0.9 grams) was under-predicted based on these original kinetics (0.658 grams) and over predicted based on the larger kinetics coefficients(1.49 grams). As was done in run #4, the measured heated surface temperature for this run (run #5) was used to generate the known surface boundary condition for both the heating and cooling periods. Similar to run #4, the original kinetics prediction of the mass loss is not as big an under-prediction as that which was experienced in runs #1, 2, and 3. This is as expected by the same reasons discussed for Run #4. Likewise for these same reasons, the 50 times larger kinetics coefficients prediction is substantially over-predicted compared to the predictions of runs #1 and 2.

Figure 28 compares the temperature predictions based on the original CMA kinetics coefficients at the locations of thermocouples #2, 3 and 5 with the measured data.

Table 15 Predicted and measured mass loss for run #5

Case	Heating (30.9 sec.)		Cool-Down (891.5 sec.)		Total Mass Loss
	Mass Loss (grams)	End Temp.[a] (°C)	Mass Loss (grams)	End Temp.[a] (°C)	(grams)
Orig. CMA Kinetics Coefficients	0.263	1934	0.395	61	0.658
50 times Larger Kinetics	0.690	1934	0.796	61	1.486
Measurement					0.9 ± 0.05

[a]Measured temperature at end of time period by thermocouple #0 at heated surface.

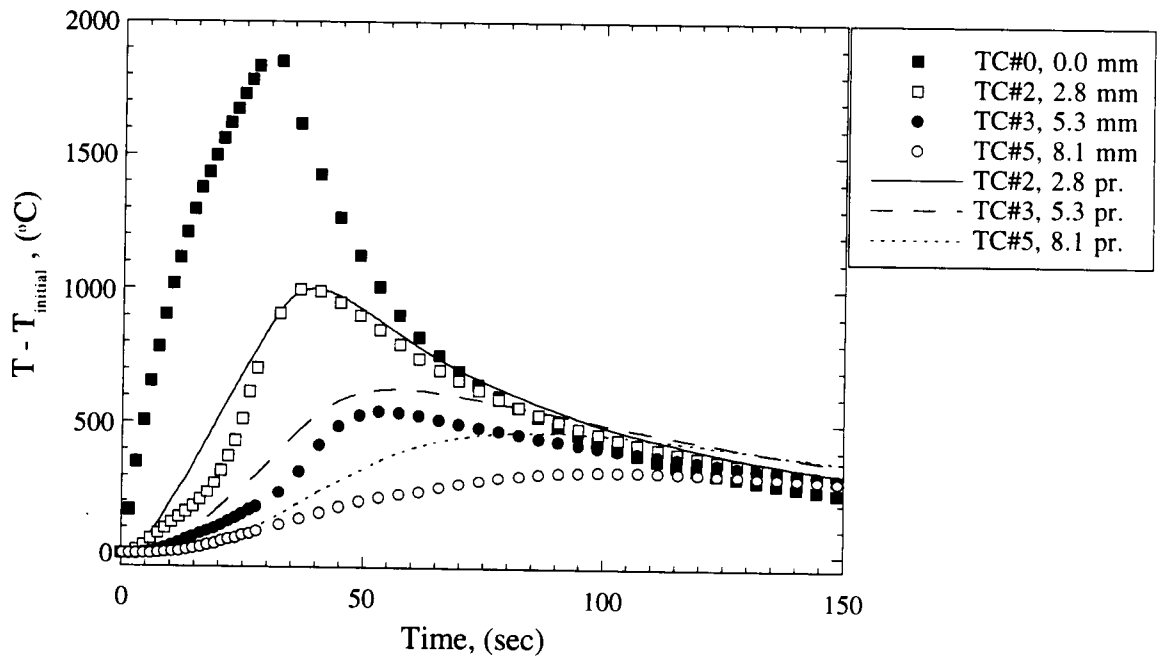


Figure 28 Comparison of run #5 cement-potted in-depth thermocouple measurements with prediction using original CMA kinetics coefficients

As seen in previous runs and discussed for run #4, the predictions do not capture the trend in the change of the slope of the temperature measurement profile during the period of increasing temperature at the thermocouple locations. For instance the measurement of TC #2 is under-predicted by nearly 200 °C at t = 20 sec before the prediction and measurement are matched near t = 30 sec. The temperature measurements of the air-potted thermocouples #1, 4, and 6 (2.6 mm, 5.5 mm, and 8.6 mm, respectively) are compared in Fig. 29 with predictions performed using the larger kinetics coefficients. Again, the predictions do not capture the trend in the change in slope of the measurement profile of TC #1, but the deviation during the period of increasing temperature is much less than that for TC #2.

During the period of increasing temperature, the decrease in the deviation between prediction and measurement that is noted for the air-potted thermocouples as compared to the cemented-potted thermocouples suggests that the change in slope of the measured temperature profile is, in part, due to instrument installation. Thermocouples are invasive measuring devices and, in the absence of axial conduction, will always measure temperature during a temperature rise as being somewhat lower than actual because of the required existence of a temperature gradient. The presence of the near linear measurement profile of the air-potted TC #2 during heat-up suggests that the cement-potted TC #1 is experiencing a time dependent measurement lag. In other words, it suggests that the air is providing better heat transfer between the host material and the thermocouple bead. A list of thermal diffusivities for the potting compounds and the carbon-phenolic is given in Appendix B (Table B-6). Notice that the thermal diffusivity of air (169 mm^2/sec at near 1000 °C) is an order of magnitude greater than that of Boron Nitride paint (18.8 mm^2/sec at near 1000 °C), and two orders of magnitude

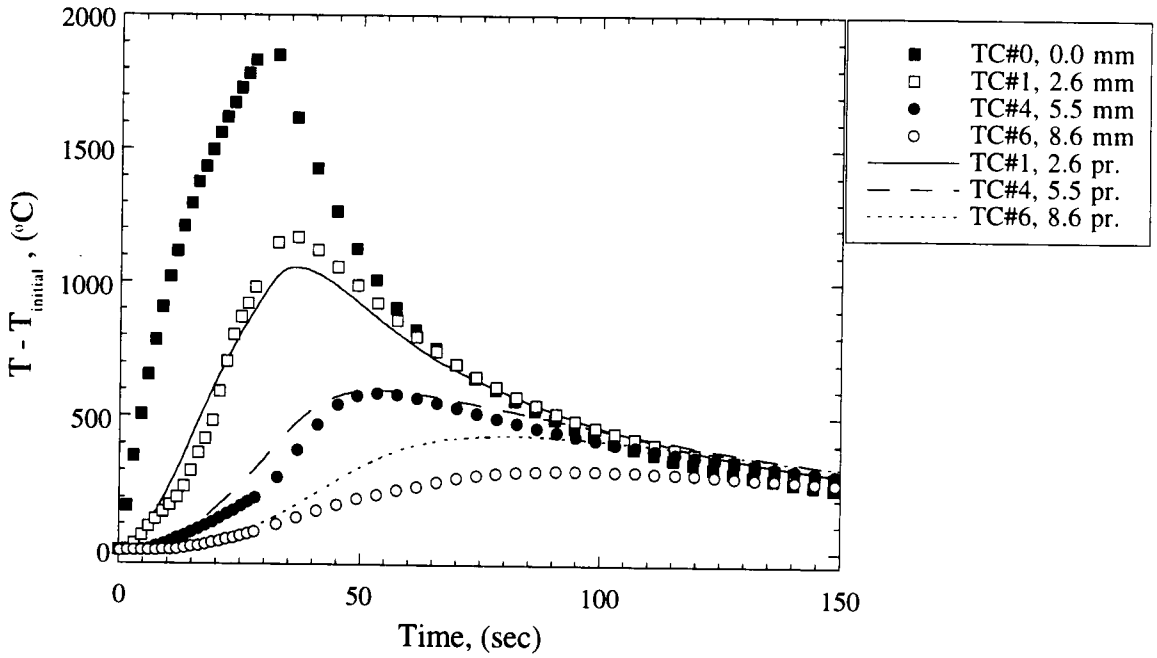


Figure 29 Comparison of run #5 air-potted in-depth thermocouple measurements with prediction using 50 times larger kinetics coefficients

greater than all of the remaining potting materials and the carbon-phenolic (0.35 - 2.9 mm^2/sec at near 1000 ^oC). In addition to the high thermal diffusivity, air allows for radiation heat transfer to occur between the carbon-phenolic and the thermocouple bead. This radiation heat transfer begins to be dominant mode of heat transfer at high temperatures. Thus, air will respond more quickly to changes in the local thermal environment at high temperatures than will other potting materials. Although the "air-potted" thermocouples are actually surrounded by a complex mixture of pyrolysis gases, it is assumed that, for the purposes of simplifying the following analyses, these gases will behave on the same order of magnitude as air with respect to thermal diffusivity.

To stress the statement that 'air-potted' thermocouples will respond faster than cement-potted thermocouples during high temperature transient experiments, the transient (temperature dependent) behavior of their effective time constants was explored. Assume a lumped capacitance model for the thermocouple bead consisting of two concentric spheres: the center sphere representing the thermocouple bead with a radius of 0.1905 mm, and the surrounding spherical shell representing the thermocouple potting compound. This surrounding shell has an outer radius of 0.375 mm, the radius of the drilled hole, and an inner radius of that of the thermocouple bead. Since the thermocouple lead wires are routed along an isotherm in the carbon-phenolic material, and since any effect they might have on the model would be present for both of the cases being compared, 'air-potting' and cement-potting, axial conduction along the lead wires are neglected in this analysis.

For the thermocouple bead, the time constant is given by

$$\tau = R_t C_{t,eff} = (R_t)\left((mc_p)_{TC,bead} + (mc_p)_{air}\right), \tag{5}$$

where the effective capacitance of the bead is assumed to be equal to the sum of the capacitances of the bead and the potting material, and the thermal resistance is defined as follows. For the cement-potted thermocouple, it is assumed that there is perfect installation, or more specifically the hole is completely and evenly filled with the potting cement and there is perfect thermal contact between the outer surface of the cement and the host carbon-phenolic. Energy can traverse the cement by conduction, therefore R_t for the cement is given by

$$R_{conduction} = \frac{1}{4\pi k_{potting\ material}}\left(\frac{1}{R_{inner}} - \frac{1}{R_{outer}}\right). \tag{6}$$

Equation 6 is dependent on temperature through the temperature dependence of the thermal conductivity. For the case of the 'air-potted' thermocouple, energy is transferred to the thermocouple bead by both conduction and radiation. The host carbon-phenolic is assumed to act as a blackbody and the thermocouple bead is assumed to have an emissivity of $\varepsilon = 0.5$. Conservatively assuming the surrounding carbon-phenolic temperature to be equal to that of the thermocouple bead, the thermal resistance due to radiation is given as

$$R_{radiation} = \left(4\sigma\varepsilon A_i T_{TC}^3\right)^{-1}. \tag{7}$$

where T_{TC} is the temperature of the thermocouple bead and A_i is the surface area of the bead. R_t for the 'air-potted' case is then the combination of $R_{conduction}$ and $R_{radiation}$ added in parallel. Note the strong dependence on temperature introduced by Eq. 7.

Figure 30 shows the thermal resistance and Fig. 31 shows the effective time constant as a function of temperature for both air and Alumina cement used as potting materials. Note from Fig. 31 that after the surrounding carbon-phenolic has reached a temperature of 1500 K, the 'air-potted' thermocouple has a lower time constant than the cement-potted thermocouple, and moreover, the time constant of the 'air-potted' thermocouple is further decreasing with increasing temperature while the time constant of the cement-potted thermocouple is increasing with increasing temperature. Recalling the assumption of perfect installation for the cement-potted thermocouple, if voids in the cement and contact resistance between the cement and carbon-phenolic were not neglected, the Alumina time constant curve would be vertically shifted upward by a substantial amount since the contact resistance would be due to an air gap. Moreover, this additional thermal contact resistance would be added in series with the thermal resistance of the cement. This would result in a lower transition temperature after which 'air-potting' would appear to provide a faster thermal response for a thermocouple than cement-potting. Exactly at what temperature this transition would occur may be impossible to determine since the imperfections in the installation can not be described or modelled in detail.

In light of the above analyses, a possible scenario for the changing slope of the temperature measurement profile during the period of increasing temperature at the thermocouple location could be as follows. Thermocouple #2 of this run (2.8 mm, run

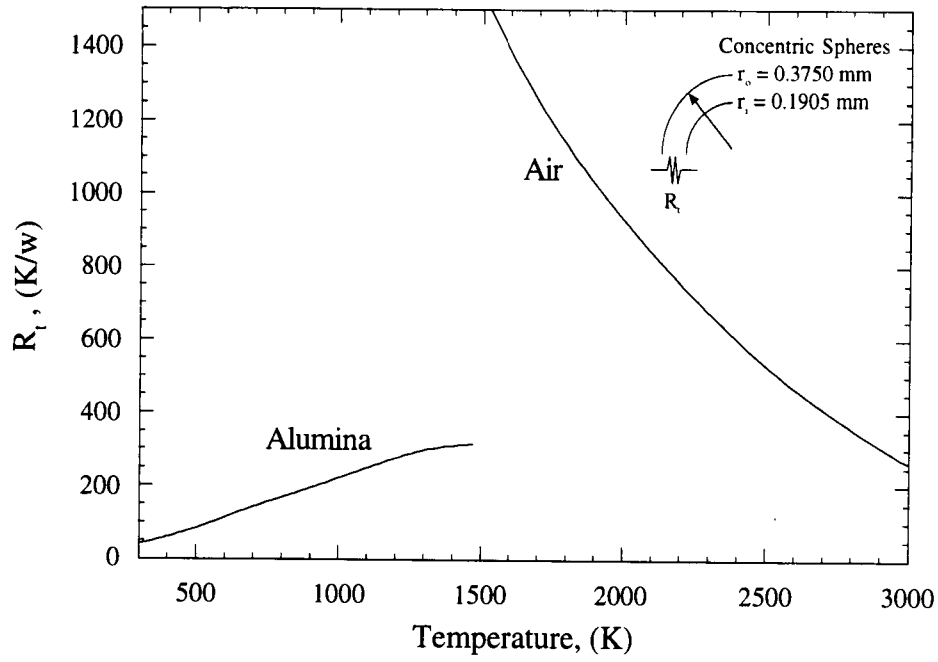


Figure 30 Thermal resistance vs. temperature for different potting materials

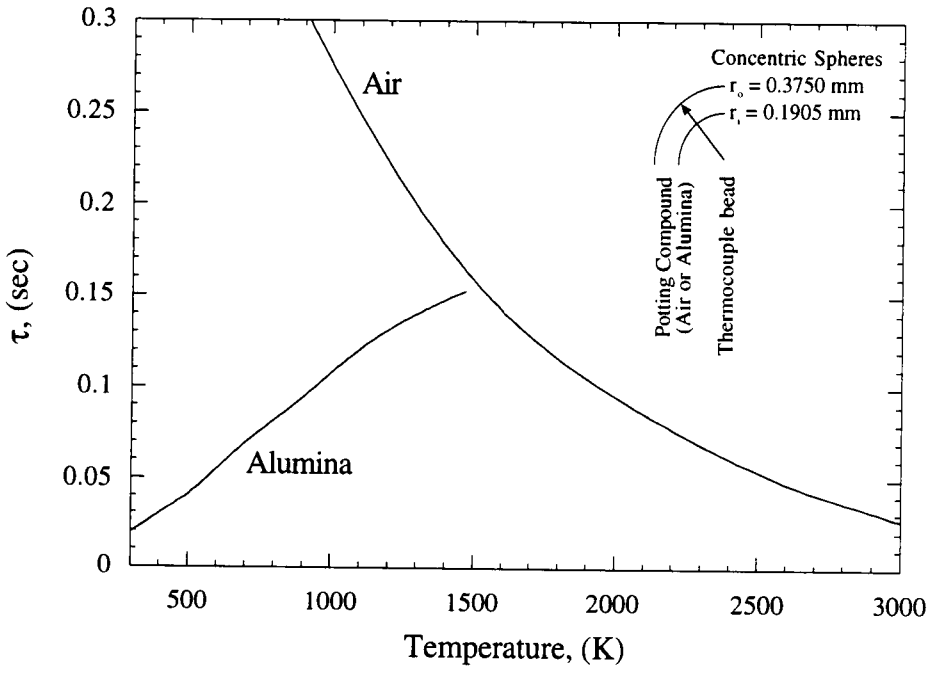


Figure 31 Effective time constant vs. temperature for different potting materials

#5) shall be used as the example since it exhibits the most pronounced changing slope trend (Figs. 27 and 28). As the location of this thermocouple is first heated, the increasing effective time constant of the cement potting material produces a thermocouple response lag resulting in the initial relatively low slope. Due to different thermal expansion characteristics between the cement and the host carbon-phenolic, separation between the cement and host occurs. This allows the introduction of a layer of air between the cement and carbon-phenolic. As temperature increases, the decreasing effective time constant enhances the heat transfer from the carbon-phenolic to the cement resulting in an increase of the slope. As the thermocouple location is further heated, increased separation can occur allowing for the introduction of additional air. The 'air-potted' TC #1 (Fig. 29) takes full advantage of the decreasing effective time constant and thus has less curvature in its slope during heating. Recall that for the cement-potted thermocouple the thermal resistance of the introduced air layer is in series with the resistance of the cement.

The predicted DOC as a function of depth from the heated surface, of both the original CMA kinetics coefficients and those of 50 times larger, is shown in Fig. 32. The "scratch" test was not performed on the uninstrumented sample of run #5, so an approximate "char" depth, as described for run #4, was observed. As shown in Fig. 32, the approximate "char" depth for run #5 was found to be 4.8 mm. Using the original CMA kinetics coefficients, the predicted "char" depth based on the Aerotherm char criterion was found to be 2.18 mm after a modeled heating period of 30.9 seconds and cooling period of near 15 minutes. Likewise, the 50 times larger kinetics coefficients predicted a "char" depth of 9.8 mm. These approximated and predicted "char" depths are listed in Table 16. The predicted "char" depth based on the original CMA kinetics

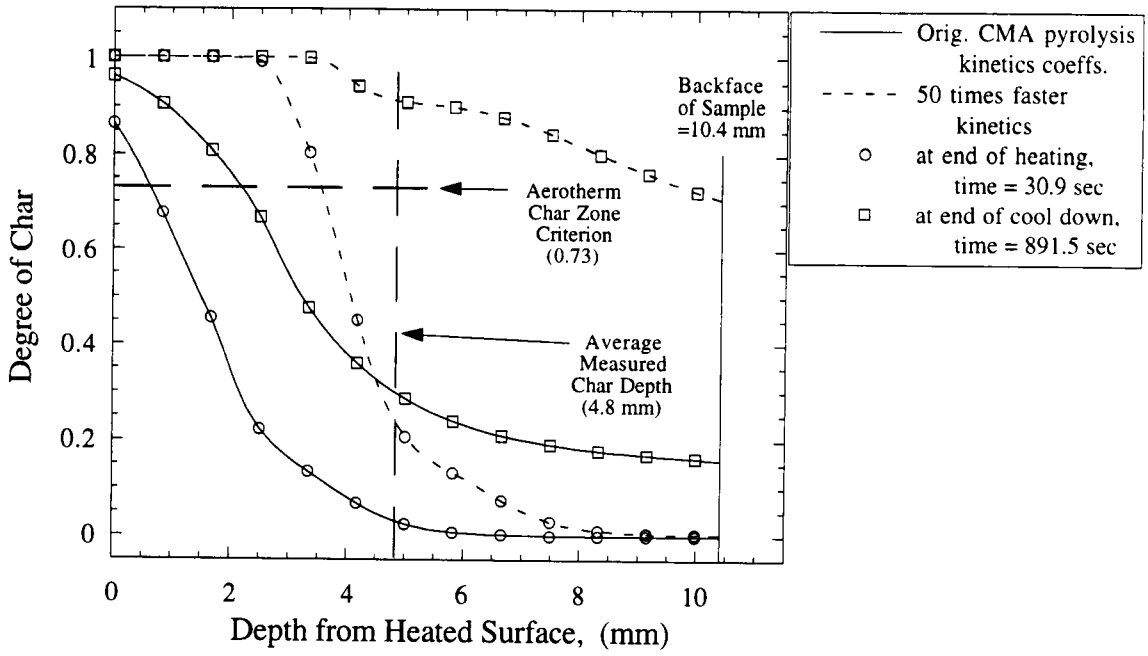


Figure 32 Predicted degree of char after 30.9 sec of heating and near 15 minutes cooling for run #5

Table 16 Comparison of the predicted and "observed" "char" depth for run #5

Time	Char Depth (mm)		
	Original CMA Kinetics Coefficients[1]	50 times Larger Kinetics Coefficients[1]	Approximated Char Depth[2]
End of the Heating (t = 30.9 sec)	0.6	3.54	--
End of the Cool-down (t = 922.4 sec)	2.18	9.8	4.8

[1]Aerotherm char criterion of 0.73 is used to determine the predicted values.
[2]The listed value is an in-house estimation based on observation.

coefficients under-predicts the "measured" "char" depth while the predicted "char" depth based on the 50 times larger kinetics coefficients over-predicts the "measured" "char". The difference in the amount of over- and under-prediction compared to runs #1 and 2 are attributed to the measured temperature boundary condition during the cool-down period, as was discussed for the mass loss of this run.

The heating rate of the air-potted thermocouples in run #5 are presented in Fig. 33. For this run, our test facility heated the surface of the test sample at an initial heating rate of near 130 ^{o}C/sec, over two and one-half times the maximum of 50 ^{o}C/sec for the range of heating rates over which TGA data has been obtained for the CMA pyrolysis kinetics model. With the more realistic measured temperature boundary condition used in the predictions during the cool-down period, this run shows, as did run #4, that the original CMA pyrolysis kinetics coefficients under-predict the mass loss and "char" depth while the 50 times larger coefficients over-predict them. A multiplying factor for the kinetics coefficients could possible be found by trial and error, but these values would be case specific and not very useful. It is important to note, though, that the 'accepted' original CMA kinetics coefficients appear to be at least an order of magnitude to small to accurately model heating rates higher than the maximum of 50 ^{o}C/s for which these published values were found.

3.6 Run #6

Seven thermocouples were used in this run; one Type C, and six Type K. The distances of thermocouple beads from the heated surface of the test sample, as measured

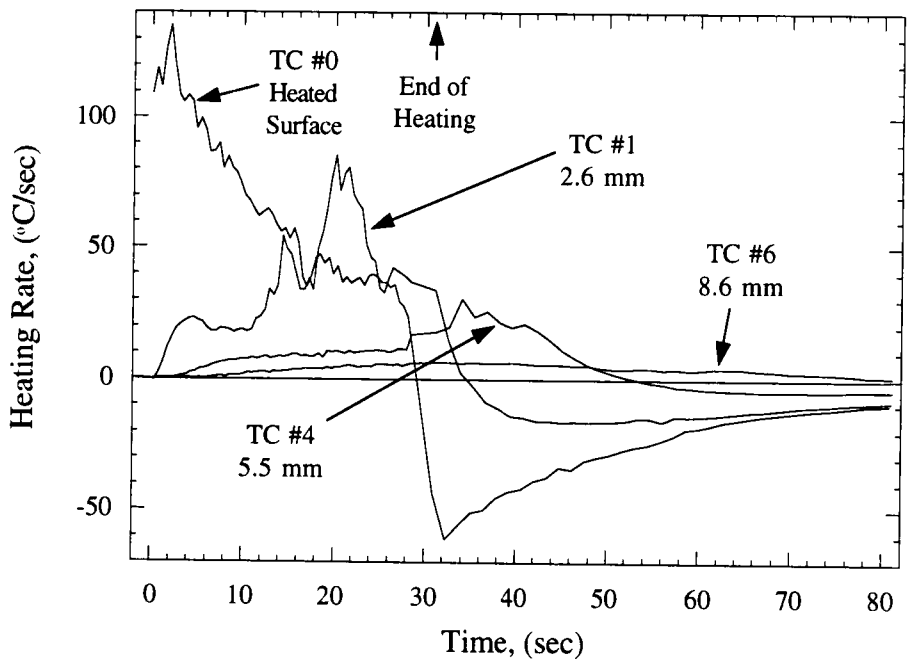


Figure 33 Time history of heating rates for run #5 air-potted thermocouples

from the x-ray, are listed in Table 17. Thermocouples #1, 4, and 6 were potted with Boron Nitride paint while thermocouples #2, 3, and 5 were potted with Cotronics C-989 Alumina-based cement. Of all the Alumina-based cements used in run #5, C-989 was the easiest to work with to ensure complete filling of the thermocouple wells. The discussion in run #5 regarding air-potting of the thermocouples was not realized before the completion of this and subsequent runs, therefore run #5 was the only one to utilize air-potting. Heating was applied to the samples of this run for 33.9 seconds, at the end of which, a heat flux of 151 ± 4 was calculated. The output of all seven thermocouples was recorded over this heating period and over a near 15 minute cooling period.

As in previous tests, the heater began glowing red in the center at the start of this run, then the glowing quickly spread outward in both directions, and pyrolysis gas flow from the samples was very strong. For this run, no flame was observed during this test.

As in run #4, the thermocouples of run #6 can be divided into three sets, each set consisting of two thermocouples each at similar depths from the heated surface: (1) TC's #1 and 2 at 2.4 and 2.8 mm, (2) TC's #3 and 4 at 5.3 and 5.5 mm, and (3) TC's #5 and 6 at 7.4 and 8.5 mm. Figure 34 shows the temperature measurements for the seven thermocouples for this run. The thermocouples potted with Boron Nitride, TC's 1, 4, and 6, are represented by different line styles. As can be seen, TC #1 (2.4 mm) appears to be corrupted from near 17 to 42 seconds. The potting compound for this thermocouple is Boron Nitride paint. Although Boron Nitride paint has a high thermal conductivity, it does not posses any refractory strength characteristics. Post-firing observations revealed this thermocouple had become loosened in its hole, so secondary junctions are likely.

Table 17 Thermocouple locations for run #6

Thermocouple	Distance from Heated Face (mm)	Potting Compound
TC #0	Surface Boundary	BN paint
TC #1	2.4±0.05	BN paint
TC #2	2.8±0.05	C-989[a]
TC #3	5.3±0.05	C-989[a]
TC #4	5.5±0.05	BN paint
TC #5	8.4±0.05	C-989[a]
TC #6	8.5±0.05	BN paint

[a]C-989 is an Alumina-based cement supplied by Cotronics.

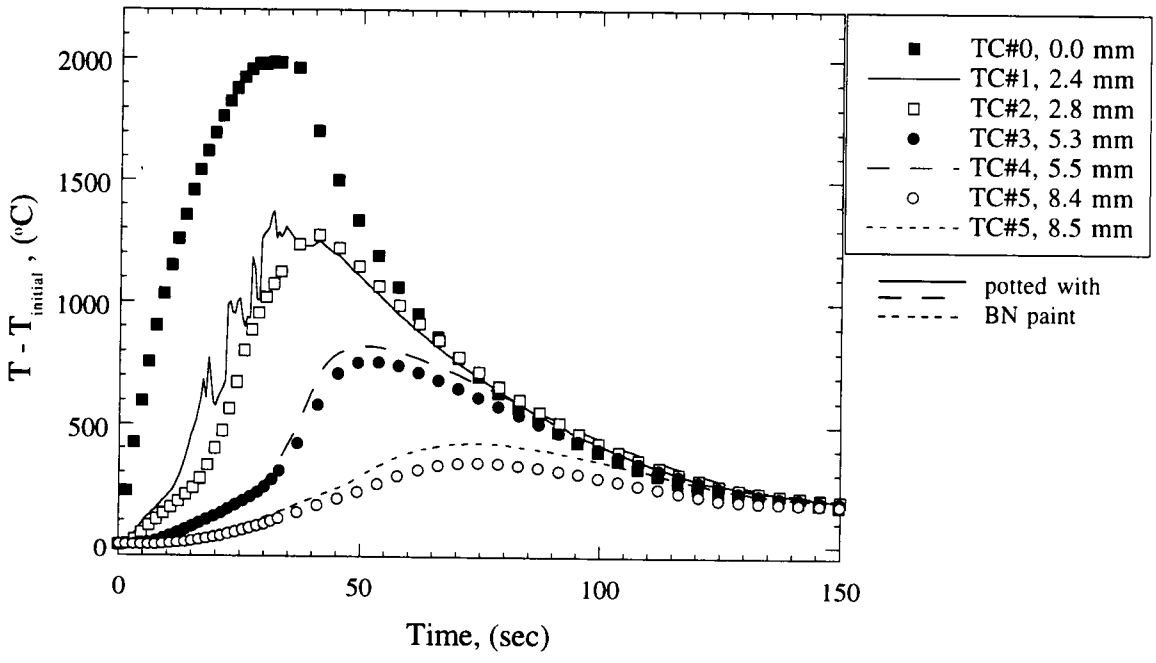


Figure 34 Comparison of measured thermocouple temperatures for run #6.

It is interesting to note that for the second and third pairs of thermocouples, the two thermocouples potted in Boron Nitride paint, TC's #4 and 6, exhibited measured temperature profiles higher than those of their respective partners, TC's #3 and 5, even though they were further away from the heated surface. This is not surprising, however. The thermal diffusivity of the Boron Nitride paint is two orders of magnitude higher than that of the C-989, (18.8 vs. 0.65 mm^2/sec). Also, the Boron Nitride is a water based paint that draws up substantially when it dries. Therefore, the possibility of having air voids within the thermocouple well is good. These large air voids would result in a faster effective time response for the thermocouple as discussed in run #5.

The temperature measurements of thermocouples #0, 2, 3, and 5 (the heated surface, 2.8 mm, 5.3 mm, and 8.4 mm, respectively), are shown in Fig. 35. Since these thermocouples represent a set of thermocouples, potted with the same material, that spans the range of in-depth locations and that exhibits no anomalies such as possible secondary junctions, this set is presented as part of the thermal response database. Note a maximum temperature near 2010 ^oC was achieved at the surface at the end of the heating period (t = 33.9 sec).

The recorded traces of the electrical "leakage" showed that for the HPBN which was insulating the uninstrumented (top) sample, the voltage became non-zero near t = 6.2 sec. The plate maintained its insulating effectiveness until about t = 8.4 sec, when the maximum voltage, as set by the Lambda DC power supply, was achieved. The measured voltage across the plate insulating the instrumented (bottom) sample was not recorded due to an open circuit and is therefore considered to be approximately equal to the top that of the uninstrumented (top) sample. The HPBN plates were white before the

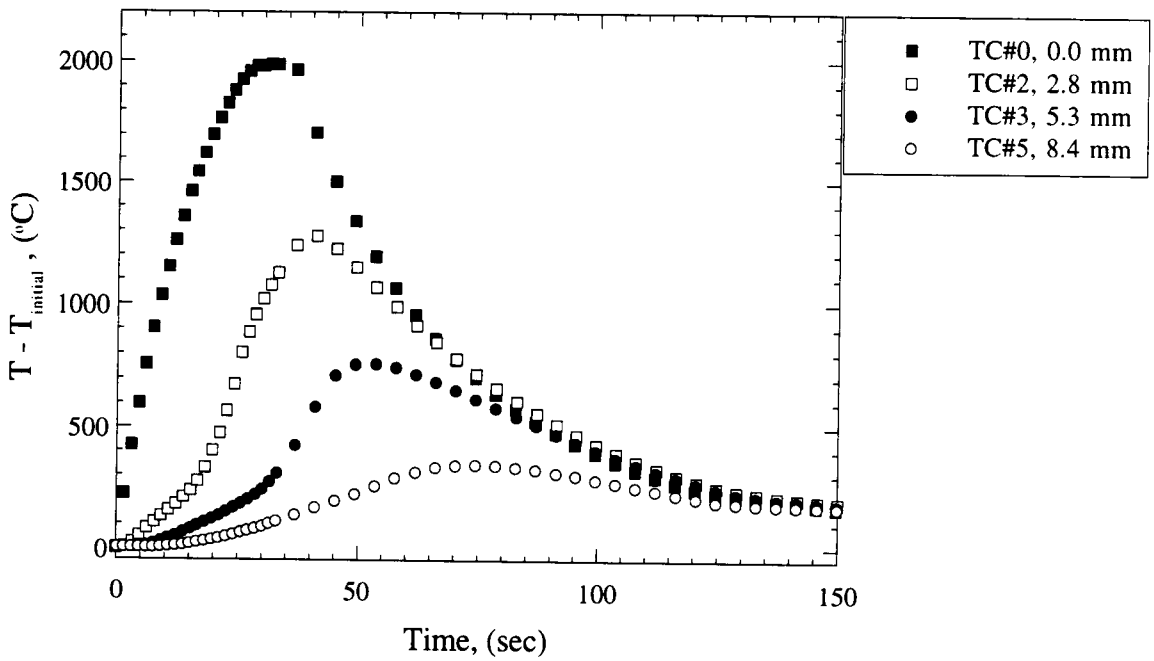


Figure 35 Measured thermocouple temperatures for run #6

experimental run. After firing, similar to run #2, what appeared to be carbon was noted to have unevenly diffused a short distance into the plates, but the electrical resistance of the insulation was in tact upon cooling. After the plates had lost their insulating effectiveness during the run ($t > 8$ sec), the change in the slopes of the in-depth thermocouple can be seen to occur. Again, the temperature at the time the insulation lost its effectiveness was near 900 ^{o}C, in the range of the maximum use temperature. The correlation between the time of lost insulation effectiveness and the heated surface temperature of the sample is consistent for all of the runs. Therefore, there is still no evidence to dismiss Joulean heating in the test sample as a partial cause for the upward change in slope of the thermocouple response.

Table 18 lists the mass loss of the uninstrumented test sample. A prediction was made using original CMA pyrolysis kinetics coefficients as supplied by Aerotherm. As can be seen from the table, the experimental measurement of the mass loss (1.1 grams) was under-predicted based on these original kinetics (0.764 grams). Similar to run #4, the prediction of the mass loss is not as big an under-prediction as that which was experienced in runs #1, 2, and 3. This is as expected by the same reasons discussed for Run #4. As was done in run #4, the measured heated surface temperature for this run (run #6) was used to generate the known surface boundary condition for both the heating and cooling periods.

Figure 36 compares the temperature predictions based on the original CMA kinetics coefficients at the locations of thermocouples #2, 3 and 5 with the measured data. As seen in previous runs and discussed for run #5, the predictions do not capture the trend

Table 18 Predicted and measured mass loss for run #6

Case	Heating (33.9 sec.)		Cool-Down (902 sec.)		Total Mass Loss
	Mass Loss (grams)	End Temp.[a] (°C)	Mass Loss (grams)	End Temp.[a] (°C)	(grams)
Orig. CMA Kinetics Coefficients	0.353	2010	0.411	58	0.764
Measurement					1.1 ± 0.05

[a]Measured temperature at end of time period by thermocouple #0 at heated surface.

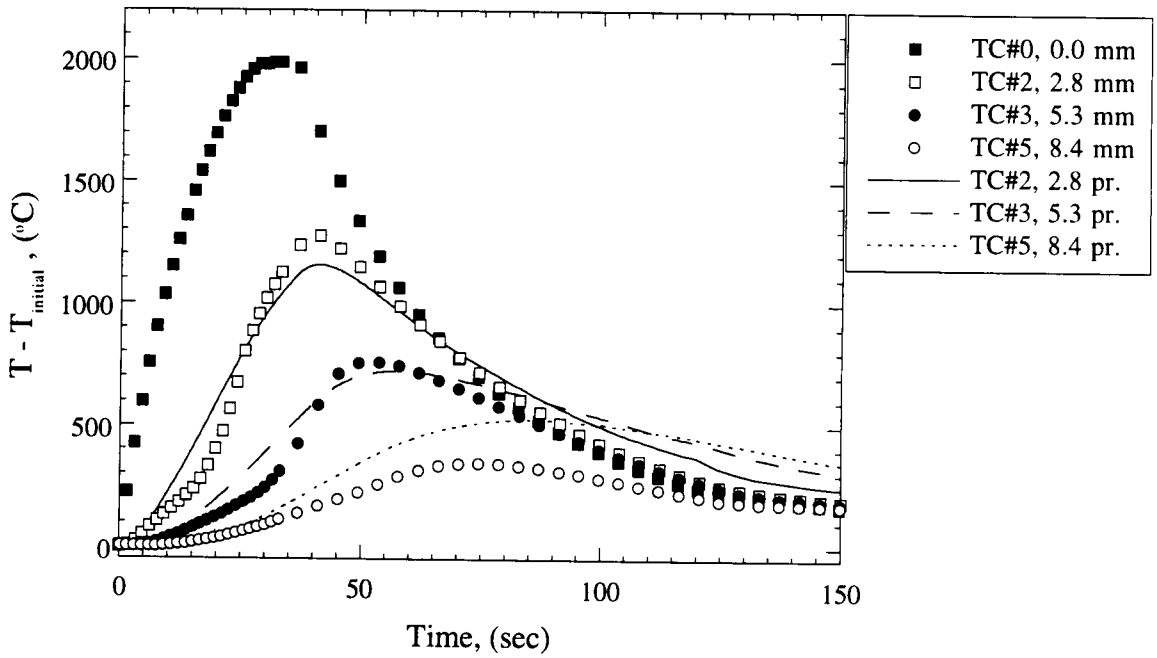


Figure 36 Comparison of run #6 in-depth temperatures with prediction

in the change of the slope of the temperature measurement profile during heating of the thermocouple locations because the predictions ignore installation effects.

The predicted DOC as a function of depth from the heated surface is shown in Fig. 37. The prediction shown is based on the original CMA kinetics coefficients. The "scratch" test was not performed on the uninstrumented sample of run #6, so an approximate "char" depth, as described for run #4, was observed. As shown in Fig. 37, the approximate "char" depth for run #6 was found to be 5.1 mm. The predicted "char" depth based on the Aerotherm char criterion was found to be 2.96 mm after a modeled heating period of 33.9 seconds and cooling period of near 15 minutes. These approximated and predicted "char" depths are listed in Table 19. Again, the predicted "char" depth is under-predicting the "measured" "char" depth due to shortcomings in the use of the "slow" three-reaction constant coefficients model of the pyrolysis process.

The heating rate of the thermocouples in run #6 are presented in Fig. 38. For this run, our test facility heated the surface of the test sample at an initial heating rate of near 150 ^{o}C/sec, three times the maximum of 50 ^{o}C/sec for the range of heating rates over which TGA data has been obtained for the CMA pyrolysis kinetics model. The location of TC #2 (2.8 mm) was heated at a rate of near 100 ^{o}C/sec at about t = 25 sec, two times the maximum for this range. With the more realistic measured temperature boundary condition used in the predictions during the cool-down period, this run shows, as did run #4, that the pyrolysis kinetics model under-predicts the mass loss and "char" depth and thus is too slow to adequately represent higher heating rates such as that for this run.

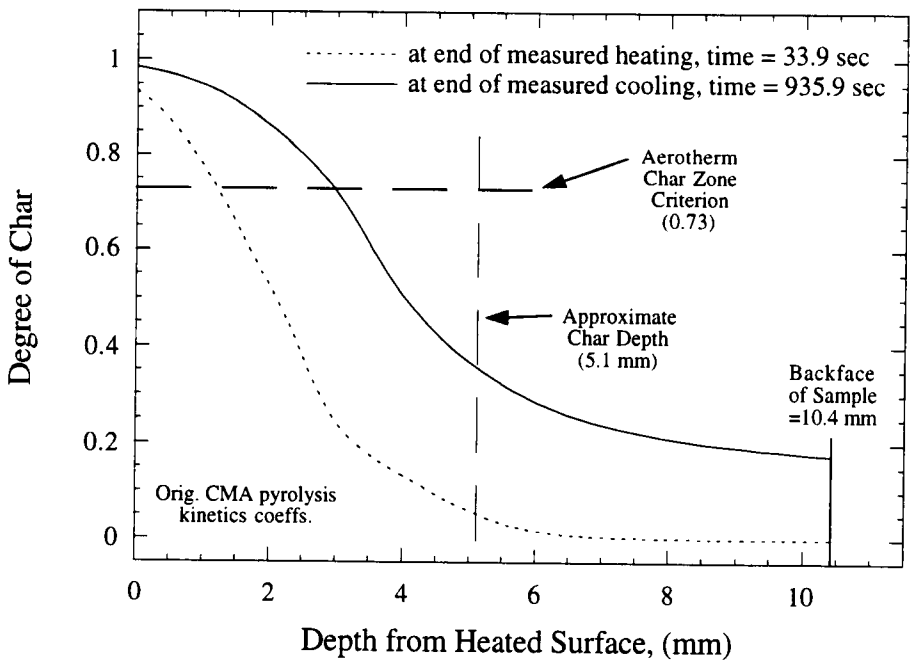


Figure 37 Predicted degree of char after 33.9 sec of heating and near 15 minutes cooling for run #6

Table 19 Comparison of the predicted and "observed" "Char" Depth for run #6

Time	"Char" Depth (mm)	
	Original CMA Kinetics Coefficients[1]	Approximated Char Depth[2]
End of the Heating (t = 33.9 sec)	1.2	--
End of the Cool-down (t = 902.0 sec)	2.96	5.1

[1] Aerotherm char criterion of 0.73 is used to determine the predicted values.
[2] The listed value is an in-house estimation based on observation.

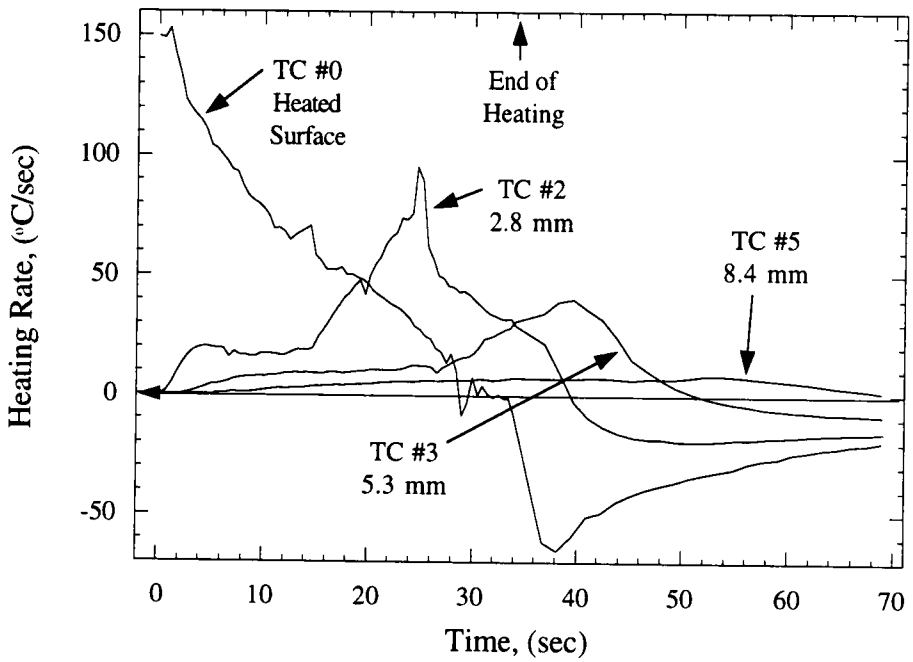


Figure 38 Time history of heating rates for run #6 thermocouples

3.7 Run #7

Seven thermocouples were used in this run; one Type C, and six Type K. The distances of thermocouple beads from the heated surface of the test sample, as measured from the x-ray, are listed in Table 20. Thermocouples #2, 4, and 5 were potted with Boron Nitride paint while thermocouples #1, 3, and 6 were potted with Cotronics C-989 Alumina-based cement. Heating was applied to the samples for 27.9 seconds. The calculated heat flux at the end of this period was found to be 166 ± 4 W/cm^2.

Similar to previous tests, the heater began glowing red in the center at the start of this run, then the glowing quickly spread outward in both directions, and pyrolysis gas flow from the samples was very strong. For this run, no flame was observed during this test.

The thermocouples of run #7 can be divided into three sets, each set consisting of two thermocouples each at similar depths from the heated surface: (1) TC's #1 and 2 at 2.6 and 2.9 mm, (2) TC's #3 and 4 both at 5.3 mm, and (3) TC's #5 and 6 at 7.9 and 8.5 mm. Recall, the Boron Nitride paint used to pot thermocouple #5 (7.9 mm) has very little strength upon drying. The adhesive bond supplied by the paint between the thermocouple and sample was compromised during placement of the sample in the test stand and the thermocouple was inadvertently pulled from the hole prior to firing. The measured output from this displaced thermocouple is not representative of any location in the sample and is therefore disregarded. Figure 39 shows the temperature measurements for the first two pairs of thermocouples, TC's #1 and 2, and TC's #3 and 4. Thermocouples #2 and 4 (2.9 and 5.3 mm) were potted with Boron Nitride paint and are

Table 20 Thermocouple locations for run #7

Thermocouple	Distance from Heated Face (mm)	Potting Compound
TC #0	Surface Boundary	BN paint
TC #1	2.6±0.05	C-989[a]
TC #2	2.9±0.05	BN paint
TC #3	5.3±0.05	C-989[a]
TC #4	5.3±0.05	BN paint
TC #5	7.9±0.05	BN paint
TC #6	8.5±0.05	C-989[a]

[a]C-989 is an Alumina-based cement supplied by Cotronics.

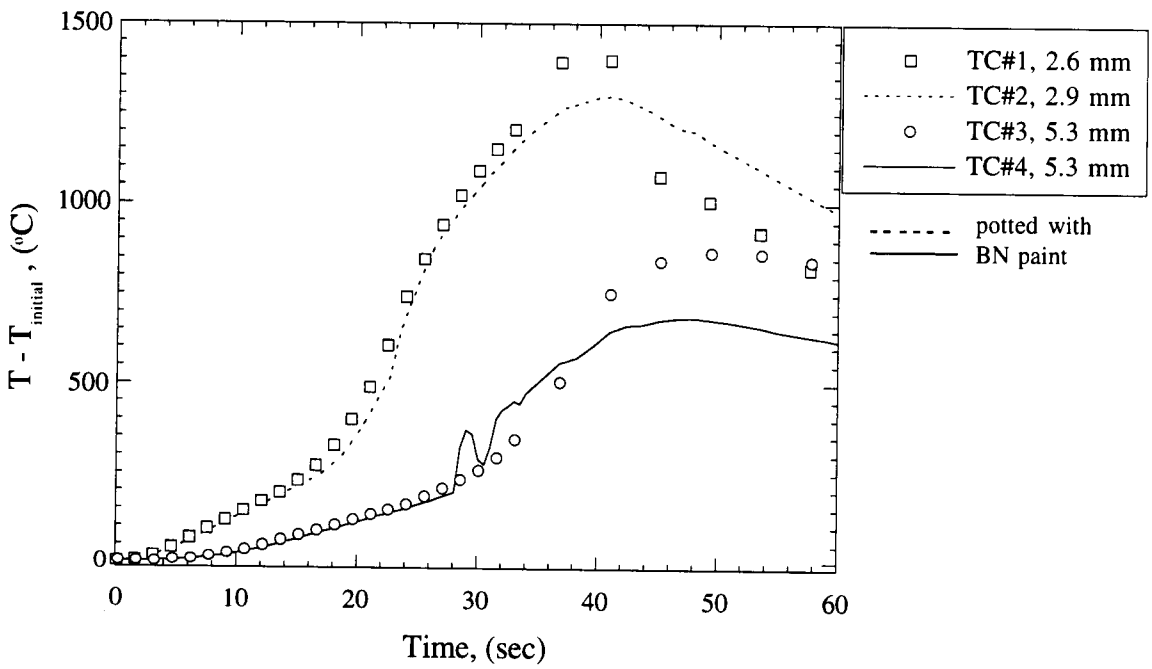


Figure 39 Comparison of measured thermocouple temperatures for run #7

distinguished on Fig. 39 by different line styles. As can be seen from Fig. 39, the measurements of TC's #2 and 4, the ones potted with Boron Nitride, seem reasonable compared to the measurements of TC's 1 and 3, the ones potted with C-989. For example, TC #2 (2.9 mm) potted with Boron Nitride paint is 0.3 mm further from the heated surface than TC #1 (2.6 mm), and the temperature measured by TC #2 is slightly lower than that measured by TC #1. Figure 39 also shows that the temperature measured by TC #4 (5.3 mm, BN paint) becomes corrupted after near t = 28 sec. Since there is only one Boron Nitride-potted thermocouple (TC #2) that gives reasonable measurements over the entire measurement period, and since all three thermocouples potted with C-989 (TC's #1, 3, and 6) give reasonable, uncorrupted measurements over this whole period, the measurements of these three thermocouples are presented as the set of thermal responses to be included in the database.

The temperature measurements of thermocouples #0, 1, 3, and 6 (the heated surface, 2.6 mm, 5.3 mm, and 8.5 mm, respectively) are shown in Fig. 40. Note a maximum temperature near 2038 ^{o}C was achieved at the surface at the end of the heating period (t = 27.9 sec).

The recorded traces of the electrical "leakage" showed that for the HPBN which was insulating the uninstrumented (bottom) sample, the voltage became non-zero near t = 4.4 sec. The plate maintained its insulating effectiveness until about t = 6.2 sec, when the maximum voltage, as set by the Lambda DC power supply, was achieved. The measured voltage across the plate insulating the instrumented (bottom) sample became non-zero at 4.2 sec and the plate maintained its insulating effectiveness until t = 6.6 sec.

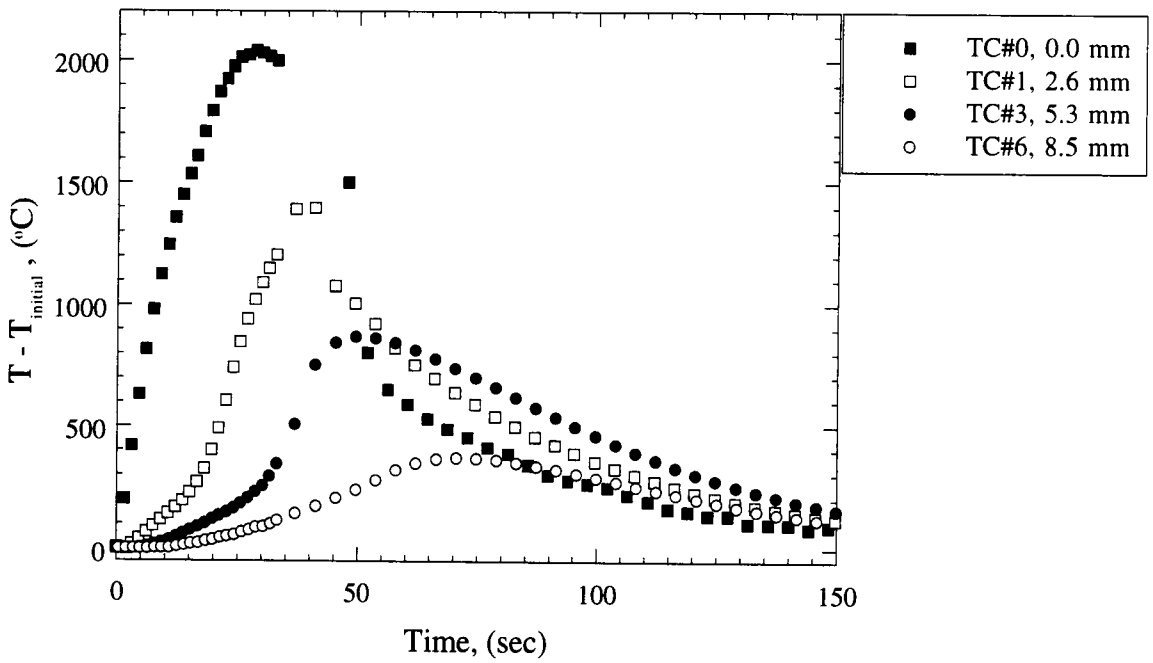


Figure 40 Measured thermocouple temperatures for run #7

As seen and discussed in previous runs, the heated surface temperature of the test sample was near 900 °C at the time insulation effectiveness was lost.

Table 21 lists the mass loss of the uninstrumented test sample. A prediction was made using original CMA pyrolysis kinetics coefficients. Similar to run #6, the experimental measurement of the mass loss (1.1 grams) was under-predicted based on this kinetics model (0.705 grams). The measured heated surface temperature for this run (run #6) was used to generate the known surface boundary condition for both the heating and cooling periods.

Figure 41 compares the temperature predictions based on the CMA kinetics coefficients at the locations of thermocouples #1, 3 and 6 with the measured data. As seen in previous runs and discussed for run #5, the predictions do not capture the trend in the change of the slope of the temperature measurement profile during heating of the thermocouple locations.

The predicted DOC as a function of depth from the heated surface is presented in Fig. 42. The prediction shown is based on the original CMA kinetics model. The "scratch" test was not performed on the uninstrumented sample of run #7, so an approximate "char" depth, as described for run #4, was observed. As shown in Fig. 42, the approximate "char" depth for run #7 was found to be 5.3 mm. The predicted "char" depth based on the Aerotherm char criterion was found to be 2.67 mm after a modeled heating period of 27.9 seconds and cooling period of near 15 minutes. These approximated and predicted "char" depths are listed in Table 22. Again, the predicted

Table 21 Predicted and measured mass loss for run #7

Case	Heating (27.9 sec.)		Cool-Down (910 sec.)		Total Mass Loss
	Mass Loss (grams)	End Temp.[a] (°C)	Mass Loss (grams)	End Temp.[a] (°C)	(grams)
Orig. CMA Kinetics Coefficients	0.270	2038	0.435	20	0.705
Measurement					1.1 ± 0.05

[a]Measured temperature at end of time period by thermocouple #0 at heated surface.

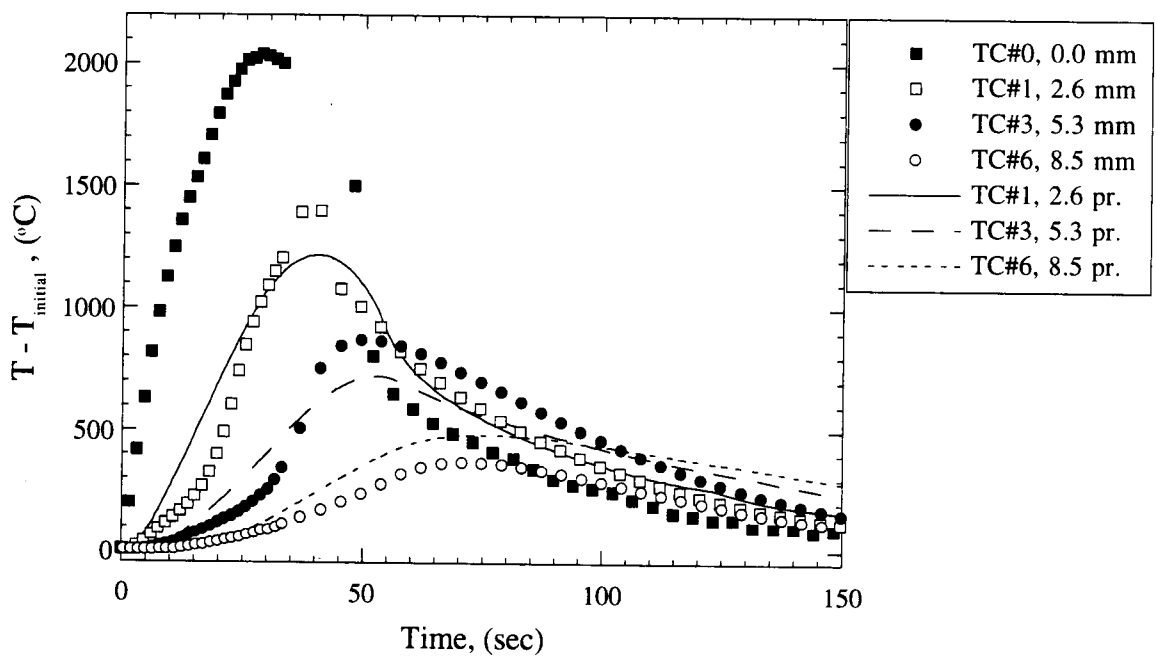


Figure 41 Comparison of run #7 in-depth temperatures with prediction

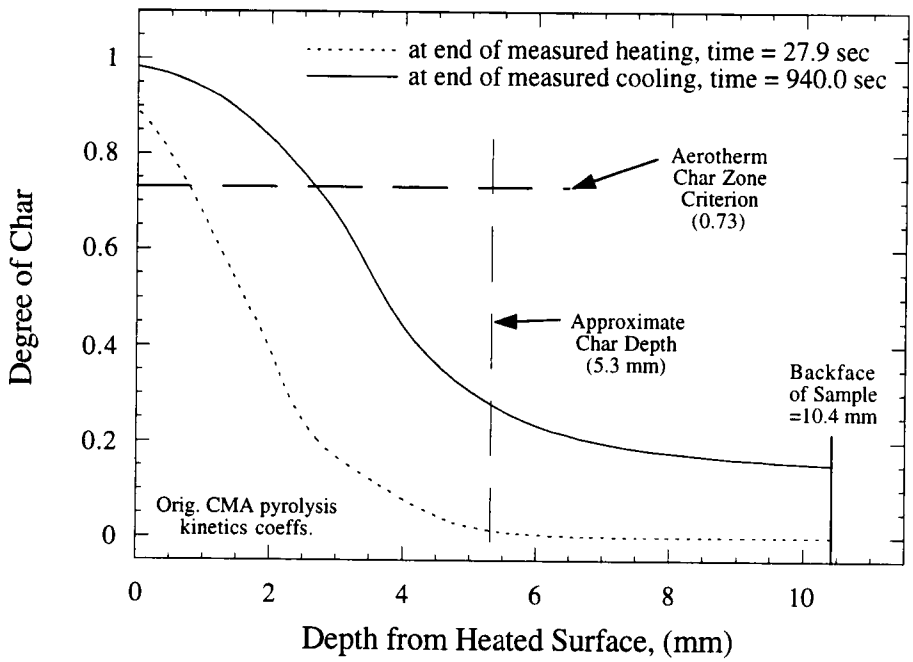


Figure 42 Predicted degree of char after 27.9 sec of heating and near 15 minutes cooling for run #7

Table 22 Comparison of the predicted and "observed" "Char" Depth for run #7

Time	"Char" Depth (mm)	
	Original CMA Kinetics Coefficients[1]	Approximated Char Depth[2]
End of the Heating (t = 27.9 sec)	0.775	--
End of the Cool-down (t = 940 sec)	2.67	5.3

[1]Aerotherm char criterion of 0.73 is used to determine the predicted values.

[2]The listed value is an in-house estimation based on observation.

"char" depth is under-predicting the "measured" "char" depth due to shortcomings in the use of the "slow" three-reaction constant coefficients model of the pyrolysis process.

For this run, our test facility heated the surface of the test sample at an initial heating rate of near 150 °C/sec, three times the maximum of 50 °C/sec for the range of heating rates over which TGA data has been obtained for the CMA pyrolysis kinetics model. The location of TC #1 (2.6 mm) was heated at a rate of near 100 °C/sec at about t = 23 sec, two times the maximum for this range. With the more realistic measured temperature boundary condition used in the predictions during the cool-down period, this run shows again, as did run #4, that the pyrolysis kinetics model under-predicts the mass loss and "char" depth and thus is too slow to adequately represent higher heating rates such as these for this run.

3.8 Run #8

Seven thermocouples were used in this run; one Type C, and six Type K. The distances of thermocouple beads from the heated surface of the test sample, as measured from the x-ray, are listed in Table 23. Thermocouples #2, 4, and 5 were potted with Boron Nitride paint while thermocouples #1, 3, and 6 were potted with Cotronics C-989 Alumina-based cement. Heating was applied to the samples for 51.56 seconds. At the end of the heating period, the surface heat flux was calculated to be 283 ±18 W/cm^2. The output of all seven thermocouples was recorded over this heating period and over a near 15 minute cooling period.

Table 23 Thermocouple locations for run #8

Thermocouple	Distance from Heated Face (mm)	Potting Compound
TC #0	Surface Boundary	BN paint
TC #1	2.4±0.05	C-989[a]
TC #2	2.7±0.05	BN paint
TC #3	4.7±0.05	C-989[a]
TC #4	5.3±0.05	BN paint
TC #5	7.8±0.05	C-989[a]
TC #6	8.3±0.05	BN paint

[a]C-989 is an Alumina-based cement supplied by Cotronics.

Similar to previous tests, the heater began glowing red in the center at the start of this run, then the glowing quickly spread outward in both directions, and pyrolysis gas flow from the samples was very strong. The highest level of power input yet was applied to run #8. While there was no flame from ignition of the pyrolysis gases, the temperature was raised high enough to decompose the HPBN causing sparking of the Boron metal, and high enough to burn out five of the seven instrumented thermocouples.

The thermocouples of run #8 can be divided into three sets, each set consisting of two thermocouples each at similar depths from the heated surface: (1) TC's #1 and 2 at 2.4 and 2.7 mm, (2) TC's #3 and 4 at 4.7 and 5.3 mm, and (3) TC's #5 and 6 at 7.8 and 8.3 mm. Figures 43, 44, and 45 show the temperature measurements of each of these pairs, respectively. Figure 43 shows that TC's #1 and 2 burn out at about t = 23 seconds near 1350 ^{o}C. Figure 44 shows that TC's #3 and 4 burn out at about t = 36 seconds, also near 1350 ^{o}C. This is as expected since the upper limit of the temperature range of Type K thermocouples is near 1370 ^{o}C. Figure 45 shows that the set of thermocouples farthest from the heated surface, TC's #5 and 6, were not burned out and actually gave plausible output traces over the entire measurement period. These two thermocouples did not reach their maximum use temperature. Thermocouples #2, 4, and 6 were potted with Boron Nitride paint and are distinguished on the figures by dashed lines. As can be seen from Figs. 43, 44, and 45 the measurements of TC's #2, 4, and 6, the ones potted with Boron Nitride, seem reasonable compared to the measurements of TC's 1, 3, and 5, the ones potted with C-989, with respect to their distances from the heated surface. In view of the discussion in run #5, the close measurement profiles of TC's 3 and 4 shown in Fig. 44, coupled with the difference in depth from the heated surface of 0.6 mm, suggests the presence of air filled voids within the well of the Boron Nitride-potted TC #4. And since

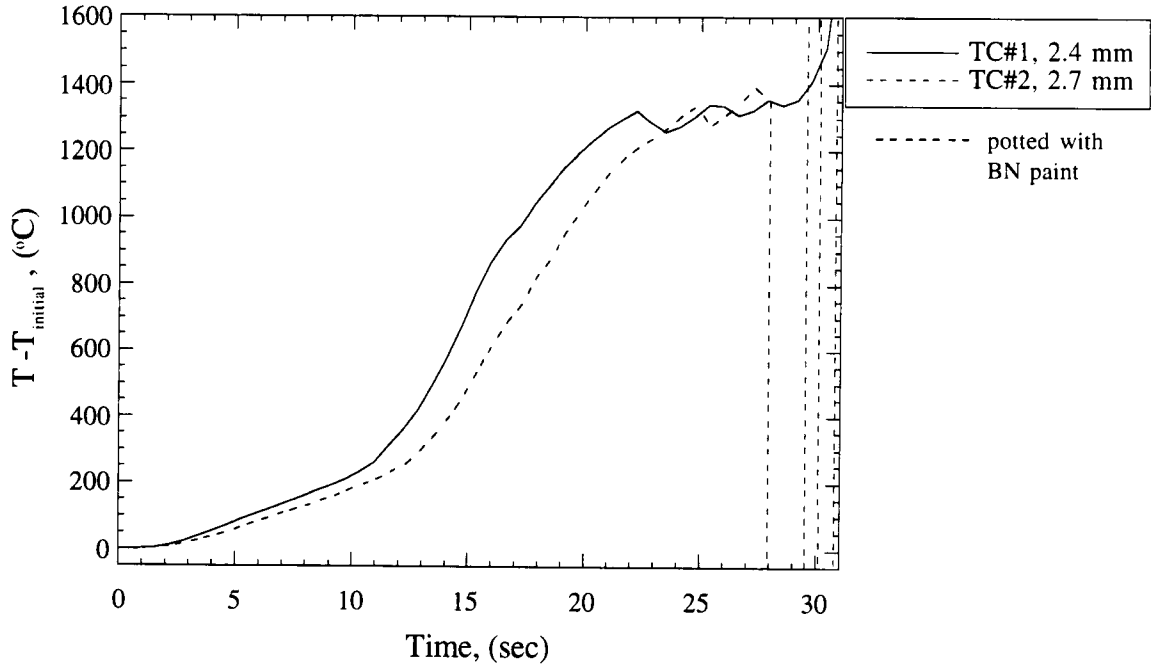


Figure 43 Comparison of measured thermocouple temperatures for thermocouples #1 and 2 for run #8

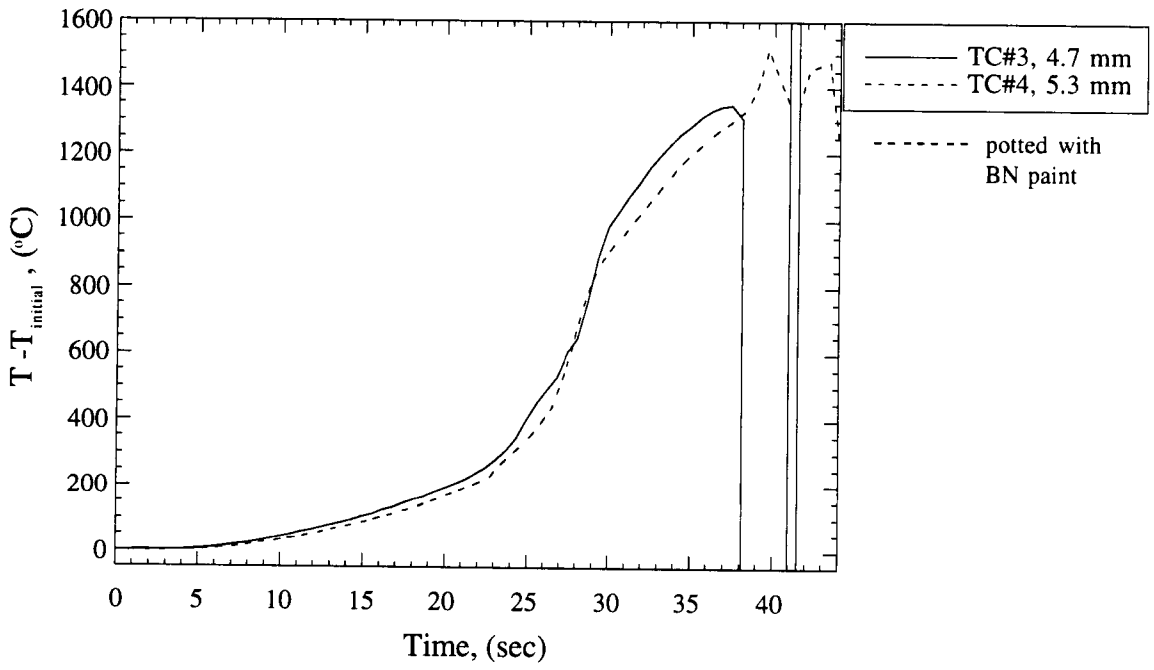


Figure 44 Comparison of measured thermocouple temperatures for thermocouples #3 and 4 for run #8

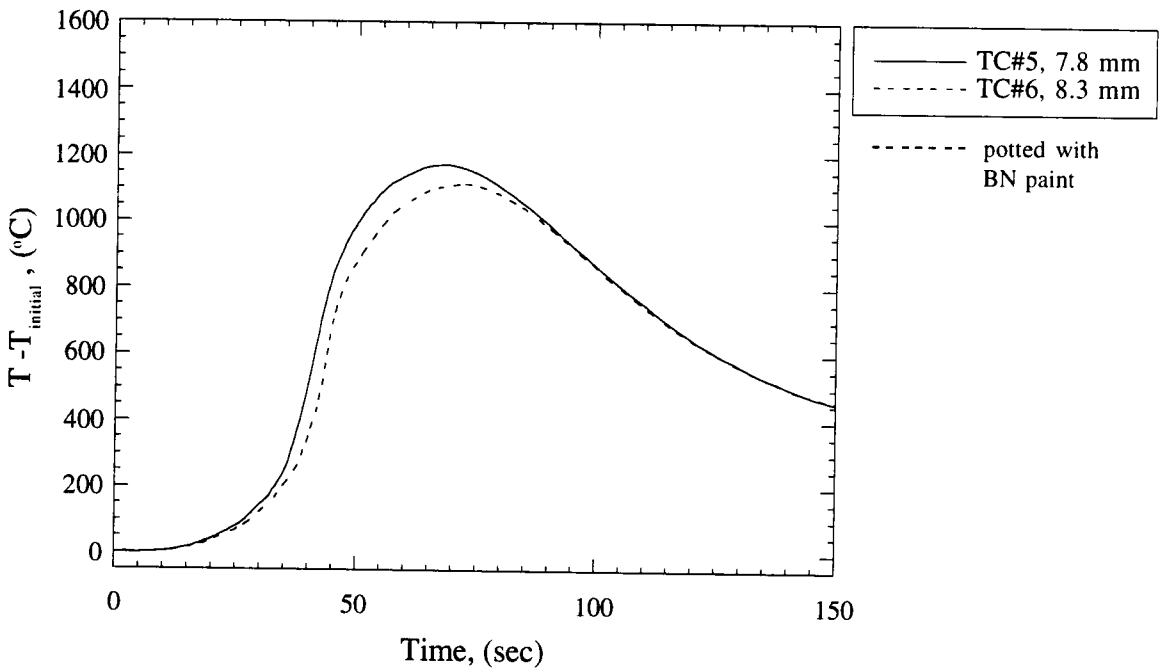


Figure 45 Comparison of measured thermocouple temperatures for thermocouples #5 and 6 for run #8

thermocouples cannot measure higher than their surroundings, this close agreement of the measurements also suggests that the cement-potted thermocouple exhibits substantial error.

The temperature measurements of the cement-potted thermocouples are shown in Fig. 46. Only the portions of the measured output traces (before thermocouple burn outs) are represented. Note a maximum temperature near 2200 °C was achieved at the surface near t = 22 seconds. It is at this time that the surface thermocouple burned out. In an inert environment, Type C thermocouples have a maximum-use temperature of near 2760 °C and a short-time maximum-use temperature of near 3000 °C. The maximum measured temperature of 2200 °C is not surprising considering the presence of the oxidizing pyrolysis gases.

The recorded traces of the electrical "leakage" showed that for the HPBN which was insulating the uninstrumented (bottom) sample, the voltage became non-zero near t = 3.0 sec. The plate maintained its insulating effectiveness until about t = 5.4 sec, when the maximum voltage, as set by the Lambda DC power supply, was achieved. The measured voltage across the plate insulating the instrumented (bottom) sample became non-zero at 3.1 sec and the plate maintained its insulating effectiveness until t = 4.8 sec. Consistent with previous runs, the heated surface of the test sample reached 900 °C near the time of insulating effectiveness breakdown, in this run near t = 5 sec, and the in-depth thermocouples exhibited the trend of an increasing change in slope afterwards. After firing, the plates appeared dark gray and a hollow concave indention on the heated side of the insulating plate due to the decomposition was observed. The plates did not regain any

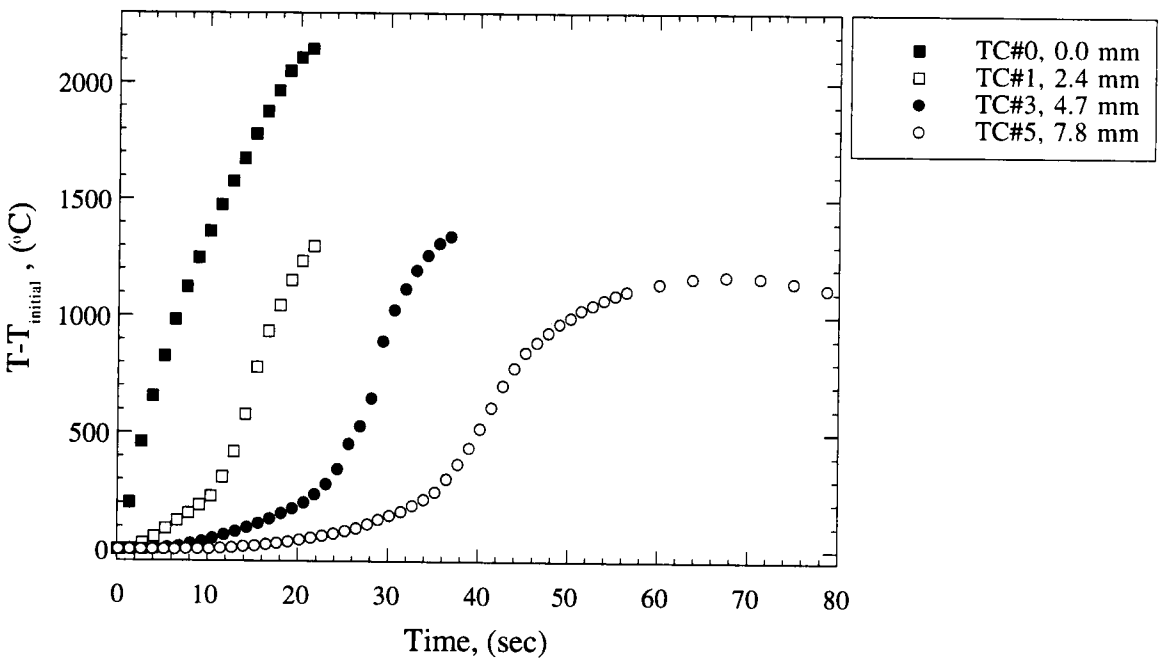


Figure 46 Measured thermocouple temperatures for run #8

of their high electrical resistance upon cooling, so Joulean heating was possible during the later part of the run.

Figure 47 compares the temperature predictions, based on the original CMA kinetics coefficients, at the locations of thermocouples #1, 3 and 5 with the measured data for $t < 22$ seconds. This was the only time period over which a measured boundary condition was available. As seen in previous runs and discussed for run #5, the predictions do not capture the trend in the change of the slope of the temperature measurement profile during heating of the thermocouple location near the heated surface (2.4 mm). If a longer boundary condition was available, the predictions would also first over-predict, then under-predict the temperature measurement profiles of the other thermocouples (4.7 and 7.8 mm) shown in Fig. 47.

The predicted mass loss and DOC were not found because of the unavailability of an adequate boundary condition over the heating and cooling periods. The mass loss itself was not measured because the HPBN plates were strongly adhered to the samples after the run. Attempts to separate the sample for weighing would have broken off pieces of the sample invalidating the mass measurement. The observation of an approximate "char" depth, as discussed in run #4, resulted in a depth of near 10 mm. This value, though, is not considered to be accurate because the discolored strip around the sides was not uniform.

The heating rate of TC's #1, 3, and 5 in run #8 are presented in Fig. 48. For this run, our test facility heated the surface of the test sample at initial heating rates of near 240 ^{o}C/sec, almost five times the maximum of 50 ^{o}C/sec for the range of heating rates

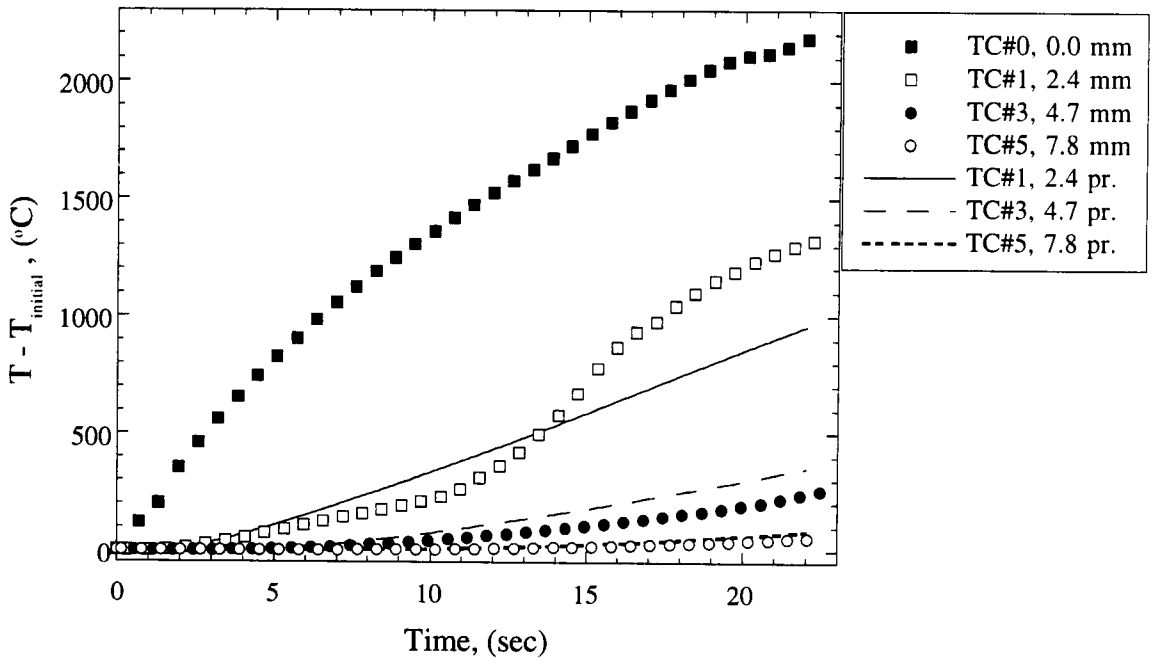


Figure 47 Comparison of run #8 in-depth temperatures with prediction

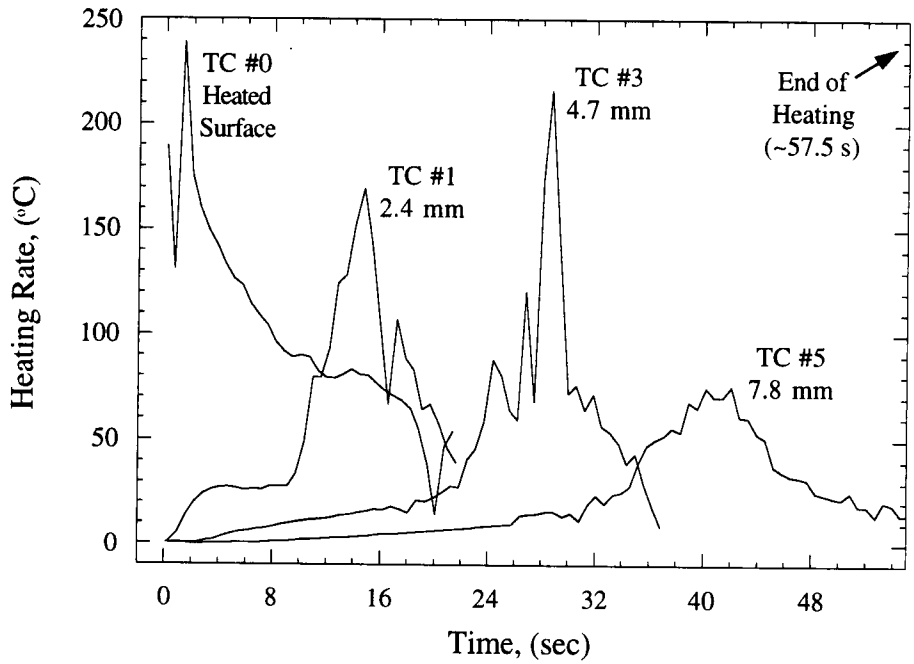


Figure 48 Time history of heating rates for run #8 thermocouples

over which TGA data has been obtained for the CMA pyrolysis kinetics model. The locations of TC's #1, 3, and 5 (2.4 mm, 4.7 mm, and 7.8 mm) were heated at a rates of near 170 ^{o}C/sec at about t = 14 sec, 220 ^{o}C/sec at about t = 28 sec, and 70 ^{o}C/sec near t = 41 sec, respectively. All of these rates are well over the maximum range for the rates over which the kinetics model has a valid database.

Chapter 4

4.0 Conclusions and Future Considerations

The proposed experimental facility has the capability of producing initial heating rates over 250 °C/sec and obtaining maximum temperatures over 2000 °C. A limited database, compiling the results of the eight experiments presented here, is found in Appendix A. In Tables A-6 through 14, tabulated values for the measured boundary condition and thermocouple outputs believed to be accurate are given. This data could be used to verify numerical codes modeling high heating rates.

Although the presented experimental facility has met the stated heating rate and maximum temperature goals, it still does not reproduce conditions (> 500 °C/sec and >3000 °C) experienced by the SRM nozzle liner during actual flight. This facility was limited in the amount of power it could supply by the regulated AC power supply. Even if technical limitations such as these are removed, the ability to collect quality data at higher temperature conditions must be improved.

To collect temperature data at these levels, Type C or Type S thermocouples could be used at the in-depth locations near the heated surface. Also, in view of the discussion presented in run #5, potting these thermocouples in "air", bare in the hole, would allow for a faster thermocouple response at high temperatures. In addition, since the details of the installation of a cement-potted thermocouple may be impossible to determine, for example the degree of uniformity of the filling of the drilled hole and a way of quantifying the contact resistance between the cement and the host material, 'air-

potting' might be a better installation method of choice for all the thermocouples in high heat rate, highly transient experiments such as the one for this project. Through the use of guides, more control can be implemented on the placement of the thermocouple bead in the drilled hole, and the details of the installation can be specified with more confidence. This would allow for more confidence in the analysis of the time response of the installed thermocouple, which in turn would allow for the correction of the thermocouple lag time. The benefits and limitations of such a process should be further explored.

The problem of maintaining and measuring a valid boundary condition at these extreme levels is not as easily addressed. But it might not be necessary. If a numerical model is suggested that can predict the results of previously performed experiments at the lower heating rates and temperatures as well as predict the results of the database presented here, it would seem reasonable that the confidence developed by these predictions could be extended to predictions of actual flight conditions.

The currently "accepted" kinetics model used by the CMA code has been shown to be unable to predict the thermal response of carbon-phenolic subjected to a high heat flux. Through "tweaking" of the kinetics coefficients, the CMA coefficients have been shown to be in error by at least an order of magnitude. An improved kinetics model can lead to accurate prediction of the "char" depth, and therefore the mass loss, which is an important design parameter for a SRM. It was noted that the predicted temperatures had negligible dependence on the pyrolysis kinetics coefficients. The analysis of run #5 concerning the thermocouple installation suggests that the disparity between the predicted and measured slopes of the thermal response could be due to measurement error. The

analysis suggests that the measurements should be adjusted by a time dependent correction factor towards the predicted values. Therefore, the possibility that the predicted temperatures are accurate exists and should be further examined. With an improved kinetics model, accurate predictions of the in-depth temperatures as well as the "char" depth (mass loss) are possible.

References

References

[1] Beck, T. A., P. A. Johnson, M. L. Gordon, and B. Laub, "IUS Nozzle Thermal Characterization," Acurex report FR-84-21/ATD, August, 1984, pp. 46-51

[2] Clayton, F. I., "Derivation of New Thermal Decomposition Model for Carbon-Phenolic Composites," Technical report to Hercules Incorporated, Magna, Utah, Subcontract 1157-03027, August, 1994.

[3] Keyhani, M,. "UT1D Predictions of Thermocouples in the FM5055 Sections of the SPIP 48-3 Nozzle" University of Tennessee, Knoxville, TN, January, 1994.

[4] Keyhani, M., and V. Krishnan, "Thermal Response of a Decomposing Polymer," Heat Transfer in Porous Media, Eds., M. Faghri and L. C. Burmeister, ASME HTD-Vol. 240, 1993, pp. 35-42.

[5] Keyhani, M., and V. Krishnan, "A One-Dimensional Model for Thermal response of a Decomposing Polymer," proceedings, Computational Mechanics of Porous Solid Materials and Their Thermal Decomposition, Eds.,. Salamon, N. J., and Sullivan, R. M., ASME AMD-Vol. 136, 1992, pp. 81-90.

[6] Keyhani, M., and V. Krishnan, "A One-Dimensional Thermal Model With an Efficient Scheme for Surface Recession," 1992 JANNAF Rocket Nozzle Technology Subcommittee Meeting, Lockheed Missiles and Space Company, Sunnyvale, California, 1992.

[7] Keyhani, M., and S. Liter, "Experimental Investigation of Thermal Response of Decomposing Polymers - Code Verification," Technical report to Hercules Incorporated, Magna, Utah, Subcontract 1157-03175, January, 1995.

[8] Keyhani, M., and R. A. Polehn, "Finite Difference Modeling of Anisotropic Flows," Journal of Heat Transfer, Vol. 117, No. 2, pp. 458-464, 1995.

[9] Krishnan, V., "A One-Dimensional Model for the Thermal Response of a Decomposing Polymer," M. S. Thesis, University of Tennessee, Knoxville, TN, August, 1992.

[10] Pitman, F., "Experimental and Numerical Investigation of Heat Transfer in Polymers," M. S. Thesis, University of Tennessee, Knoxville, TN, August, 1993.

[11] Polehn, R. A., "Thermal Response of an Axisymmetric, Charring-Decomposing Polymer," Ph. D. Dissertation, University of Tennessee, Knoxville, TN, May, 1994.

[12] Polehn, R. A., and M. Keyhani, "Comparison of Pore Pressure Prediction Schemes for Flow Through Variable Permeability Media," 1993 JANNAF Rocket Nozzle Technology Subcommittee Meeting, Marshal Space Flight Center, Alabama, 1993.

[13] Polehn, R. A., and M. Keyhani, "Difficulties in Modeling Two-Dimensional Flows in a Decomposing Composite," 1992 JANNAF Rocket Nozzle Technology Subcommittee Meeting, Lockheed Missiles and Space Company, Sunnyvale, California, 1992.

[14] Polehn, R. A., M. Keyhani, and M. Parang, "Transient Compressible Flow in Variable Permeability Media," Journal of Thermophysics and Heat Transfer, Vol. 8, No. 2, 1994, pp. 374-381.

[15] Ross, R. and F. Strobel, "CMA90S Input Guide and User's Manual," Aerotherm division of the Acurex Corporation, December, 1990, pp. 38-39.

[16] Stokes, E. H., "Compressibility of Carbon-Phenolic Pyrolysis Gas Products and a Discussion of Other Factors Contributing to Internal Gas Pressure Calculation," 1990 JANNAF Rocket Nozzle Technology Subcommittee Meeting, October 23-25, 1990.

[17] Stokes, E. H., "Kinetics of Pyrolysis Mass Loss from Phenolic Resin Based Composites," Technical report to Marshal Space Flight Center, Alabama, Contract NAS8-37801, October, 1993, pp. 235-245.

[18] Stokes, E. H. and J. R,. Koenig, "The Physical, Mechanical, and Thermal Properties of the FM 5055 404 Aft Inlet Ring," Southern Research Institute report # SRI-MME-88-201-6032-1, March, 1988, pp. 41-120.

Appendices

Appendix A

High heating rate database

Table A-1 Instrumented test sample dimensions for each experiment

Case	Width (mm)	Height (mm)	Length (mm)
Experiment #1	19.9 ± 0.05	10.4 ± 0.05	40.0 ± 0.05
Experiment #2	20.0 ± 0.05	10.4 ± 0.05	39.9 ± 0.05
Experiment #3	19.9 ± 0.05	10.4 ± 0.05	39.9 ± 0.05
Experiment #4	20.0 ± 0.03	10.4 ± 0.03	39.9 ± 0.05
Experiment #5	20.0 ± 0.03	10.4 ± 0.03	39.9 ± 0.05
Experiment #6	20.0 ± 0.05	10.4 ± 0.05	39.8 ± 0.08
Experiment #7	19.9 ± 0.05	10.4 ± 0.05	39.9 ± 0.05
Experiment #8	19.9 ± 0.05	10.4 ± 0.05	39.9 ± 0.05

Table A-2 Uninstrumented test sample dimensions for each experiment

Case	Width (mm)	Height (mm)	Length (mm)
Experiment #1	19.9 ± 0.08	10.4 ± 0.08	39.9 ± 0.05
Experiment #2	20.2 ± 0.05	10.4 ± 0.05	39.9 ± 0.05
Experiment #3	20.0 ± 0.05	10.4 ± 0.03	39.9 ± 0.05
Experiment #4	20.0 ± 0.03	10.4 ± 0.03	39.9 ± 0.05
Experiment #5	20.0 ± 0.03	10.5 ± 0.03	39.9 ± 0.05
Experiment #6	19.9 ± 0.08	10.4 ± 0.05	40.0 ± 0.08
Experiment #7	19.9 ± 0.03	10.4 ± 0.05	40.0 ± 0.08
Experiment #8	19.9 ± 0.03	10.4 ± 0.05	39.9 ± 0.05

Table A-3 Uncoated graphite heater dimensions for each experiment

Case	Width (mm)	Height (mm)	Length[a] (mm)
Experiment #1	19.9 ± 1.3	1.2 ± 0.05	45.6 ± 0.25
Experiment #2	19.9 ± 1.3	1.2 ± 0.05	46.7 ± 0.25
Experiment #3	19.9 ± 0.05	1.2 ± 0.05	46.5 ± 0.25
Experiment #4	19.9 ± 0.05	1.2 ± 0.05	46.4 ± 0.25
Experiment #5	19.9 ± 0.05	1.2 ± 0.05	46.1 ± 0.25
Experiment #6	19.9 ± 0.05	1.2 ± 0.05	47.0 ± 0.25
Experiment #7	19.9 ± 0.05	1.2 ± 0.05	46.4 ± 0.25
Experiment #8	19.9 ± 0.05	1.2 ± 0.05	46.2 ± 0.25

[a]The listed value is the distance between the local voltage probes.

Table A-4 Current, voltage, resistance, and calculated surface heat flux at the end of heating for each experiment

Case	Measured Current (Amps)	Local Voltage (Volts AC)	Calculated Resistance (Ohms)	Final Heat Flux (W/cm^2)
Experiment #1	293 ± 6	5.0 ± 0.1[a]	0.0171 ± 0.0005	81 ± 6
Experiment #2	–	–	–	–
Experiment #3	290 ± 6	5.3 ± 0.1[a]	0.0183 ± 0.0005	83 ± 6
Experiment #4	325 ± 7	6.4 ± 0.1[a]	0.0197 ± 0.0005	113 ± 7
Experiment #5	363 ± 7	7.0 ± 0.1[a]	0.0193 ± 0.0005	138 ± 8
Experiment #6	376 ± 8	7.5 ± 0.1[a]	0.0199 ± 0.0005	151 ± 9
Experiment #7	389 ± 8	7.9 ± 0.1[a]	0.0203 ± 0.0005	166 ± 10
Experiment #8	510 ± 10	10.2 ± 0.6[b]	0.020 ± 0.001[c]	283 ± 41

[a]The listed value was measured across the local voltage probes.

[b]The listed value was calculated from an approximated resistance.

[c]The listed value was approximated from the calculated resistance values.

Table A-5 Total mass loss and "char" depth of uninstrumented test sample for each experiment

Case	Measured Total Mass Loss (grams)	"Char" Depth from Heated Surface (mm)
Experiment #1	0.3 ± 0.05	2.3[1]
Experiment #2	0.7 ± 0.05	2.9[1]
Experiment #3	1.1 ± 0.05	3.4[1]
Experiment #4	1.3 ± 0.05	5.1[2]
Experiment #5	0.9 ± 0.05	4.8[2]
Experiment #6	1.1 ± 0.05	5.1[2]
Experiment #7	1.1 ± 0.05	5.3[2]
Experiment #8	--	--
Calculated Maximum	1.67	--

[1]The listed value is the average of 4 experimental measurements made by MSFC using the "Scratch" Test.

[2]The listed value is an approximation made by observation.

Table A-6 Experimental temperature data for run #1

Boundary Condition: Power (Watts(time)) = $1185.9 + 138.89t - 21.421t^2 + 1.0326t^3$

$T_{initial} = 21.5 \pm 2.2$ °C Heating Time = 13.3 sec

Time (sec) (1.7 mm)	$T-T_{initial}$ (°C) (1.7 mm)	Time (sec) (5.4 mm)	$T-T_{initial}$ (°C) (5.4 mm)
0.00	0.00	0.00	0.00
0.08	0.28	0.16	0.00
0.52	0.94	0.59	0.01
0.74	3.06	0.81	0.11
1.18	14.49	1.25	0.50
1.40	23.10	1.47	0.53
1.83	42.64	1.91	0.10
2.05	52.72	2.12	0.18
2.49	72.92	2.56	0.24
2.71	82.77	2.78	0.43
3.15	101.53	3.22	0.90
3.36	110.22	3.44	1.16
3.80	126.91	3.87	1.97
4.02	135.09	4.09	2.65
4.46	150.15	4.53	3.92
4.68	156.86	4.75	4.61
5.11	168.46	5.19	6.59
5.33	173.21	5.41	7.62
5.77	187.36	5.84	9.70
5.99	196.14	6.06	11.02
6.43	215.83	6.50	13.87
6.65	228.22	6.72	15.07
7.08	252.81	7.16	18.22
7.30	265.70	7.38	20.02
7.74	293.46	7.81	23.49
7.96	308.81	8.03	24.86
8.40	341.84	8.47	28.12
8.62	359.46	8.69	30.51
9.05	395.97	9.13	34.60
9.27	414.97	9.34	36.04
9.71	453.77	9.78	40.14
9.93	474.47	10.00	42.73
10.36	521.99	10.44	46.63
10.58	550.72	10.66	48.76

Table A-7 Experimental temperature data for run #2

$T_{initial}$ = 19.8 ± 2.2 °C Heating Time = 9.8 sec

Time (sec) (surface)	$T-T_{initial}$ (°C) (surface)	Time (sec) (1.9 mm)	$T-T_{initial}$ (°C) (1.9 mm)	Time (sec) (2.9 mm)	$T-T_{initial}$ (°C) (2.9 mm)	Time (sec) (6.6 mm)	$T-T_{initial}$ (°C) (6.6 mm)
0.00	0.00	0.00	0.00	0.00	0.00	0.00	-0.00
0.07	6.00	0.12	-0.33	0.18	0.07	0.23	0.11
0.62	157.50	0.68	0.93	0.73	0.19	0.79	0.02
0.90	228.03	0.96	5.04	1.01	1.40	1.07	0.15
1.46	346.56	1.51	24.84	1.57	9.01	1.63	0.04
1.74	400.53	1.79	37.95	1.85	15.72	1.90	0.10
2.57	537.48	2.63	79.98	2.68	41.34	2.74	0.17
2.85	581.21	2.91	92.80	2.96	50.69	3.02	0.36
3.41	659.44	3.47	116.91	3.52	68.84	3.58	0.56
3.69	699.67	3.74	127.22	3.80	77.86	3.86	0.81
4.25	769.23	4.30	143.43	4.36	94.92	4.41	1.43
4.52	803.29	4.58	151.49	4.64	103.33	4.69	1.97
5.08	869.09	5.14	165.12	5.19	119.40	5.25	3.19
5.36	901.80	5.42	171.21	5.47	128.02	5.53	3.83
5.92	967.60	5.97	197.77	6.03	145.96	6.08	5.64
6.20	994.17	6.25	212.45	6.31	153.88	6.36	6.56
6.75	1051.41	6.81	240.98	6.86	169.33	6.92	8.76
7.03	1079.24	7.09	255.33	7.14	185.22	7.20	9.99
7.59	1140.19	7.64	288.29	7.70	200.06	7.76	12.61
7.87	1166.47	7.92	308.75	7.98	194.72	8.04	14.26
8.43	1220.04	8.48	369.34	8.54	205.12	8.59	17.09
8.70	1246.76	8.76	393.98	8.82	226.78	8.87	18.73
9.26	1294.46	9.32	453.60	9.37	226.46	9.43	22.17
9.54	1319.50	9.60	507.47	9.65	254.95	9.71	23.77
10.10	1321.69	10.15	597.75	10.21	310.77	10.26	27.67
10.38	1309.65	10.43	648.04	10.49	322.77	10.54	29.57
10.93	1292.83	10.99	722.59	11.04	352.90	11.10	33.58
11.77	1264.41	11.82	782.07	11.88	431.19	11.94	40.58
12.60	1236.38	12.66	803.60	12.72	522.99	12.77	48.62
12.88	1230.48	12.94	807.63	12.99	546.48	13.05	51.24
13.44	1210.00	13.50	808.33	13.55	572.54	13.61	56.54
14.28	1186.00	14.33	806.12	14.39	614.35	14.44	64.71
14.56	1178.70	14.61	817.91	14.67	622.97	14.72	67.43
15.11	1165.39	15.17	834.77	15.22	636.41	15.28	73.21
16.78	1120.39	16.84	814.39	16.90	658.43	16.95	90.90
17.62	1096.79	17.68	803.78	17.73	669.91	17.79	99.66
18.74	1068.84	18.79	799.62	18.85	677.78	18.90	110.91
19.57	1046.93	19.63	793.61	19.68	680.89	19.74	119.43
20.41	1027.19	20.46	786.85	20.52	681.57	20.57	127.31

Table A-8 Experimental temperature data for run #3

$T_{initial}$ = 26.1 ± 2.2 °C Heating Time = 32.2 sec

Time (sec) (surface)	$T-T_{initial}$ (°C) (surface)	Time (sec) (2.1 mm)	$T-T_{initial}$ (°C) (2.1 mm)	Time (sec) (2.6 mm)	$T-T_{initial}$ (°C) (2.6 mm)	Time (sec) (5.5 mm)	$T-T_{initial}$ (°C) (5.5 mm)
0.00	0.00	0.00	0.00	0.00	0.00	0.00	0.00
0.07	0.00	0.32	0.13	0.45	0.00	0.13	0.06
0.57	38.34	0.82	0.31	0.94	0.00	0.63	0.02
1.07	77.22	1.32	2.01	1.44	0.38	1.13	0.03
2.06	142.52	2.31	12.46	2.44	4.58	2.13	0.05
3.06	212.82	3.31	29.66	3.43	13.91	3.12	0.31
3.56	243.07	3.80	39.79	3.93	20.02	3.62	0.66
4.55	300.99	4.80	61.30	4.92	34.37	4.61	2.16
5.05	329.04	5.30	72.27	5.42	42.28	5.11	3.30
5.55	355.95	5.80	83.11	5.92	50.51	5.61	4.78
7.04	435.95	7.29	112.46	7.41	76.00	7.10	10.98
7.54	461.96	7.79	121.61	7.91	84.14	7.60	13.56
8.03	487.48	8.28	130.40	8.41	92.02	8.10	16.42
8.53	512.09	8.78	138.85	8.91	99.59	8.59	19.41
9.53	560.22	9.78	154.63	9.90	114.67	9.59	25.87
10.52	606.37	10.77	170.54	10.90	129.47	10.59	32.73
11.02	628.49	11.27	178.04	11.39	136.72	11.08	36.36
12.02	670.83	12.27	193.76	12.39	150.68	12.08	43.58
12.51	691.64	12.76	201.66	12.89	157.32	12.58	47.42
13.01	711.92	13.26	209.53	13.38	163.92	13.07	51.19
14.01	752.08	14.26	226.83	14.38	177.61	14.07	59.00
15.00	789.28	15.25	244.31	15.38	191.76	15.06	66.71
15.50	807.26	15.75	253.16	15.87	198.67	15.56	70.42
16.00	825.03	16.25	262.38	16.37	206.62	16.06	74.22
16.50	842.49	16.74	272.36	16.87	214.32	16.56	77.82
17.99	892.77	18.24	305.22	18.36	235.15	18.05	90.59
18.49	908.81	18.73	316.73	18.86	242.16	18.55	96.51
18.98	925.53	19.23	329.26	19.36	250.88	19.05	100.99
19.98	958.17	20.23	355.90	20.35	271.69	20.04	109.40
20.48	974.38	20.73	369.41	20.85	282.18	20.54	112.22
21.47	1005.39	21.72	398.20	21.85	303.36	21.53	124.76
22.47	1035.80	22.72	433.95	22.84	330.29	22.53	128.06
22.96	1050.99	23.21	449.51	23.34	342.88	23.03	136.13
23.46	1065.59	23.71	466.93	23.84	357.87	23.52	142.95
23.96	1080.06	24.21	487.51	24.33	373.09	24.02	146.77
25.45	1122.26	25.70	546.23	25.83	422.75	25.52	158.55
26.45	1148.98	26.70	589.81	26.82	455.61	26.51	163.43
27.94	1187.07	28.19	650.55	28.31	528.98	28.00	179.96
28.94	1212.23	29.19	688.99	29.31	597.64	29.00	184.24

Table A-9 Experimental temperature data for run #4

$T_{initial}$ = 21.6 ± 2.2 °C Heating Time = 46.7 sec

Time (sec) (surface)	$T-T_{initial}$ (°C) (surface)	Time (sec) (2.8 mm)	$T-T_{initial}$ (°C) (2.8 mm)	Time (sec) (5.2 mm)	$T-T_{initial}$ (°C) (5.2 mm)	Time (sec) (8.0 mm)	$T-T_{initial}$ (°C) (8.0 mm)
0.00	0.00	0.00	-0.00	0.00	-0.00	0.00	0.00
2.55	263.73	2.86	9.28	2.61	0.14	2.74	0.04
5.54	522.70	5.85	56.32	5.60	6.10	5.73	0.29
8.53	739.10	8.84	108.66	8.59	23.01	8.71	2.17
11.51	933.11	11.82	151.35	11.58	44.95	11.70	7.30
14.50	1095.98	14.81	196.38	14.56	68.05	14.69	15.57
17.49	1237.32	17.80	246.92	17.55	92.12	17.67	25.91
20.47	1369.29	20.79	328.46	20.54	117.87	20.66	38.39
23.46	1488.25	23.77	444.33	23.52	144.07	23.65	52.64
26.45	1598.50	26.76	619.62	26.51	168.28	26.64	68.38
29.44	1696.92	29.75	780.54	29.50	197.51	29.62	85.35
32.42	1781.75	32.73	868.01	32.49	230.85	32.61	103.55
35.41	1851.13	35.72	956.24	35.47	268.04	35.60	122.03
38.40	1912.84	38.71	1034.83	38.46	319.94	38.58	140.93
41.38	1961.80	41.70	1112.92	41.45	402.83	41.57	160.59
46.69	2021.75	46.97	1221.49	46.74	612.90	46.86	196.62
55.07	1621.13	55.35	1227.57	55.12	851.73	55.24	259.08
63.44	1346.97	63.73	1117.43	63.50	871.32	63.61	357.10
71.82	1145.38	72.11	1006.76	71.88	840.59	71.99	442.09
80.20	991.76	80.48	909.63	80.26	797.51	80.37	489.21
88.58	868.81	88.86	826.03	88.64	750.80	88.75	509.96
96.96	768.13	97.24	752.79	97.01	703.82	97.13	513.26
105.34	684.56	105.62	687.43	105.39	657.86	105.51	504.87
113.71	614.48	114.00	629.81	113.77	614.01	113.88	489.01
122.09	555.08	122.38	578.11	122.15	573.06	122.26	468.60
130.47	504.11	130.75	532.23	130.53	534.65	130.64	445.85
159.80	372.70	160.08	404.15	159.85	419.27	159.97	364.35
189.12	288.99	189.40	313.58	189.18	328.66	189.29	290.60
218.45	233.20	218.73	249.66	218.50	259.94	218.62	230.31
275.70	169.71	275.98	177.90	275.76	180.36	275.87	165.43
339.93	134.80	340.22	140.12	339.99	141.47	340.10	133.25
397.19	116.58	397.47	119.27	397.24	119.18	397.36	111.67
454.44	103.71	454.72	104.35	454.50	103.24	454.61	95.88
511.69	93.79	511.98	93.44	511.75	91.49	511.86	84.23
568.95	85.84	569.23	84.89	569.00	82.46	569.12	75.42
683.45	72.98	683.74	71.53	683.51	69.12	683.62	62.55
754.67	66.62	754.95	65.15	754.73	62.75	754.84	56.53
825.89	61.78	826.17	59.51	825.94	57.14	826.06	51.55
945.98	51.82	946.26	49.66	946.04	47.39	946.15	42.08

Table A-10 Experimental temperature data for run #5

$T_{initial}$ = 19.0 ± 2.2 °C Heating Time = 30.9 sec

Time (sec) (surface)	$T-T_{initial}$ (°C) (surface)	Time (sec) (2.8 mm)	$T-T_{initial}$ (°C) (2.8 mm)	Time (sec) (5.3 mm)	$T-T_{initial}$ (°C) (5.3 mm)	Time (sec) (8.1 mm)	$T-T_{initial}$ (°C) (8.1 mm)
0.00	0.00	0.00	0.00	0.00	-0.00	0.00	0.00
1.51	164.91	1.57	-0.10	1.63	1.31	1.69	0.21
3.45	402.78	3.51	0.41	3.57	18.74	3.63	0.10
5.39	604.11	5.45	5.02	5.51	48.07	5.57	0.76
7.32	782.08	7.38	13.12	7.44	78.76	7.50	2.59
9.26	944.36	9.32	24.89	9.38	105.27	9.44	5.83
11.19	1085.11	11.25	38.52	11.32	134.06	11.38	10.48
13.13	1208.13	13.19	53.11	13.25	161.44	13.31	16.60
15.07	1321.43	15.13	68.01	15.19	188.68	15.25	24.10
17.00	1418.54	17.06	83.36	17.12	223.54	17.18	32.10
18.94	1499.53	19.00	96.71	19.06	272.88	19.12	40.14
20.88	1583.06	20.94	114.89	21.00	339.41	21.06	51.07
22.81	1655.16	22.87	134.11	22.93	413.77	22.99	59.42
24.75	1729.30	24.81	152.85	24.87	512.76	24.93	71.01
26.68	1800.37	26.74	171.91	26.81	647.44	26.87	81.10
30.92	1911.24	30.98	217.41	31.03	855.78	31.09	103.73
36.46	1617.99	36.52	318.63	36.57	998.32	36.63	136.21
42.00	1368.81	42.05	443.80	42.11	978.63	42.16	167.49
47.54	1169.06	47.59	519.94	47.65	918.73	47.70	194.45
53.07	1007.69	53.13	542.84	53.18	848.61	53.24	217.13
58.61	875.14	58.67	537.12	58.72	776.97	58.78	233.03
64.15	776.75	64.20	519.01	64.26	714.10	64.31	251.89
69.69	697.73	69.74	499.22	69.80	661.03	69.85	273.33
75.22	631.18	75.28	481.14	75.33	613.69	75.39	289.80
80.76	574.64	80.82	463.36	80.87	570.83	80.93	302.87
86.30	525.49	86.35	446.16	86.41	532.86	86.46	312.43
116.75	341.13	116.81	367.08	116.86	387.01	116.92	316.91
147.21	242.83	147.26	304.17	147.32	298.28	147.37	286.44
177.67	188.43	177.72	253.64	177.77	239.80	177.83	246.68
208.12	155.81	208.18	212.80	208.23	199.05	208.29	211.67
266.26	120.20	266.32	158.47	266.37	149.01	266.43	158.03
324.41	99.42	324.46	122.31	324.52	117.41	324.57	120.58
382.55	85.20	382.60	97.15	382.66	95.87	382.71	94.38
440.69	74.51	440.74	79.83	440.80	80.73	440.85	76.18
558.36	60.17	558.41	60.26	558.47	62.32	558.52	56.87
676.03	50.72	676.08	49.23	676.14	51.62	676.19	45.84
734.17	47.21	734.23	45.18	734.28	47.60	734.33	42.02
869.84	40.28	869.89	37.84	869.95	40.15	870.00	35.14
922.44	37.81	922.50	35.77	922.55	37.91	922.61	33.00

Table A-11 Experimental air-potted temperature data for run #5

$T_{initial}$ = 19.0 ± 2.2 °C Heating Time = 30.9 sec

Time (sec) (surface)	$T-T_{initial}$ (°C) (surface)	Time (sec) (2.6 mm)	$T-T_{initial}$ (°C) (2.6 mm)	Time (sec) (5.5 mm)	$T-T_{initial}$ (°C) (5.5 mm)	Time (sec) (8.6 mm)	$T-T_{initial}$ (°C) (8.6 mm)
0.00	0.00	0.00	0.00	0.00	0.00	0.00	0.00
1.51	164.91	1.75	4.22	1.88	0.07	1.82	0.05
3.45	402.78	3.69	36.52	3.81	0.98	3.75	0.28
5.39	604.11	5.63	79.90	5.75	5.68	5.69	0.49
7.32	782.08	7.56	116.89	7.68	15.01	7.62	1.21
9.26	944.36	9.50	152.95	9.62	27.74	9.56	3.00
11.19	1085.11	11.44	188.67	11.56	42.31	11.50	6.57
13.13	1208.13	13.37	240.10	13.49	57.64	13.43	11.09
15.07	1321.43	15.31	322.80	15.43	73.76	15.37	16.29
17.00	1418.54	17.24	397.68	17.37	90.94	17.31	23.06
18.94	1499.53	19.18	483.41	19.30	107.67	19.24	30.41
20.88	1583.06	21.12	627.20	21.24	127.60	21.18	38.54
22.81	1655.16	23.05	770.46	23.17	147.08	23.11	47.91
24.75	1729.30	24.99	870.13	25.11	167.60	25.05	57.31
26.68	1800.37	26.93	941.39	27.05	187.98	26.99	67.67
30.92	1911.24	31.14	1101.65	31.25	250.31	31.20	91.82
36.46	1617.99	36.68	1167.62	36.79	377.04	36.74	125.47
42.00	1368.81	42.22	1099.94	42.33	498.75	42.27	158.66
47.54	1169.06	47.76	1011.04	47.87	570.89	47.81	188.40
53.07	1007.69	53.29	921.87	53.40	586.74	53.35	212.55
58.61	875.14	58.83	838.94	58.94	577.73	58.89	233.95
64.15	776.75	64.37	761.99	64.48	557.07	64.42	254.91
69.69	697.73	69.91	694.89	70.02	532.47	69.96	274.08
75.22	631.18	75.44	637.55	75.55	507.28	75.50	287.53
80.76	574.64	80.98	587.53	81.09	483.54	81.04	296.39
86.30	525.49	86.52	544.01	86.63	461.23	86.57	300.86
116.75	341.13	116.97	378.32	117.08	363.46	117.03	291.50
147.21	242.83	147.43	282.37	147.54	293.80	147.48	258.46
177.67	188.43	177.88	223.57	177.99	242.17	177.94	221.70
208.12	155.81	208.34	185.05	208.45	202.29	208.40	189.81
266.26	120.20	266.48	140.19	266.59	151.33	266.54	143.25
324.41	99.42	324.62	112.55	324.73	118.02	324.68	110.32
440.69	74.51	440.91	80.08	441.02	78.71	440.96	71.27
498.83	66.45	499.05	70.18	499.16	67.29	499.11	60.24
558.36	60.17	558.58	62.88	558.69	59.50	558.63	52.72
676.03	50.72	676.25	52.49	676.36	48.85	676.30	42.79
734.17	47.21	734.39	48.63	734.50	44.91	734.44	39.19
869.84	40.28	870.06	41.28	870.16	37.75	870.11	32.83
922.44	37.81	922.66	38.81	922.77	35.56	922.72	30.83

Table A-12 Experimental temperature data for run #6

$T_{initial}$ = 22.4 ± 2.2 °C Heating Time = 33.9 sec

Time (sec) (surface)	$T-T_{initial}$ (°C) (surface)	Time (sec) (2.8 mm)	$T-T_{initial}$ (°C) (2.8 mm)	Time (sec) (5.3 mm)	$T-T_{initial}$ (°C) (5.3 mm)	Time (sec) (8.4 mm)	$T-T_{initial}$ (°C) (8.4 mm)
0.00	0.00	0.00	0.00	0.00	0.00	0.00	0.00
1.56	223.36	1.80	3.31	1.68	0.04	1.62	0.06
3.55	482.23	3.80	31.60	3.67	1.05	3.61	0.14
5.54	704.65	5.79	70.76	5.66	7.25	5.60	0.08
7.53	901.10	7.78	106.75	7.65	17.75	7.59	1.50
9.52	1072.81	9.77	139.26	9.65	32.34	9.58	3.46
11.51	1222.97	11.76	173.36	11.64	47.78	11.57	7.16
13.50	1357.03	13.75	208.16	13.63	65.25	13.57	12.28
15.49	1489.61	15.74	248.42	15.62	83.02	15.56	18.33
17.49	1595.52	17.74	312.64	17.61	101.17	17.55	26.02
19.48	1696.49	19.73	400.65	19.60	119.81	19.54	34.01
21.47	1786.21	21.72	502.10	21.59	140.08	21.53	43.29
23.46	1862.32	23.71	636.80	23.58	160.78	23.52	53.76
25.45	1923.26	25.70	802.95	25.58	184.40	25.51	64.75
27.44	1965.64	27.69	911.10	27.57	206.17	27.50	76.16
29.43	1981.62	29.68	999.31	29.56	234.30	29.50	88.21
31.43	1985.43	31.67	1076.44	31.55	272.58	31.49	100.87
33.42	1984.37	33.67	1141.50	33.54	323.63	33.48	113.61
39.50	1786.96	39.73	1281.17	39.61	525.39	39.56	156.70
45.08	1502.31	45.31	1222.65	45.20	709.21	45.14	196.31
50.67	1285.48	50.90	1119.69	50.78	758.39	50.73	234.09
56.25	1104.33	56.48	1013.29	56.37	749.38	56.31	278.92
61.84	956.06	62.06	914.39	61.95	717.13	61.90	315.98
67.42	832.26	67.65	823.26	67.54	674.31	67.48	338.44
73.01	726.33	73.23	738.80	73.12	627.07	73.06	346.07
89.76	491.85	89.99	526.67	89.88	482.98	89.82	317.66
120.48	243.39	120.71	275.61	120.59	267.99	120.54	208.81
151.20	168.87	151.42	189.50	151.31	183.93	151.25	171.12
239.16	102.28	239.38	116.90	239.27	121.22	239.21	121.61
297.80	86.55	298.03	96.36	297.91	98.96	297.86	97.94
356.44	76.13	356.67	82.67	356.55	83.54	356.50	81.40
415.08	68.10	415.31	72.69	415.19	72.42	415.14	69.63
473.72	61.43	473.95	65.09	473.84	63.96	473.78	60.98
532.36	56.61	532.59	59.00	532.48	57.57	532.42	54.41
649.65	48.45	649.87	49.53	649.76	47.81	649.70	44.71
708.29	45.02	708.51	45.72	708.40	43.97	708.34	40.96
766.93	41.65	767.15	42.33	767.04	40.46	766.98	37.74
884.21	36.22	884.44	36.68	884.32	35.19	884.27	32.47
935.87	33.53	936.10	34.47	935.98	32.68	935.93	30.47

Table A-13 Experimental temperature data for run #7

$T_{initial}$ = 22.3 ± 2.2 °C Heating Time = 27.9 sec

Time (sec) (surface)	$T-T_{initial}$ (°C) (surface)	Time (sec) (2.6 mm)	$T-T_{initial}$ (°C) (2.6 mm)	Time (sec) (5.3 mm)	$T-T_{initial}$ (°C) (5.3 mm)	Time (sec) (8.5 mm)	$T-T_{initial}$ (°C) (8.5 mm)
0.00	-0.00	0.00	-0.00	0.00	0.00	0.00	-0.00
1.56	199.89	1.62	2.06	1.74	0.48	1.93	0.83
3.55	489.58	3.61	23.96	3.73	0.31	3.92	-0.12
5.54	756.23	5.60	57.58	5.72	6.26	5.91	0.83
7.53	979.30	7.59	93.10	7.71	16.16	7.90	2.88
9.52	1168.13	9.58	126.51	9.70	28.41	9.89	4.23
11.51	1321.02	11.57	161.99	11.70	43.21	11.88	6.75
13.50	1451.18	13.56	195.38	13.69	62.75	13.87	14.39
15.49	1562.52	15.55	240.90	15.68	81.24	15.86	21.22
17.48	1675.12	17.54	305.33	17.67	98.02	17.85	26.98
19.47	1794.28	19.53	400.17	19.66	119.37	19.85	37.35
21.46	1888.18	21.52	524.66	21.65	139.99	21.84	46.79
23.45	1958.98	23.52	697.80	23.64	157.56	23.83	55.22
25.44	2012.36	25.51	848.21	25.63	185.08	25.82	66.52
27.43	2030.39	27.50	969.50	27.62	214.96	27.81	79.82
29.43	2030.68	29.49	1067.47	29.61	248.09	29.80	89.24
31.42	2015.66	31.48	1150.90	31.60	295.13	31.79	101.33
33.41	1991.08	33.47	1219.22	33.59	362.47	33.78	117.89
50.65	1036.32	50.71	979.32	50.82	869.34	50.99	252.42
56.24	650.54	56.29	844.24	56.41	851.88	56.57	309.36
61.82	582.21	61.87	753.54	61.99	813.68	62.16	349.05
67.40	525.00	67.46	677.81	67.57	765.32	67.74	367.54
72.98	453.45	73.04	603.97	73.15	713.07	73.32	370.50
89.73	300.58	89.79	435.20	89.90	551.02	90.07	327.71
151.14	77.28	151.20	116.78	151.31	155.01	151.48	105.09
239.07	50.99	239.12	65.48	239.23	64.37	239.40	56.54
297.68	39.35	297.74	58.35	297.85	57.90	298.02	52.86
356.30	35.49	356.36	53.17	356.47	52.71	356.64	48.47
414.92	31.98	414.97	48.73	415.09	48.26	415.26	44.36
473.53	30.54	473.59	44.89	473.70	44.43	473.87	40.89
532.15	31.03	532.21	41.56	532.32	41.13	532.49	37.75
590.77	27.55	590.82	38.66	590.94	38.17	591.11	34.97
649.39	23.00	649.44	36.02	649.55	35.52	649.72	32.54
708.00	25.45	708.06	33.67	708.17	33.14	708.34	30.34
776.39	24.27	776.45	31.15	776.56	30.63	776.73	27.81
883.85	18.15	883.91	27.59	884.02	27.19	884.19	24.93
908.98	14.87	909.03	26.82	909.14	26.42	909.31	24.10
942.47	16.29	942.53	25.93	942.64	25.51	942.81	23.36

Table A-14 Experimental temperature data for run #8

$T_{initial}$ = 20.5 ± 2.2 °C Heating Time = 22 sec measured

Time (sec) (surface)	$T-T_{initial}$ (°C) (surface)	Time (sec) (2.4 mm)	$T-T_{initial}$ (°C) (2.4 mm)	Time (sec) (4.7 mm)	$T-T_{initial}$ (°C) (4.7 mm)	Time (sec) (7.8 mm)	$T-T_{initial}$ (°C) (7.8 mm)
0.00	0.00	0.00	0.00	0.00	0.00	0.00	0.00
0.08	-0.00	0.31	0.00	0.55	0.00	0.16	0.00
0.70	118.57	0.94	0.41	1.17	0.28	0.78	0.18
1.33	200.54	1.56	3.75	1.80	0.43	1.41	0.15
1.96	350.18	2.19	12.20	2.42	0.52	2.03	0.34
2.58	460.02	2.82	24.67	3.05	0.72	2.66	0.27
3.21	560.31	3.44	39.70	3.68	1.56	3.28	0.16
3.83	653.89	4.07	56.20	4.30	2.84	3.91	0.12
4.46	742.97	4.69	73.30	4.93	5.04	4.54	0.07
5.08	826.54	5.32	90.53	5.55	7.99	5.16	0.14
5.71	905.59	5.94	107.48	6.18	11.64	5.79	0.32
6.33	982.78	6.57	123.87	6.80	15.37	6.41	0.57
6.96	1054.48	7.20	140.68	7.43	19.74	7.04	0.87
7.59	1122.84	7.82	157.18	8.06	24.38	7.66	1.17
8.21	1188.14	8.45	174.81	8.68	29.70	8.29	1.60
8.84	1248.43	9.07	192.42	9.31	35.54	8.92	2.21
9.46	1305.90	9.70	209.90	9.93	41.88	9.54	2.87
10.09	1361.61	10.32	230.90	10.56	48.63	10.17	3.77
10.71	1418.08	10.95	261.19	11.18	55.69	10.79	4.90
11.34	1473.80	11.57	311.00	11.81	63.00	11.42	6.19
11.97	1525.43	12.20	360.86	12.43	70.52	12.04	7.71
12.59	1575.25	12.83	419.49	13.06	78.37	12.67	9.39
13.22	1624.80	13.45	497.28	13.69	86.90	13.30	11.14
13.84	1675.47	14.08	577.53	14.31	95.68	13.92	13.01
14.47	1727.69	14.70	672.90	14.94	104.93	14.55	15.04
15.09	1778.31	15.33	778.91	15.56	114.58	15.17	17.27
15.72	1828.65	15.95	869.02	16.19	124.83	15.80	19.77
16.35	1876.63	16.58	934.09	16.81	134.92	16.42	22.56
16.97	1922.56	17.21	976.07	17.44	145.94	17.05	25.49
17.60	1966.90	17.83	1043.10	18.07	156.17	17.67	28.62
18.22	2009.83	18.46	1098.75	18.69	165.37	18.30	31.91
18.85	2050.30	19.08	1150.81	19.32	178.44	18.93	35.39
19.47	2084.56	19.71	1191.11	19.94	191.04	19.55	39.03
20.10	2108.58	20.33	1233.03	20.57	205.02	20.18	42.87
20.72	2117.49	20.96	1268.96	21.19	220.73	20.80	46.85
21.35	2146.66	21.58	1297.86	21.82	238.39	21.43	51.13
21.98	2180.46	22.21	1322.34	22.45	255.73	22.05	55.64

Appendix B

Material properties

Table B-1 Temperature-dependent material properties for carbon-phenolic

Material Property	Temperature	Metric Value	English Value
Thermal conductivity, virgin with-ply [18]	338.9 K (610.0 R)	1.127 W/m-K	0.000181 Btu/ft-s-R
	422.2 K (760.0 R)	1.483 W/m-K	0.000238 Btu/ft-s-R
	477.8 K (860.0 R)	1.545 W/m-K	0.000248 Btu/ft-s-R
	533.3 K (960.0 R)	1.545 W/m-K	0.000248 Btu/ft-s-R
	588.9 K (1060.0 R)	1.526 W/m-K	0.000245 Btu/ft-s-R
	644.4 K (1160.0 R)	1.501 W/m-K	0.000241 Btu/ft-s-R
Thermal conductivity, virgin across-ply [18]	338.9 K (610.0 R)	0.810 W/m-K	0.000130 Btu/ft-s-R
	422.2 K (760.0 R)	0.922 W/m-K	0.000148 Btu/ft-s-R
	477.8 K (860.0 R)	0.978 W/m-K	0.000157 Btu/ft-s-R
	533.3 K (960.0 R)	1.022 W/m-K	0.000164 Btu/ft-s-R
	588.9 K (1060.0 R)	1.040 W/m-K	0.000167 Btu/ft-s-R
	644.4 K (1160.0 R)	1.009 W/m-K	0.000162 Btu/ft-s-R
Thermal conductivity, char with-ply [18]	366.7 K (660.0 R)	1.601 W/m-K	0.000257 Btu/ft-s-R
	477.8 K (860.0 R)	1.863 W/m-K	0.000299 Btu/ft-s-R
	588.9 K (1060.0 R)	2.205 W/m-K	0.000354 Btu/ft-s-R
	700.0 K (1260.0 R)	2.205 W/m-K	0.000354 Btu/ft-s-R
	811.1 K (1460.0 R)	2.348 W/m-K	0.000377 Btu/ft-s-R
	922.2 K (1660.0 R)	2.510 W/m-K	0.000403 Btu/ft-s-R
	1088.9 K (1960.0 R)	2.741 W/m-K	0.000440 Btu/ft-s-R
Thermal conductivity, char across-ply [18]	366.7 K (660.0 R)	0.953 W/m-K	0.000153 Btu/ft-s-R
	477.8 K (860.0 R)	1.171 W/m-K	0.000188 Btu/ft-s-R
	588.9 K (1060.0 R)	1.358 W/m-K	0.000218 Btu/ft-s-R
	700.0 K (1260.0 R)	1.514 W/m-K	0.000243 Btu/ft-s-R
	811.1 K (1460.0 R)	1.644 W/m-K	0.000264 Btu/ft-s-R
	922.2 K (1660.0 R)	1.676 W/m-K	0.000269 Btu/ft-s-R
	1088.9 K (1960.0 R)	1.676 W/m-K	0.000269 Btu/ft-s-R
Heat capacity, virgin [1]	255.6 K (460.0 R)	1044 J/Kg-K	0.250 Btu/lbm-R
	294.4 K (530.0 R)	1073 J/Kg-K	0.257 Btu/lbm-R
	444.4 K (800.0 R)	1466 J/Kg-K	0.351 Btu/lbm-R
	555.6 K (1000.0 R)	1759 J/Kg-K	0.421 Btu/lbm-R
	644.4 K (1160.0 R)	1880 J/Kg-K	0.450 Btu/lbm-R
	833.3 K (1500.0 R)	1921 J/Kg-K	0.460 Btu/lbm-R

	1111.1 K (2000.0 R)	1963 J/Kg-K	0.470 Btu/lbm-R
	1389.9 K (2500.0 R)	2013 J/Kg-K	0.482 Btu/lbm-R
	1666.7 K (3000.0 R)	2059 J/Kg-K	0.493 Btu/lbm-R
Heat capacity, char [1]	255.6 K (460.0 R)	731 J/Kg-K	0.175 Btu/lbm-R
	294.4 K (530.0 R)	781 J/Kg-K	0.187 Btu/lbm-R
	444.4 K (800.0 R)	1090 J/Kg-K	0.261 Btu/lbm-R
	555.6 K (1000.0 R)	1316 J/Kg-K	0.315 Btu/lbm-R
	644.4 K (1160.0 R)	1428 J/Kg-K	0.342 Btu/lbm-R
	833.3 K (1500.0 R)	1671 J/Kg-K	0.400 Btu/lbm-R
	1111.1 K (2000.0 R)	1813 J/Kg-K	0.434 Btu/lbm-R
	1389.9 K (2500.0 R)	1938 J/Kg-K	0.464 Btu/lbm-R
	1666.7 K (3000.0 R)	2059 J/Kg-K	0.493 Btu/lbm-R
Heat of formation, virgin [15]	297.8 K (536.0 R)	-909000 J/Kg	-391.72 Btu/lbm
Heat of formation, char [15]	297.8 K (536.0 R)	0.0 J/Kg	0.0 Btu/lbm
Molecular weight, pyrolysis gas [16]	672.2 K (1210.0 R)	32 g/mole	32.0 lbm/lb-mole
	811.1 K (1460.0 R)	26 g/mole	26.0 lbm/lb-mole
Viscosity, pyrolysis gas [15]	277.8 K (500.0 R)	5.020×10^{-7} Kg/m-s	3.366×10^{-7} lbm/ft-s
	400.0 K (720.0 R)	6.155×10^{-7} Kg/m-s	4.127×10^{-7} lbm/ft-s
	1600.0 K (2880.0 R)	1.490×10^{-6} Kg/m-s	9.988×10^{-7} lbm/ft-s
	2000.0 K (3600.0 R)	1.716×10^{-6} Kg/m-s	1.151×10^{-6} lbm/ft-s
Enthalpy, pyrolysis gas [1]	277.8 K (500.0 R)	-4.00×10^{6} J/Kg	-1721.0 Btu/lbm
	500.0 K (900.0 R)	-2.74×10^{6} J/Kg	-1182.5 Btu/lbm
	600.0 K (1080.0 R)	-2.18×10^{6} J/Kg	-940.0 Btu/lbm
	700.0 K (1260.0 R)	-1.61×10^{6} J/Kg	-693.6 Btu/lbm
	800.0 K (1440.0 R)	-993000 J/Kg	-428.1 Btu/lbm
	900.0 K (1620.0 R)	-400000 J/Kg	-172.6 Btu/lbm
	1000.0 K (1800.0 R)	194000 J/Kg	83.6 Btu/lbm
	1100.0 K (1980.0 R)	815000 J/Kg	351.3 Btu/lbm
	1200.0 K (2160.0 R)	1.43×10^{6} J/Kg	614.8 Btu/lbm
	1300.0 K (2340.0 R)	2.02×10^{6} J/Kg	870.0 Btu/lbm
	1400.0 K (2520.0 R)	2.65×10^{6} J/Kg	1140.0 Btu/lbm
	1500.0 K (2700.0 R)	3.19×10^{6} J/Kg	1375.0 Btu/lbm
	2000.0 K (3600.0 R)	6.16×10^{6} J/Kg	2654.5 Btu/lbm

Table B-2 Porosity and permeability for carbon-phenolic

Material Property	Degree of Char	Metric Value	English Value
Porosity[a]	0.0	0.060	
	1.000	0.345	
Permeability, with-ply[b]	0.000	3.2×10^{-18} m^2	3.44×10^{-17} ft^2
	0.040	2.7×10^{-18} m^2	2.91×10^{-17} ft^2
	0.096	7.1×10^{-19} m^2	7.64×10^{-18} ft^2
	0.180	1.0×10^{-17} m^2	1.08×10^{-16} ft^2
	0.400	4.9×10^{-17} m^2	5.27×10^{-16} ft^2
	0.464	1.0×10^{-16} m^2	1.08×10^{-15} ft^2
	0.500	5.0×10^{-16} m^2	5.38×10^{-15} ft^2
	0.600	3.3×10^{-15} m^2	3.55×10^{-14} ft^2
	0.700	1.0×10^{-14} m^2	1.08×10^{-13} ft^2
	1.000	1.0×10^{-13} m^2	1.08×10^{-12} ft^2
Permeability, across-ply[b]	0.000	1.0×10^{-24} m^2	1.08×10^{-23} ft^2
	0.400	1.0×10^{-17} m^2	1.08×10^{-16} ft^2
	0.464	1.0×10^{-16} m^2	1.08×10^{-15} ft^2
	0.500	5.0×10^{-16} m^2	5.38×10^{-15} ft^2
	0.600	3.3×10^{-15} m^2	3.55×10^{-14} ft^2
	0.700	1.0×10^{-14} m^2	1.08×10^{-13} ft^2
	1.000	1.0×10^{-13} m^2	1.08×10^{-12} ft^2

[a]Upper value from refererence [18], lower value is an educated guess [11].

[b]Unpublished paper by F. I. Clayton "Influence of Real Gas Effects on the Predicted Response of Carbon Phenolic Material Exposed to Elevated Temperature and Pressure Environments," 1993.

Table B-3 Decomposition kinetics for carbon-phenolic[a]

Material property	Metric Value	English Value
Component A virgin density	50.44 kg/m^3	3.142 lbm/ft^3
Component A char density	0.0 kg/m^3	0.0 lbm/ft^3
Component A pre-expon. factor	1873.6 s^{-1}	
Component A order of reaction	1.23	
Component A activation energy	38643 J/g-mole	16618 Btu/lb-mole
Component A cutoff temperature	310 K	558 R
Component B virgin density	315.3 kg/m^3	19.64 lbm/ft^3
Component B char density	0.0 kg/m^3	0.0 lbm/ft^3
Component B pre-expon. factor	118.56 s^{-1}	
Component B order of reaction	1.17	
Component B activation energy	49787 J/g-mole	21410 Btu/lb-mole
Component B cutoff temperature	360 K	648 R
Component C virgin density	2575.9 kg/m^3	60.47 lbm/ft^3
Component C char density	2540.07 kg/m^3	158.241 lbm/ft^3
Component C pre-expon. factor	1.918×10^9 s^{-1}	
Component C order of reaction	1.12	
Component C activation energy	213910 J/g-mole	91987 Btu/lb-mole
Component C cutoff temperature	925 K	1665 R
Resin fraction	0.500	

[a]Revised kinetics from phone conservation with F. Strobel, June 1993 [11].

Table B-4 Material properties used for POCO graphite, grade EDM3

Material Property	Temperature	Metric Value	English Value
Thermal conductivity[a]	294.4 K (530.0 R)	183.4 W/m-K	0.02944 Btu/ft-s-R
	344.4 K (620.0 R)	105.5 W/m-K	0.01694 Btu/ft-s-R
	533.3 K (960.0 R)	90.8 W/m-K	0.01458 Btu/ft-s-R
	811.1 K (1460.0 R)	75.6 W/m-K	0.01214 Btu/ft-s-R
	1088.9 K (1960.0 R)	62.5 W/m-K	0.01003 Btu/ft-s-R
	1366.7 K (2460.0 R)	53.4 W/m-K	0.00858 Btu/ft-s-R
	1644.4 K (2960.0 R)	46.5 W/m-K	0.00746 Btu/ft-s-R
Heat capacity[a]	255.6 K (460.0 R)	593 J/Kg-K	0.1420 Btu/lbm-R
	494.4 K (890.0 R)	1253 J/Kg-K	0.3000 Btu/lbm-R
	627.8 K (1130.0 R)	1462 J/Kg-K	0.3500 Btu/lbm-R
	811.1 K (1460.0 R)	1636 J/Kg-K	0.3917 Btu/lbm-R
	1366.7 K (2460.0 R)	1914 J/Kg-K	0.4583 Btu/lbm-R
	1922.2 K (3460.0 R)	2054 J/Kg-K	0.4917 Btu/lbm-R
Solid density[a]	---	1814 Kg/m^3	112.998 lbm/ft^3
Porosity[a]	---	0.2	
Permeability[b]	---	$9.29x10^{-13}$ m^2	$1.0x10^{-11}$ ft^2

[a]Properties for similar material, AXF-5Q graphite, from manufacturer.
[b]Educated guess [11]. Value was picked to minimize effect on pressure computation.

Table B-5 Material properties used for Boron Nitride paint

Material property	Metric Value	English Value
Thermal conductivity[a]	31.0 W/m-K	0.005 Btu/ft-s-R
Heat capacity[a]	488.7 J/Kg-K	0.117 Btu/lbm-R
Solid density[a]	2263 Kg/m^3	141.0 lbm/ft^3
Porosity[b]	0.2	
Permeability[b]	$9.29x10^{-13}$ m^2	$1.0x10^{-11}$ ft^2

[a]Room temperature values for pure Boron Nitride from manufacturer.
[b]Educated guess [11]. Values were picked to minimize effect on pressure computation.

Table B-6 Thermophysical properties[a] of thermocouple potting materials and carbon-phenolic

Thermocouple potting material	Thermal Conductivity (W/m-K)	Density (Kg/m^3)	Specific Heat (J/Kg-K)	Thermal Diffusivity (10^{-6} m^2/sec)
Air	0.0667	0.3482	1141	168
Cotronics Hi-Seal C7030	1.20	2400	950[b]	0.53
Cotronics Resbond C989	1.30	2000	1000[b]	0.65
Cotronics Resbond C903HP	5.77	2000	1000[b]	2.9
ORPAC Al_2O_3 paste	4	2400	1050	1.59
Sauereisen Insultemp #10 Cement[a]	2.87	2344	981.6	1.25
ZYP Coatings Boron Nitride paint	20.9	2270	490	18.8
ZYP Coatings RS-1000 cement	1.67	2560	1 000[b]	0.65
Carbon-phenolic, virgin with-ply	1.501	1471	1963	0.52
Carbon-phenolic, char with-ply	2.741	1270	1813	1.19
Carbon-phenolic, virgin across-ply	1.009	1471	1963	0.35
Carbon-phenolic, char across-ply	1.676	1270	1813	0.73

[a]Listed values are for temperatures near 1000 °C.

[b]Educated guess. Values are typical of similar materials.

Table B-7 Material properties used for Hot Pressed Boron Nitride (HPBN) plates

Material property	Metric Value parallel (perpendicular)[a]
Thermal conductivity[b]	71.3 (121.2) W/m-K
Heat capacity[b]	828 J/Kg-K
Solid density[b]	1914 Kg/m^3
Thermal Diffusivity	45.0 (76.4) mm^2/s

[a]Orientation to the pressing direction

[b]Room temperature values for pure Boron Nitride from manufacturer.

Vita

Scott Gayton Liter was born in Fort Sam Houston outside of San Antonio, Texas on April 20, 1971. He grew up the son of an Army officer and attended public schools throughout the United States. In 1989, he graduated from Lowell High School in San Francisco, California. The following school year he entered the University of Tennessee at Knoxville (UTK) and was awarded a Bachelor of Science degree in Aerospace Engineering in May 1994. Immediately afterwards, he continued his education at UTK in the Mechanical Engineering Master's program. He received the Master of Science degree in Mechanical Engineering, Thermal Science Specialty, in May 1996 from the UTK Graduate School. In January of 1996, he went to the University of Michigan at Ann Arbor with a letter of completion of the requirements for a Master's degree at UTK. He is currently in Ann Arbor pursuing a doctoral degree Mechanical Engineering, Thermal Sciences.